6-2012

Paleoclimatic Regimes of the African Sahara Desert During Pleistocene and the Origin of Groundwater in the Nubian Sandstone Aquifer System

Abdou A. Abouelmagd
Western Michigan University

PALEOCLIMATIC REGIMES OF THE AFRICAN SAHARA DESERT DURING PLEISTOCENE AND THE ORIGIN OF GROUNDWATER IN THE NUBIAN SANDSTONE AQUIFER SYSTEM

by

Abdou A. Abouelmagd

A Dissertation
Submitted to the
Faculty of The Graduate College
in partial fulfillment of the
requirements for the
Degree of Doctor of Philosophy
Department of Geosciences
Advisor: Alan Kehew, Ph.D.

Western Michigan University
Kalamazoo, Michigan
June 2012

It is Allah (God) who sends the winds so that they raise a cloud. Then He spreads it in the sky as He pleases and places it layer upon layer and thou seest the rain issuing forth from its midst. And when He causes it to fall on whom He pleases of His servants, behold! They rejoice.

(Holy Qur'an, 30:48)

ACKNOWLEDGMENTS

First and foremost, praise is to God, who gave me the patience and effort to carry out this research. Second, my great appreciation towards the Department of Geosciences at Western Michigan University for granting me generous scholarships and teaching assistantships that helped me a lot since the first day of matriculation in the PhD program.

I would like to thank my advisor, Dr. Alan Kehew, for guiding me through the long process of my dissertation. He was always there to answer my questions and make suggestions. I would also like to express my deepest appreciation to Dr. Mohamed Sultan, a committee member and department chair, for giving me the opportunity to conduct my research work among his research group at the ESRS lab facility. His continuous guidance, financial support, and critical revision are highly appreciated and would not be forgotten.

I would also like to extend my gratitude to my committee members, Dr. R.V Krishnamurthy and Dr. Neil Sturchio for the invaluable discussions and suggestions throughout each phase of the project. I am also grateful to Dr. Elen Cutrim (deceased) for her guidance and support throughout the early stage of this research. In addition, my sincere appreciation to Dr. Adam Milewski, Mr. Mohamed Ahmed and all ESRS Lab colleagues for their assistance and sincere cooperation and support over the years.

Lastly, I should not forget to thank my family (parents and sisters) in my home country, Egypt and my wife and children here in US for their patience, continuous support and encouragement to work hard and finalize this research in its final form.

Abdou A. Abouelmagd

PALEOCLIMATIC REGIMES OF THE AFRICAN SAHARA DESERT DURING PLEISTOCENE AND THE ORIGIN OF GROUNDWATER IN THE NUBIAN SANDSTONE AQUIFER SYSTEM

Abdou A. Abouelmagd, Ph.D.

Western Michigan University, 2012

This study involves an integrated three-fold approach to better understand the paleoclimatic regimes over the North African Sahara Desert with emphasis on the origin of groundwater in the Nubian Sandstone Aquifer System. Specifically, the nature and origin of the paleo-wind regimes that produced the precipitation that recharged the fossil aquifers in North Africa in the previous wet climatic periods are deciphered using inferences from stable isotope data, noble gases, remote sensing and GIS.

In the first phase, the progressive depletion trend of stable isotopic composition in the fossil groundwaters under influence of paleowesterlies across North African Sahara Desert is simulated using a Rayleigh Distillation Model. Then, the precipitation events that gave rise to precipitation with isotopic signatures similar to those of the fossil groundwater in North African Aquifers (e.g., Nubian Sandstone Aquifer System) are identified. In the second phase, the temporal satellite data (METEOSAT First Generation) are used to identify the directions of the modern wind regimes influencing those precipitation events.

To substantiate the findings from the first two phases, groundwater samples are collected from the Nubian Aquifer underlying Egyptian Sinai Peninsula to extract the recharge temperatures using dissolved noble gas concentrations in the samples and

to determine their ages. The following observations and findings support recharge of the Sahara fossil aquifers by intensification of paleowesterlies during wet cool glacial periods: (1) modern rare west to east propagation clouds produce precipitation that is progressively depleted in its isotopic composition (O, H) with distance traveled across the Sahara; the observed isotopic compositions and patterns for modern precipitation are similar to those reported for the North African fossil aquifers, and (2) groundwater samples from the fossil aquifers are depleted in their isotopic composition and their ages are found to be consistent with the deposition during cool glacial periods. The average recharge temperatures (from dissolved noble gas concentrations) are lower than current mean annual air temperatures by approximately 4.0 °C and the groundwater ages for the Nubian Sandstone Aquifer range from ^{14}C: 32 x 10^3 yrs B.P. to 26 x 10^3 yrs B.P.

TABLE OF CONTENTS

CHAPTER

CHAPTER

LIST OF TABLES

LIST OF FIGURES

LIST OF ABBREVIATIONS

AMS	Accelerator Mass Spectrometer
AMSL	above Mean Sea Level
ARL	Air Resources Laboratory
BMSL	below Mean Sea Level
BP	Before Present
BTM	Back Trajectory Model
BUFR	Binary Universal Form for the Representation of meteorological data
CMW	Cloud Motion Winds
DEM	Digital Elevation Model
DIC	Dissolved Inorganic Carbon
ED	Eastern Desert of Egypt
GIS	Geographic Information System
GMWL	Global Meteoric Water Line
HRI	High Resolution Image
HYSPLIT	Hybrid Single-Particle Lagrangian Integrated Trajectory
IAEA	International Atomic Energy Agency
ITCZ	Intertropical Convergence Zone
LGM	Last Glacial Maximum
MAAT	Mean Annual Air Temperature

MFG	Meteosat First Generation
MTP	Meteosat Transition Program
NAO	North Atlantic Oscillation
NCDC	National Climatic Data Center
NGTs	Noble Gas Recharge Temperatures
NOAA	National Oceanic and Atmospheric Administration
NDR	Number of Data Records
NRD	Number of Rainy Days
NSAS	Nubian Sandstone Aquifer System
pmC	Percent Modern Carbon
SP	Sinai Peninsula
STP	Standard Temperature and Pressure
SWAT	Soil and Water Assessment Tool
U-MARF	Unified Meteorological Archiving and Retrieval Facility
UTC	Universal Coordinated Time
WD	Western Desert of Egypt
WGS	World Geodetic System
WISER	Water Isotope System for Data Analysis, Visualization and Electronic Retrieval Database

CHAPTER I

INTRODUCTION

1.1 Rationale and Problem Statement

The lack of an adequate water supply needed to sustain the rising population in the Sahara Desert countries motivates efforts to better understand the nature, origin and hydrogeologic setting of the major aquifer systems in the area. Such studies could assist in developing sustainable exploitation plans and relevant management practices for these systems. Of prime importance, are investigations addressing the mechanisms and timing of recharge of these aquifers and modern contributions to these systems.

Regarding the paleoclimatic regimes of the Sahara Desert, there is a general consensus that they alternated between dry and wet periods throughout the Pleistocene Epoch, from which the (fossil aquifers) are believed to have been recharged in previous wet climatic periods. On the other hand, the nature of these wet periods remains a subject of contention. Two main hypotheses have been advocated to address the origin of the fossil groundwater underneath the African Sahara Desert: (1) intensification of paleowesterlies during glacial periods (Sonntag et al., 1978; Sultan et al., 1997; Brookes, 2003; Sturchio et al., 2004) and (2) intensification of paleomonsoons during interglacial periods (Rossignol-Strick, 1983; Prell and Kutzbach, 1987; Yan and Petit-Maire, 1994; Osmond and Dabous, 2004).

The findings from the two advocated hypotheses were inferred from numerous terrestrial and marine paleoclimatic indicators such as; (1) using the stable isotope

data (δ^2H and $\delta^{18}O$) of the fossil groundwaters; (2) studying the stable isotopes of cave formations (speleothems); (3) dating the organic black rich layer (sapropel); and (4) studying the fluctuations of pluvial lake levels during the Quaternary (e.g. Lake Lisan; the precursor of the Dead Sea).

The present study provides comprehensive analysis utilizing three-fold approach to better understand the paleoclimatic regimes that prevailed during the Pleistocene over the North African Sahara Desert with emphasis on the Nubian Sandstone Aquifer System (NSAS) and by using inferences from (1) stable isotope data of meteoric and fossil waters, (2) dissolved noble gas concentrations, and (3) remote sensing and GIS.

The findings resulting from applying the integrated three-fold approach presented in this study support the hypothesis that advocates the intensification of paleowesterlies in recharging the fossil groundwater aquifers in the North African Sahara Desert and refutes the hypothesis involving intensification of monsoons. To the best of my knowledge, the novelty of current study, by applying the three-fold approach that presented in this study is the first of its kind and yielded significant results that can be used successfully in investigating other comparative fossil aquifers in the African continent and elsewhere.

1.2 Research Objectives

The ultimate goal of the present work is to reconstruct the paleoclimatic regimes over the Sahara Desert in general with emphasis on the Nubian Sandstone Aquifer System in particular. To achieve this goal, the following two vital components will be addressed:

(1) Deciphering the origin and nature of the paleowind regimes that recharged the North African fossil waters in previous wet climatic periods (450,000- 10,000 yr B.P.) using inferences from stable isotope data and applying an innovative remote sensing and GIS approach.

(2) Determining paleotemperatures using dissolved noble gas concentrations in conjunction with the radiocarbon analysis for groundwater age dating.

This approach is shown to enrich our understanding of the timing and source of recharge to the fossil groundwater aquifers beneath the Sahara Desert and can be applied to other comparative fossil aquifers elsewhere.

1.3 Study Area

The Sahara Desert is the largest (surface area: 9×10^6 km^2) "non-polar" desert region on Earth. It covers most of northern Africa (length: 4800 km; width: 1900 km), extends from the Atlantic Ocean (west) to the Red Sea (east) and from the Mediterranean Sea (north) to central Africa (south), and encompasses 11 countries (Western Sahara, Morocco, Algeria, Tunisia, Libya, Egypt, Sudan, Chad, Niger, Mali, and Mauritania) with a total population of 250 million (WPP, 2009). It has one of the

harshest and most arid climates in the world, with almost half of the Sahara receiving less than 2 cm/year of precipitation and the remaining land receiving up to 10 cm/year (Meigs, 1953). Fig. 1 shows three significant fossil aquifers that underlie the Sahara Desert: (1) the Nubian Sandstone Aquifer System; (2) the Northwestern Sahara Aquifer; and (3) the Iullemeden Aquifer System (Wallin et al., 2005).

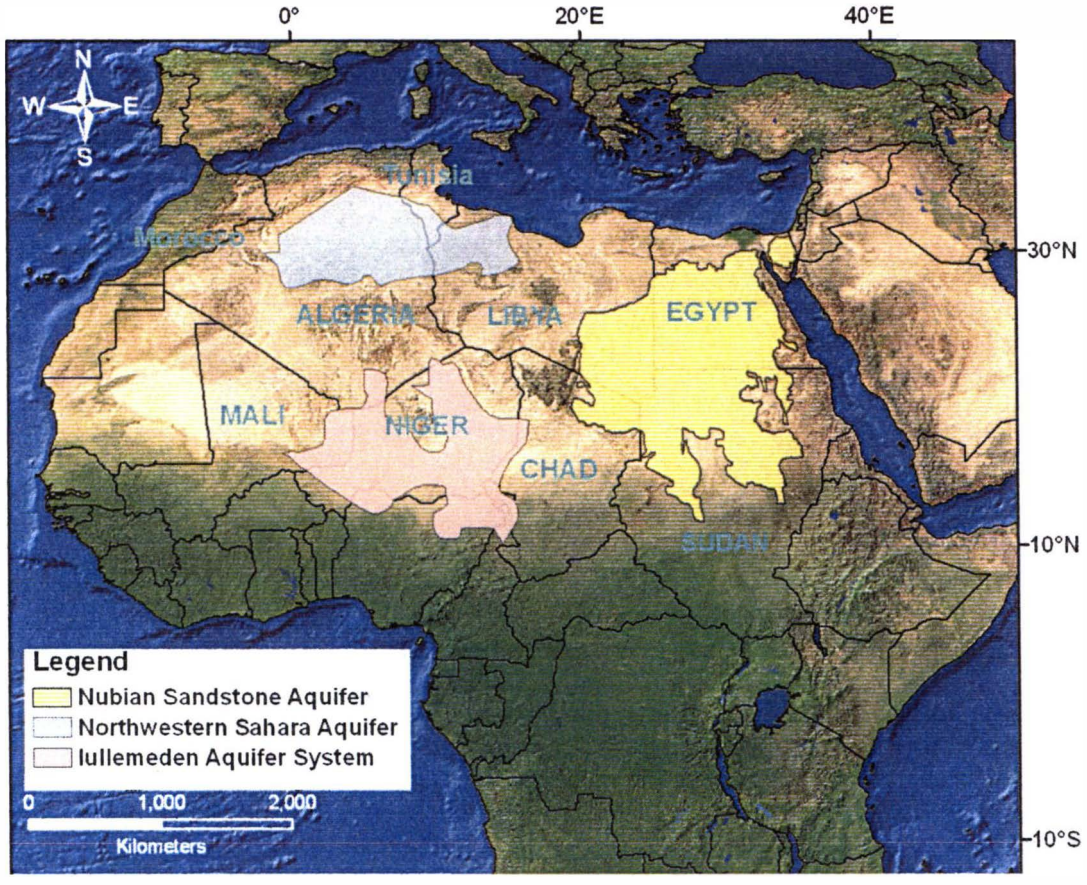

Figure 1: Spatial distribution of fossil groundwater aquifers across the North African Sahara Desert (modified after Wallin et al., 2005) over MODIS map of Africa (NASA, 2005).

The Nubian Sandstone Aquifer System (NSAS) is one of the largest fossil transboundary reservoirs in the world and contains a potential supply of fresh water

for drinking and irrigation purposes. It covers an area of about 2 million km^2 and extends between Latitude 14° and 33° N and Longitude 19° and 34° E, covering large domains in northwestern Sudan, northeastern Chad, eastern Libya, and most of Egyptian Deserts (Fig. 2). Also, it can be found underneath the central Sinai Peninsula (SP) and the southern Negev desert (Issar et al., 1972). The NSAS has an average thickness of less than 500 m to more than 3000 m in the northern regions of the Kufra (Libyan Desert) and Dakhla (Egyptian Western Desert) basins (Shata, 1982; Dabous and Osmond, 2001).

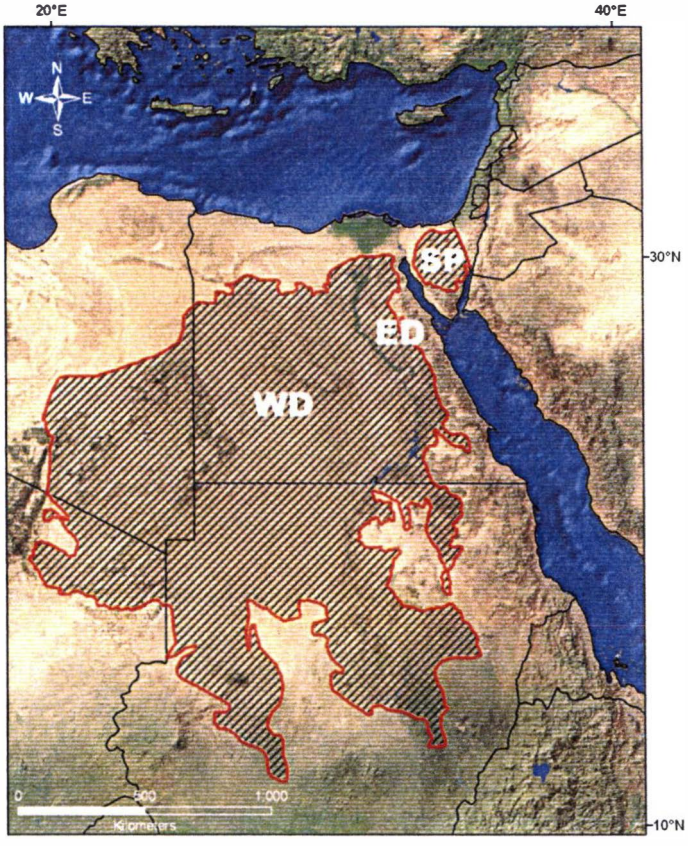

Figure 2: The location and extent of NSAS underneath the Egyptian Deserts. (a) Western Desert (WD); (b) Eastern Desert (ED); and (c) Sinai Peninsula, over MODIS map of Africa (NASA, 2005).

Accordingly, the volume of the stored groundwater in NSAS had been estimated to be ~373,000–780,000 km^3 which is equivalent to approximately 500 years worth of Nile River discharge (Thorweihe, 1990; Thorweihe and Heinl, 2002; CEDARE, 2001; Salem and Pallas, 2002).

1.4 Climatology

The isotopic composition of modern precipitation collected monthly from the International Atomic Energy Agency (IAEA) stations over North Africa is enriched compared to the depleted isotopic composition of fossil groundwaters across North Africa, which indicates that the precipitation occurred in climatic regimes different from those prevailing in the present day. Thus, the modern climate of the African Sahara desert will be briefly discussed followed by discussion of conceptual models describing the prevailing paleoclimatic regimes of the study area.

1.4.1 Modern Climatology

The onset of the current drying phase began after 5,000 yr BP in Africa and by 3,000 yr BP the aridity culminated northward in the African Sahara Desert, continuing to the present day (Street-Perrott et al, 1989). Rainfall is scarce and sporadic and is generally controlled by southward displacement of mid latitude westerly cyclonic disturbances during the winter months, whereas the southern regions (Sahel belt) are governed by the seasonal migration of the ITCZ during summer months (Hoelzmann et al., 2004). The rainfall distribution can be clearly seen from a three-hourly Tropical

Rainfall Measuring Mission (TRMM) image that shows the cumulative total precipitation from 2002 to 2009 (Fig. 3). Meteorologically, the persistent dry belt over the Sahara Desert is produced by sinking air of subtropical highs, contrary to the rising air that dominates the tropical regions where trade winds converge along the ITCZ producing intensive rainfall (Ahrens, 2008). According to Köppen classification system, the Sahara Desert has dry climates (Fig. 4) which are characterized by a deficient of precipitation most of the year and potential evaporation and transpiration exceeding precipitation (Ahrens, 2008).

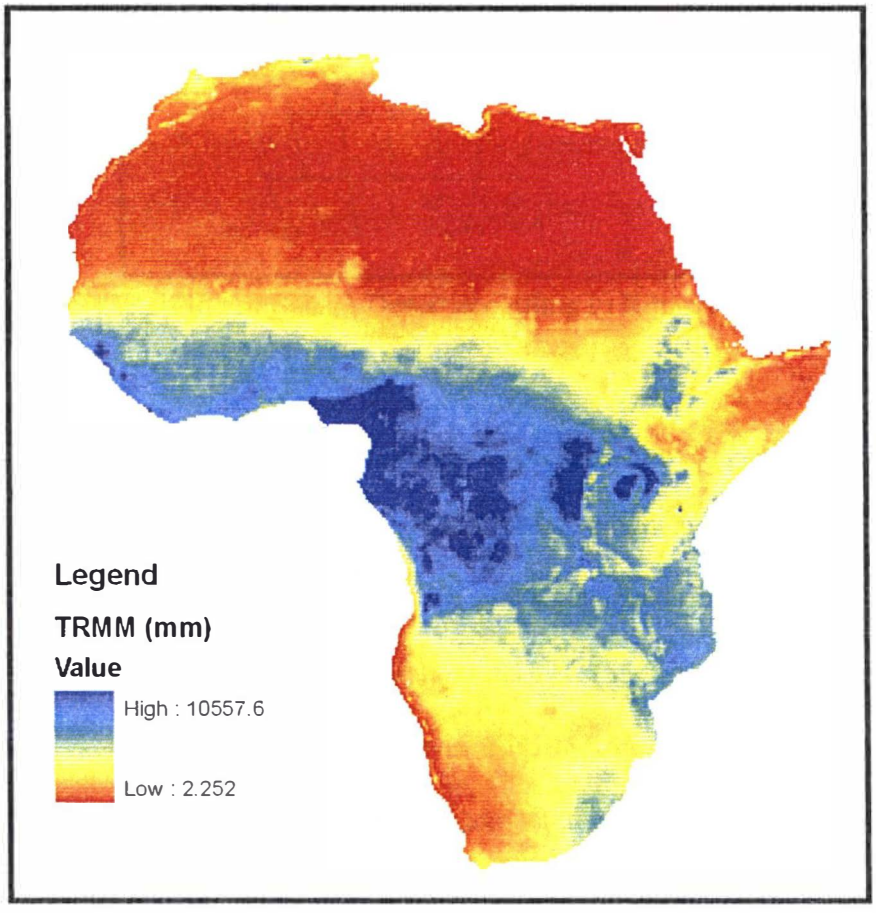

Figure 3: Total precipitation derived from TRMM three-hourly data over Africa (2002-2009).

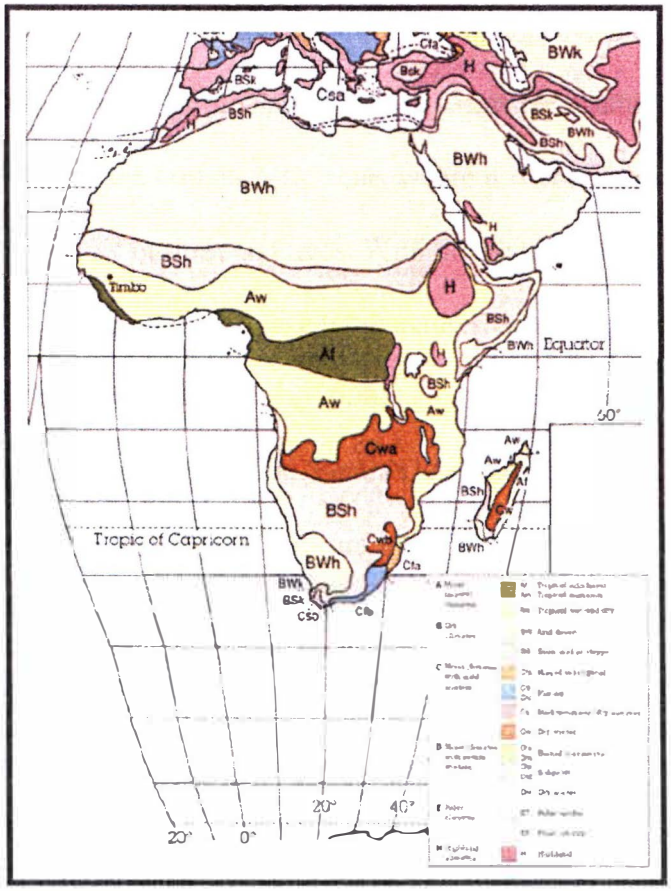

Figure 4: The aridity of Sahara Desert according to Köppen (Ahrens, 2008).

Based on the precipitation and temperature, the Sahara Desert can be divided into two primary climatic groups, the arid subtropical climates (Group BWh) and the semi-arid tropical climate (Group BSh). The arid subtropical climate is characterized by mild winters with an average temperature of 13 °C (55 °F) and scorching summers with a temperature ranging from 40 °C to 45 °C (104 °F to 113 °F). The intense sunlight can produce maximum daytime air temperature readings during the summer which exceed 50 °C (122 °F). The world's highest temperature, 58 °C (136 °F), was recoded at Azizia in western Libya in September 1922. The relative humidity is

usually between 5 and 25%. The semi-arid tropical climate covers the southern Sahel belt and northwestern margin of the Sahara Desert (Atlas Mountains). Rainfall amounts are greater than the arid climatic zone, where it is characterized by short bunch grass, scattered low bushes, and trees. With the higher elevation, the average rainfall amounts increase and the average temperatures decrease and the climate gradually becomes more humid (Ahrens, 2008).

Northerly winds prevail over the Sahara Desert coinciding with the trade wind belt, which changes direction from southward in the northern part of the eastern Sahara to westward in the southern part (El-Baz, 1998). In the eastern Sahara Desert, particularly over the Egyptian territories, N to NW wind directions prevail the country during summer and winter months, whereas NE winds dominate the northern regions during the spring and autumn (EMA, 1996).

1.4.2 Paleoclimatology

The paleoclimate of the Sahara Desert has undergone fluctuations between wet and dry periods for the last few hundred thousand years. During the dry periods, the Sahara desert extended some 200 to 500 km south of its current boundaries (Nicholson and Flohn, 1980); during the wet climatic periods, precipitation intensified (by approximately 50% to 100% of its present value; Issar and Bruins, 1983) and recharged its aquifers (e.g., Geyh, 1994).

The nature of the wet climatic periods during which the aquifers of North Africa were recharged and hence the origin of the groundwater of the fossil aquifers

in these areas are still subject of debate. One group of models claim that glacial periods were cold and dry and that interglacial periods were warm and humid (Bar-Yosef and Meadow, 1995; Sanlaville, 2000; Bar-Mathews et al., 2003; Almogi-Labin et al., 2004). Other models cite numerous field, geochronologic, and isotopic evidences in support of glacial periods being cold and humid and interglacial periods being warm and dry (Sultan et al., 1997; Frumkin et al., 2000; Bartov et al., 2002; Issar, 2003; 2010; Issar and Zohar, 2004; Vaks et al., 2006). For example, glacial periods were humid in the eastern Mediterranean, as evidenced by: (1) the isotopic compositions of speleothems collected from a cave in Jerusalem (Frumkin et al., 2000) and from a cave in the central mountain range in Israel (Vaks et al., 2003); and (2) the areal extent of deposits from Lake Lisan (precursor of the Dead Sea), reached their maximum during the LGM (24,000–14,000 years BP) (Bartov et al., 2002). If one adopts the former group of models, the wet periods would have been the interglacial periods and the aquifers of North Africa would have been recharged during these periods; if the latter models were adopted the recharge would have happened throughout the wet glacial periods.

Glacial models call on the southward migration and intensification of paleo-westerly regimes over North Africa due to a strong baroclonic zone along the ice sheet margin over northern Europe bringing moisture to northern Africa (Sonntag et al., 1978; Bradley, 1999). If these paleowesterly wind regimes were responsible for the recharge of the fossil aquifers in North Africa, one would expect a west to east progressive depletion in the isotopic composition of the aquifers across the continent.

Given the colder temperatures in glacial periods, the isotopic composition of fossil groundwater should be depleted compared to present day precipitation and the extracted recharge temperatures for these aquifers should be low compared to average present day temperatures.

1.5 Previous Studies

Previous studies present the most relevant data addressing the prevailing paleoclimatic regimes over the African Sahara Desert using numerous terrestrial and marine paleoclimate indicators. Additionally, those studies pertaining to the Nubian Sandstone Aquifer's paleoclimate, aquifer geometry, hydrogeology and groundwater age dating will be briefly discussed hereafter.

1.5.1 African Sahara Desert

Sonntag et al. (1978) showed that the west-east decrease of the stable isotopic compositions in the fossil Sahara groundwater indicated a continental effect in groundwater and leads to conclusion that North Africa must have been influenced by western drift due to intensification of westerly winds. This type of wind was responsible for carrying wet Atlantic air masses across the Sahara, causing intensive rainfall that recharged the fossil groundwater aquifers underneath the Sahara Desert.

Nicholson and Flohn (1980) indicated that the climate of the Sahara Desert has been undergoing fluctuations between wet and dry periods for the last few hundred thousand years. During the dry period (20,000–12,000 yrs B.P.), the Sahara Desert extended some 200 to 500 km south of its current boundaries.

Issar and Bruins (1983) speculated that the precipitation was intensified during the wet paleoclimatic periods by approximately 50% to 100% of its present value to recharge the fossil groundwater aquifers.

Rossignol-Strick (1983) hypothesized the intensification of monsoonal winds over the past 250,000 years based on the age record of sapropels. These organic-rich black layers that were intermittently deposited in the deep eastern Mediterranean Sea following high flood periods of the Nile River during heavy African monsoons were found to coincide in their depositional age with the astronomically driven maximum summer insolation in the northern tropics.

Prell and Kutzbach (1987) revealed contemporaneous intensification of African monsoons with increasing summer insolation in the Northern Hemisphere based on the general circulation models.

Mills and Shata (1989) indicated that the climatic conditions prevailing during the Pleistocene times were less arid than today as evidenced by presence of terraces and thick alluvial and lacustrine deposits within the southern Precambrian terrain over Sinai Peninsula, Egypt.

Crombie et al. (1997) investigated the timing of humid pluvial intervals using uranium-series disequilibrium dating of travertines from the Western Desert of Egypt. They interpreted the high precipitation, augmenting the groundwater recharge and the resultant travertine deposition are due to consequences of Milankovitch insolation cycle forcing, through enhanced Atlantic and Indian Ocean monsoons during the interglacial time periods.

Sultan et al. (1997) concluded an Atlantic source of Pleistocene carbonate deposits from previous wet climatic periods based on isotopic composition ($\delta^{18}O$: 17.1‰ to 25.9‰) of fossil (45,000 to >450,000 years old) spring carbonates (tufas) from the Western Desert of Egypt. These carbonates are consistent with deposition from depleted ($\delta^{18}O$: –10.6‰ to –11.9‰) precipitation resulting from paleowesterly wind regimes.

El-Baz (1998; 2000) observed the relation between sand accumulation patterns and origin of groundwater in the Sahara Desert using satellite images of Advanced Very High Resolution Radiometer (AVHRR), LANDSAT–TM and Space borne Imaging Radar (SIR-C). He suggested that the sand originated in the southern part of the Sahara Desert and was carried northward in river courses during past wet climates to be deposited within inland lakes. Furthermore, he recommended that groundwater exploration in the Sahara Desert include areas of depressions with large accumulations of sand.

Edmunds et al. (1999) estimated the recharge temperatures of one of the confined aquifers at the Sahel (Iullemeden Aquifer System) occurred between 23.2–28 ^{14}C kyr and was at least 5–6 °C lower than the present.

Brookes (2003) revealed the Holocene wind direction from geomorphic mapping of the aeolian landforms of Egypt's Western Desert using LANDSAT–MSS images. He reconstructed two wind directions, (1) the dominance of N–S airflow from 30° N to 20° N, which turned clockwise southward to NE–SW and is consistent with the modern wind circulation; (2) the older W airflow between 30° N and 26° N, NW

between 26° N to 20° N. The cross-cutting relation shows that the latter (paleowesterlies) are older than the former wind directions and these wind types steered moist Atlantic air masses to Egypt during the Late Pleistocene/early Holocene.

Smith et al. (2004) indicated that the Atlantic source paleowesterlies can be inferred from low ($\delta^{18}O$) isotopic ratio of the tufa deposits and gastropods compared to modern precipitation in Kharga Oasis, Egypt.

Kieniewicz and Smith (2009) indicated that the Mid-Pleistocene lacustrine deposits that exposed in Dakhla Oasis in Western Desert of Egypt provide evidence for a more humid climate than that which persists nowadays. Additionally, these sedimentary successions indicate that the rainfall was sufficient to allow for groundwater recharge and the presence of perennial surface water.

Issar (2010) concluded that the intensification of westerlies and weakness of monsoons during the last glacial periods in the Quaternary forced the wet masses to migrate from the Atlantic Ocean southward causing the Saharo-Arabian region to become more humid and green. This condition attracted ancient hominids (Homo *erectus* and Homo *sapiens*) to migrate northward as evidenced from the dating of the flint tools that have been found around the dried up lakes and swamps in the Negev Desert.

1.5.2 Nubian Sandstone Aquifer System (NSAS)

Ball (1927) and Sandford (1935a) hypothesized a model that advocates the groundwater recharge of the NSAS is due to intensive rainfall that precipitated over southern mountains in Chad and northwestern Sudan.

Knetsch et al. (1962) investigated the groundwater of the NSAS using geological and geochemical methods. They concluded that intensive rainfall occurred during a pluvial period (25,000 – 35,000) years ago and the water infiltrated over regions where the NSAS was exposed and within the depressions of western desert of Egypt.

Hellström (1940) assumed the NSAS is homogenous and has a constant thickness, hence he estimated the groundwater flow velocity within the aquifer to reach 15 meter/year. This equals to about 100,000 years for groundwater to flow 1200 km from the southern recharge areas to reach the Qattara Depression in the north.

McKee (1962) studied the genesis of the NSAS and similar sandstone aquifers beneath northern Africa and parts of Asia. The Nubian-type sandstone ranges from Cambrian through Cretaceous in age and is composed of alternating beds of sandstones and shales and was deposited largely in a marginal or continental environment.

Said (1962) showed that the upper Nubian Sandstone is overlain by a calcareous sequence of limestones, dolostones, chalks and marls which belong to the Middle Calcareous Division of Cenomanian to Upper Eocene age.

Shata et al. (1962) investigated the origin and ages of the groundwater supplies in some oases in the Western Desert of Egypt. Dating of water using the ^{14}C method indicated that the artesian water from the oases is between 25,000 and 40,000 years old and that the origin is obviously from rainwater precipitated during one or more of the pluvial periods.

Himida (1969; 1970) calculated the absolute age of groundwater in the NSAS in Kharga Oasis as up to 541,000 years using the Helium-Argon method. Additionally he computed the true velocity of groundwater from the southern recharge areas to Kharga Oasis to be 1.6 m/year. He also believed that the NSAS that underlies parts of the four countries, Egypt, Libya, Sudan and Chad is still receiving modern recharge in the highland of Chad and Sudan.

Issar et al. (1972) estimated the age of fossil groundwater stored in the NSAS that underlies the deserts of central Sinai Peninsula and the southern Negev to range between 13,000 and 30,000 years based on ^{14}C dating analysis. Also, they indicated that the fossil water was precipitated in more temperate climates than the present one based on the ($\delta^{18}O$ and $\delta^{2}H$) ratios of the water.

Mills and Shata (1989) suggested the regional groundwater flow in the NSAS underneath SP occurs generally northward and northeastward toward the Arava valley and the Dead Sea in Israel, in addition to another component flowing toward the Gulf of Suez.

Sturchio et al. (2004) measured the deep groundwater from the NSAS in the Western Desert of Egypt to be between ~2 x 10^5 to ~1 x 10^6 yr in age based on

^{81}Kr/Kr and ^{36}Cl/Cl ratios. The results were consistent with lateral flow of groundwater from a recharge area in SW Egypt. Additionally, the low δ^2H values of the ^{81}Kr-dated groundwater reveal a recurrent of Atlantic moisture source during the Pleistocene pluvial periods.

Sefelnasr (2007) developed a three-dimensional transient groundwater flow model for the NSAS based on GIS-database integration. He simulated five extraction scenarios until year 2100. The results reveal that under the present extraction rates, the free flowing wells will gradually disappear, the average depth to groundwater will range from 5 meters in the Bahariya Oasis to 36 meters in Kharga Oasis, and the groundwater volume of 354 km^3 will be extracted from the aquifer storage.

Sultan et al. (2007) identified undetected areas of discharge from Nubian Aquifer using an integrated approach utilizing isotopic data, a two-dimensional groundwater flow model and geochemical analyses along with field and remote sensing data. They showed that the discharge of the Nubian Aquifer is occurring on a larger scale, primarily through deep-seated fault systems. Additionally, the ascending Nubian groundwater in the Asyuti area along the River Nile discharges into relatively thick alluvial aquifers (75% of incoming flow) in addition to a modest contribution from surface runoff (25% on incoming flow).

Sultan et al. (2011) showed that the NSAS is still receiving modern recharge locally at the foothills of the crystalline basement terrains under the current dry climatic conditions.

CHAPTER II

METHODOLOGY

The present study adopted a three-fold approach. In the first stage, the precipitation events that gave rise to precipitation with isotopic signatures similar to those of the fossil groundwater in the North African Aquifers were identified. In the second stage, temporal satellite data (METEOSAT First Generation) was used to identify the directions of the wind regimes that precipitated these waters. To substantiate the findings from the previous two stages, a third stage was applied for groundwater sampling from the Nubian Aquifer that underlies Sinai Peninsula (SP) to extract the recharge temperatures using dissolved noble gas concentrations. The three-fold approach was executed by applying a combination of office, field and laboratory methods to achieve the objectives of the present work. In the following, a brief description of these methods and techniques is given.

2.1 Office Work

2.1.1 Rayleigh Distillation Model

The Rayleigh Distillation Model was applied in this study to investigate the progressive isotopic depletion under the direct influence of westerly winds in a west-east traverse. A simple box model was constructed over North Africa to encompass most of the area between Atlantic Ocean and Red Sea. Then, the model was divided into eight irregular boxes in which each box encompasses a certain

number of groundwater wells and the box numbers are progressively increasing eastward. In each box, it was assumed that the condensation of water was in thermodynamic equilibrium with water vapor and the subsequent removal from a cloud can be described by the Rayleigh distillation equation (Broecker and Oversby, 1971):

$$R = R_0 f^{(\alpha-1)}$$

Where R is the isotopic ratio ($^{18}O/^{16}O$) of the vapor; R_0 is the initial isotopic ratio of the vapor flux; f is the fraction of the vapor remaining in the vapor phase; and α is the isotopic fractionation factor between vapor and liquid.

Assuming that the recharge temperatures during the previous wet climatic periods over North Africa were approximately 2 to 7 °C cooler than the current mean annual air temperatures (Guendouz et al., 1997; Edmunds et al., 1999; Abouelmagd et al., 2011). As the fractionation factor α is a temperature dependent, so it was calculated for each box by applying the following equation (Majoube, 1971):

$$\ln \alpha(\delta^{18}O) = (\frac{1.137}{T^2})10^3 - (\frac{0.4156}{T}) - (2.0667)10^{-3}$$

Where (T) is the absolute temperature in degrees Kelvin.

By knowing the isotopic composition of the condensate ($\delta^{18}O_L$) in each box (fossil groundwater), the isotopic composition of the vapor ($\delta^{18}O_v$) was calculated using the following equation (Faure, 1977):

$$\delta^{18}O_L = \alpha\left(\delta^{18}O_V + 1000\ \right) - 1000$$

By using the calculated isotopic composition of the remaining vapor parcel and by assuming the initial composition of the glacial ocean was perhaps enriched by 1-1.5 ‰ in oxygen and correspondingly in hydrogen at maximum glacial conditions due to lowering of the sea level during glacial times (Fairbanks, 1989). Fractions of the remaining vapor flux (f) were calculated for each box using the following equation (Faure, 1977):

$$\delta^{18}O_V = \left[\left(\delta^{18}O\right)_o + 1000\right] f^{(\alpha-1)} - 1000$$

Where ($\delta^{18}O_v$) is the isotopic composition of the vapor; $(\delta^{18}O)_o$ is the initial isotopic ratio at the source; f is the fraction of the vapor remaining in the vapor phase; and α is the isotopic fractionation factor between vapor and liquid.

2.1.2 Stable Isotope Data Collection

The isotopic composition of the modern meteoric precipitation over the investigated area was extracted from the monthly records of the IAEA weather stations for comparisons with those of fossil water composition. The stable isotope data (δ^2H and $\delta^{18}O$) were acquired from the Water Isotope System for Data Analysis, Visualization and Electronic Retrieval database <http://nds121.iaea.org/wiser/> (WISER/IAEA, 2010). The recorded isotopic values represent composite average

monthly values encompassing contributions from one or more rainfall events that occurred throughout the month.

2.1.3 Remote Sensing and GIS

High Resolution Image (HRI) Data of the Meteosat First Generation (MFG) (acquired from EUMETSAT®) were used to identify the wind regimes that precipitated the selected rainfall events for the following reasons: (1) availability of a long (>30 years) and uninterrupted (1977 to present) stream of data produced by the Meteosat system (Meteosat 1 through 7 satellites), with adequate spatial (5 km), spectral (visible: 0.5–0.9 μm; thermal infrared [TIR]: 10.5–12.5 μm), and temporal resolution (30 minutes) that allows for effective and continuous monitoring of cloud propagation directions; (2) allows for validation of inferred cloud propagation directions using the Expanded Low-resolution Cloud Motion Winds product (MTPLRWI1), which shows wind vectors (barbs) at various heights; and (3) had data that could be readily downloaded from the Data Center Online Ordering Application (http://archive.eumetsat.int) at no cost to users. A total of 9248 images (~56 Gb) were acquired and analyzed to extract cloud propagation and wind direction information for a suite of selected months (Table 1). Two programs were utilized to read and to decode the binary format (OpenMTP) image files and wind vector (BUFR) files. Animation loops were generated using David Taylor's GeoSatSignal software V7.1.2.949 (http://www.satsignal.eu/software/geosatsignal.htm) to examine the cloud propagation directions across North Africa, using large numbers of scenes (up to 600)

acquired throughout each of the selected months. The CMW products were decoded and read using David Taylor's BUFR viewer software V.1.1.4.48 (http://www.satsignal.eu/software/bufr-viewer.html).

Initial findings pertaining to cloud propagation directions extracted from the animations loops for the selected events were further examined, validated, and refined through spatial correlations of relevant data sets in a GIS environment. For each of the selected events, the following temporal products were imported and analyzed: (1) 8-hourly TIR raster images showing cloud distribution, (2) 8-hourly shape files that display polygons representing digitized cloud boundaries extracted from individual infrared scenes, (3) 8-hourly CMW raster images showing wind direction vectors, (4) daily precipitation amounts, and (5) monthly isotopic compositions for precipitation.

Table 1: Number and size of the downloaded METEOSAT scenes of the investigated seven precipitation events.

Event	Number of Scenes	Size (Gb)
March 1982	652	3.93
December 1987	1486	8.96
December 1991	1482	8.94
October 2001	1445	8.72
February 2002	1339	8.08
March 2002	1385	8.35
April 2002	1459	8.80
Total	9248	55.78

The imported temporal data covered the time period during which the clouds were observed to travel across the entire African continent and surroundings. All images were set to a common projection (Geographic Projection – Datum: WGS84) and scale (1:50,000,000). The images were georeferenced to the global MODIS file of Africa (NASA, 2005) as a base scene using ESRI's ArcGIS 9.3 commercial software.

2.1.4 Back Trajectory Model

For each of the selected precipitation events, moisture source regions were identified using Back Trajectory Models (BTM) for simulation of the modern atmospheric circulations of the studied rainfall events. Generally, BTM uses interpolated measured meteorological data archives to estimates the most likely central parcel of air path over geographic areas at a specific time. Simply, the BTM shows the backward track of a parcel of air at different altitudes in hourly increment through a user predefined time range. The type of BTM used here is the Hybrid Single-Particle Lagrangian Integrated Trajectory (HYSPLIT) model developed by the National Oceanic and Atmospheric Administration's (NOAA) Air Resources Laboratory (ARL) (http://www.arl.noaa.gov/ready/hysplit4.html). For each precipitation event, moisture source regions were identified using BTM. The trajectories have been started at specific station, for instance "Cairo" and calculated 72 hours backward in time. Initial findings pertaining to cloud propagation directions extracted from the animations loops for the selected events and source regions

extracted from BTM analyses were further examined, validated, and refined through spatial correlations of the relevant data sets.

2.2 Field and Laboratory Work

A field trip was performed in June 2010 to target the deep groundwater wells that tap the Nubian Aquifer beneath the Sinai Peninsula (SP). Groundwater samples from eight locations were collected from deep productive wells evenly distributed over the central-south part of SP. Four samples were collected at each well for: 1) cations, anions and total alkalinity analyses; 2) stable isotope ratio analyses for hydrogen and oxygen; 3) radiocarbon for age dating analysis; and 4) dissolved noble gas concentrations to extract the recharge temperatures. The sampling and laboratory methods for each analysis type are briefly discussed hereafter.

2.2.1 Chemical Analysis

Water samples for chemical analysis of cations, anions and total alkalinity were filtered through 0.45 μm polypropylene syringe filters, and collected in tightly capped 125-mL high-density polyethylene bottles. Cations were analyzed by inductively coupled plasma-atomic emission spectrometry. Anions were analyzed by ion chromatography. The total alkalinity was determined using a UV/VIS spectrophotometric method with bromophenol blue (Sarazin et al., 1999). The total chemical analyses were performed at the Geochemistry Laboratory, Department of Geosciences, Western Michigan University.

2.2.2 Stable Isotope Analysis

Eight unfiltered and unacidified water samples for (δ^2H and $\delta^{18}O$) isotopic analysis were collected in tightly capped 30-mL glass bottles. Traditionally, the hydrogen isotope ratios were measured using the uranium reduction method (Friedman, 1953) and the oxygen isotope ratios were measured via the carbon dioxide equilibration technique (Epstein and Mayeda, 1953). However the H and O isotopic ratios in the collected groundwater samples were analyzed using a Picarro Cavity ring- down spectroscopy (CRDS) laser system. Oxygen and carbon isotopes are reported in terms of the conventional delta (δ) notation, in units of per mil (‰) deviation relative to the Standard Mean Ocean Water (V-SMOW) standards (Coplen, 1996). Hydrogen and oxygen isotope data are reported in terms of the conventional delta (δ) notation, in units of per mil deviation relative to a standard reference, whereby:

$$\delta,‰ = [(R_{sample} - R_{std})/R_{std}] \times 1000$$

Where, $R = {}^2H/{}^1H$ or ${}^{18}O/{}^{16}O$ and the standard is Vienna Standard Mean Ocean Water (Coplen, 1996).Reproducibility of δ values for ^2H is ± 1‰ and that of ^{18}O is ± 0.2‰. The samples were analyzed at ISOTECH Laboratories, Champaign, Illinois.

2.2.3 Radiocarbon Age Dating Analysis

The radiocarbon isotope (^{14}C) is produced in the atmosphere by interactions of cosmic radiation with atmospheric nitrogen via neutron bombardment (Faure, 1977). Then, the atmospheric ^{14}C is dissolved in the infiltrated rain water to reach the water table, after which the ^{14}C in groundwater starts decaying back to nitrogen (Kazemi et al., 2006). The half-life of radiocarbon, ^{14}C that is equal to 5730 years makes it a potential tool for archeological and old groundwater dating (Clark and Fritz, 1997). Groundwater ages up to 40,000 years or longer can be detected using the ^{14}C method (Kazemi et al., 2006). The ^{14}C measurements can be done using the traditional technique of radioactive decay counting and the recent AMS technique. The former method of measuring is time consuming and requires a large volume of water sample to produce a substantial amount of carbon, while the latter method is allowing rapid sampling and much smaller sample size (Kazemi et al., 2006). Therefore, unfiltered water samples were collected in tightly capped 250-mL glass bottles for ^{14}C analysis using AMS technique. During the sampling, care was taken to avoid direct contact with the atmosphere. The dissolved inorganic carbon (DIC) was extracted in vacuum by acidifying the water sample. The extracted CO_2 was cryogenically purified from the other reaction products and catalytically converted to graphite using the method of (Vogel et al. 1984). Graphite $^{14}C/^{13}C$ ratios were measured using the CAIS 0.5 MeV accelerator mass spectrometer. The sample ratios were compared to the ratio measured from the Oxalic Acid (NBS SRM 4990). The measured ^{14}C activities were reported as a percent of modern carbon (pmC). The resulted uncalibrated dates have

been given in radiocarbon years before 1950 (years BP), using the ^{14}C half-life of 5730 years and the dates have been corrected for isotopic fractionation. The analytical precision of the AMS ^{14}C results is ± 0.04%. The radiocarbon analysis was performed at the Center for Applied Isotope Studies (CAIS), University of Georgia.

2.2.4 Noble Gas Analysis

The noble gas solubility equilibrium has been successfully used in groundwater studies to reconstruct the soil temperature that prevailed during the groundwater recharge (Mazor, 1972). Thus, the extracted noble gas concentrations can be translated into climatic conditions during the air-water exchange with the atmosphere (Kipfer et al., 2002). In order to analyze the noble gas concentrations in the Nubian groundwater, duplicate samples from seven wells were collected through a transparent plastic hose into copper tube samples of ~22 cm^3 (~1 cm in diameter and 53 cm long) according to the procedure described in (Weiss, 1968; Stute et al., 1995). The wells were pumped sufficiently at least 15 minutes prior to the sampling process to flush the boreholes and get a best representation of aquifer water. A predesigned PVC tube attached to the borehole outlet with a flexible coupling (Fig. 5a) was used to avoid exchange with atmospheric air and/or partial degassing. In certain situation, the PVC tube had to be modified to adapt to the shape of the borehole outlet (Fig. 5b). The well water runs through the inline copper tubes tube for several minutes before it is sealed off using stainless steel clamps or special pliers.

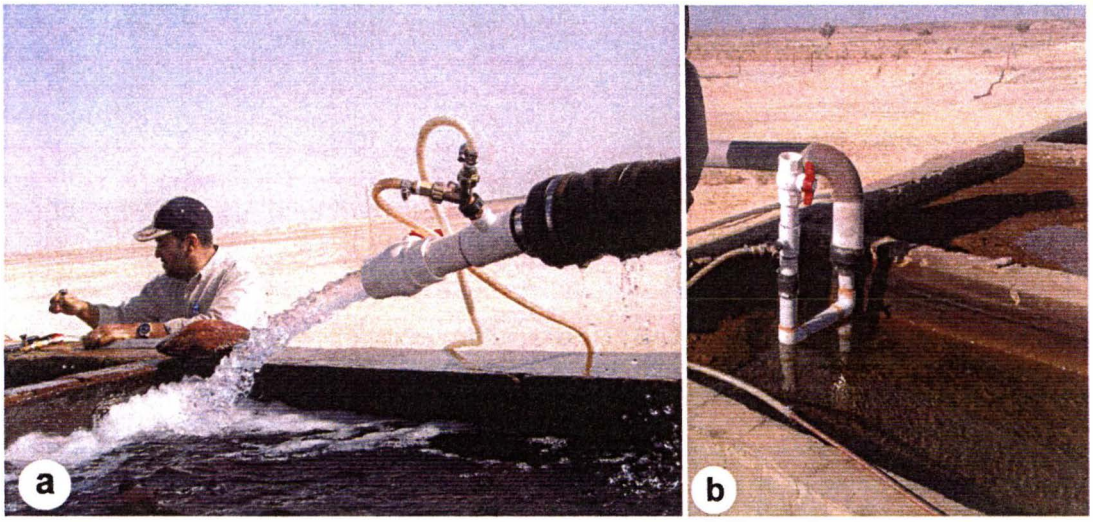

Figure 5: (a) Groundwater sampling procedure for noble gas analysis using assembled leak-tight well adaptor (white PVC tube) attached to the well outlet by flexible coupling. (b) U-shape well adaptor design to adapt different well outlets for proper air-free bubbles sample collection.

A regulator valve at one end of the copper tube was used to increase the pressure in order to minimize air bubble formation. The sampling procedure using the copper tubes developed by the Dissolved and Noble Gas Laboratory, University of Utah consists of 24 steps that were strictly followed for accurate sampling technique and described in detail hereunder (Fig. 6):

1- The well outlet was checked to fit the pre-designed well adaptor. If it doesn't fit, different size of flexible coupling can be used.

2- All the connections were checked to prevent water leakage and formation of air bubbles into the sampling string.

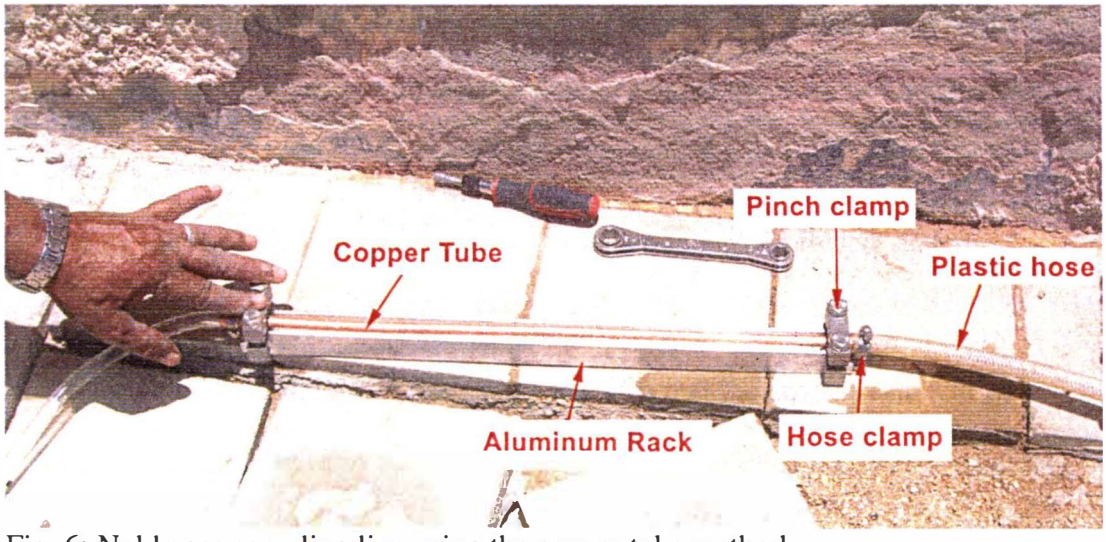

Fig. 6: Noble gas sampling line using the copper tube method.

3- The two way valve was connected to the outlet opening in the white PVC well adaptor. One way should be connected to a copper tube and the other end is a spill way to regulate the pressure

4- The copper tube was placed in the aluminum rack.

5- The two metal pinch clamps were placed at the two ends of the rack holding the copper tube in between.

6- The copper tube was inserted into the plastic hose about 2 cm and secured using hose clamps.

7- The copper tube should be centered in both directions within the clamp holder.

8- Tighten the upper portion of the pinch clamps using fingers only (a wrench should not be used at all in this stage).

9- The down gradient tube was connected with a pressure gauge at the end.

10 – The pump was started and the water flowed through the system. Purging the water smoothly and effectively prevent bubble formation.

11- Several liters of water need to be purged to flush the sampling line.

12- Taping the entire length of the tube with ratcheting wrench to help dislodge bubbles.

13- The orientation of the tube was maintained such that the downstream end was always elevated relative to the upstream end during the remainder of the sampling procedure until the clamps were closed.

14- Watching for bubbles in the downstream transparent tube.

15- A back pressure inside the copper tube was created using the downstream gauge (20 PSI should be enough).

16- The downstream pinch clamp was closed by turning one of the two bolts only one turn and then switched to do the same with the second bolt and by repeating this process will prevent shearing scissor like motion.

17- While keeping the pump operating, the upstream clamp was closed in a similar manner as the downstream one (step 16).

18- The clamps were tightening completely with no gap exist near the bolts.

19- Once both clamps were closed, the pump can be turned off.

20- The plastic hoses were removed from both ends of the copper tube and making sure that the ends of the copper tube were filled with water.

21- The black plastic caps were filled with well water and were placed on both ends of the copper tube.

22- The clamped copper tube was then removed from the aluminum holder.

23- The copper tube was carefully labeled and the labels were covered with clear tape.

24- The samples in the copper tubes do not require refrigeration.

Generally, the determination of the noble gas concentrations in the collected groundwater is divided into three analytical steps (Kipfer et al., 2002):

1. Noble gas extraction from the water.
2. Purification and separation of the extracted noble gases.
3. Quantitative analysis using a mass spectrometer.

The dissolved gases were extracted from the copper tubes on a vacuum line. Under high-vacuum, closed system, the water is transferred from the copper tube into a large stainless steel flask. The flask is heated while a smaller flask is chilled. This creates a flux of gas from the large flask, into the small flask. The small flask is then sealed before being transferred to the mass spectrometry line. The individual noble gases were separated and analyzed using a quadrupole mass spectrometer and presented as concentrations (cm^3 STP g^{-1}). The reproducibility of the measurements was ± 2% for Ne, ± 3% for Ar and ± 5% for both Kr and Xe. The noble gas measurements were performed at the Dissolved and Noble Gas Laboratory, University of Utah, Salt Lake City, Utah.

CHAPTER III

GEOLOGY AND HYDROGEOLOGY

The Nubian Sandstone Aquifer System (NSAS) is part of a group of major regional aquifers that cover about 15 million km^2 in the Sahara Desert and Arabian Peninsula. This chapter is devoted to give a brief discussion of the geologic and hydrogeologic settings of the NSAS that is located in the eastern Sahara Desert beneath the surface of the hyper-arid Western Desert of Egypt, southeastern Libya, northeastern Chad and northwestern Sudan, with emphasis on the origin and history of the fossil groundwater.

3.1 Geologic and Structural Settings

Substantial geologic and structural studies have been done on the regional geology of the NSAS at different localities, among them Sandford (1935b), Shata (1953), Knetsch and Yallouze (1955), Hermina et al. (1961), Said (1962), Barakat and Milad (1966), Issawi (1971), Hermina and Issawi (1971), El Ramly (1972), Barthel and Hermann-Degen (1981), Wycisk (1993), Klitzsch (1984 & 1994).

The geological setting of the NSAS was created between the Late Proterozoic and the Tertiary. Tectonically, a series of uplifts such as (Uweinat-Aswan and Uweinat-Howar), subdivided the NSAS into separate basins as a result of different stresses exerted on the North African plate. Accordingly, thick continental clastic deposits of Paleozoic and Mesozoic age were deposited in the Kufra and Dakhla

synclinal basins (Fig. 7), while marine carbonates and Post-Eocene continental deposits were deposited in the northern basins (Thorweihe and Heinl, 2002; Bakhbakhi, 2006).

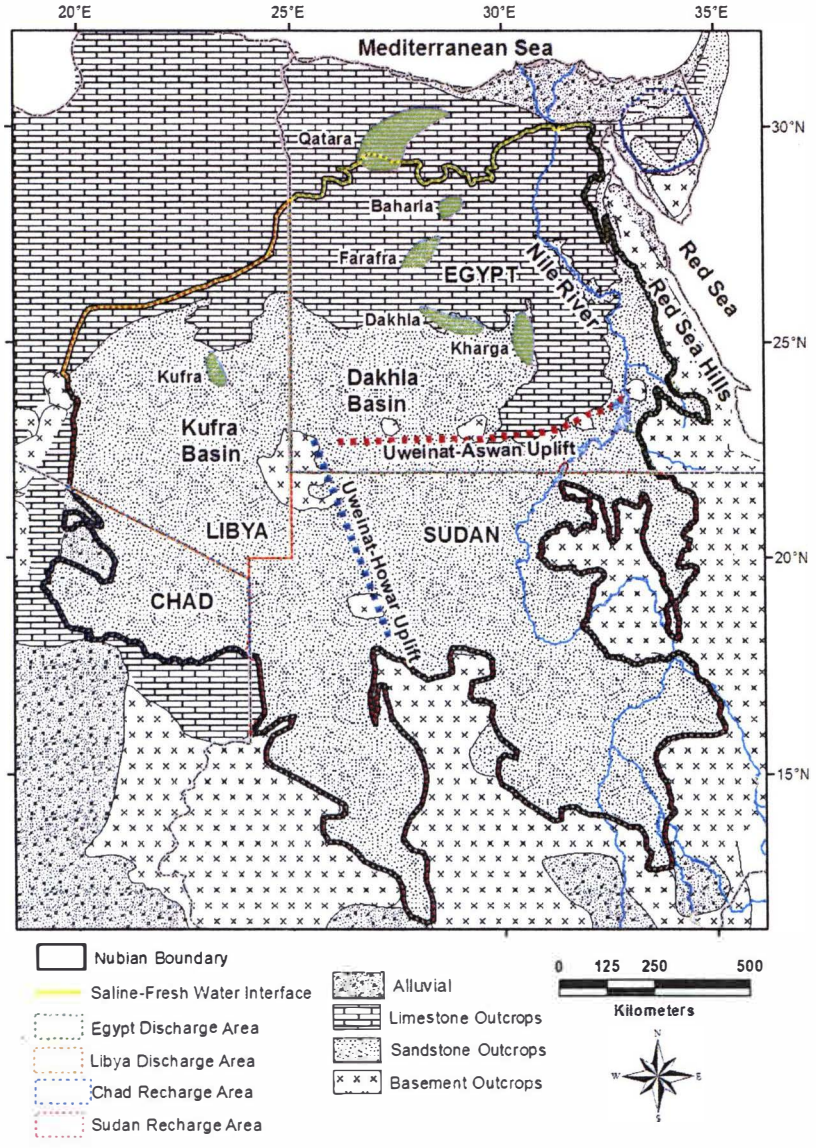

Figure 7: Regional geology of the NSAS and its outcrops (After Thorweihe, 1982; Sultan et al., 2012).

The geology of the NSAS can be outlined and categorized into four main groups of rock units (Fig. 7):

(1) The crystalline basement rocks.

(2) The Pre-Cenomanian Sandstones.

(3) The Tertiary-Upper Cretaceous carbonates.

(4) The Quaternary alluvial deposits.

3.1.1 Crystalline Basement Rocks

The Precambrian crystalline basement rocks are exposed along the Red Sea coast over the eastern Desert of Egypt, locally at Gebel Oweinat in the Western Desert of Egypt, as well as at the Ennedi and Tibesti Mountains in northeastern Chad and southern Libya. In these areas they form a closed basin and are composed of coarse grained granitoids, gneisses, schists, basalts and metasediments (Klitzsch, 1994). The Precambrian rocks are dissected by basic dykes trending NE-SW (Mokhtar, 1988). Hydrologically, they are receiving substantial mounts of rainfall compared to the interior of the basin due their higher elevations, rising to more than 3,000 meters AMSL. The basement relief had been estimated to vary from sea level in the southern regions to more than 5,000 meter BMSL in the northern regions (Bakhbakhi, 2006).

3.1.2 Pre-Cenomanian Sandstones

Geomorphologically, the NSAS is located in a huge depression structure filled with sediments ranging from Paleozoic to Lower Mesozoic in age and outcropping throughout the basin (Himida, 1970). The older sediments are generally overlain by the younger ones toward the depression center and unconformably rest on the basement rocks (Shata, 1982). The sediments are composed of unfossiliferous formations of alternating beds of continental sandstones, clays and shales of shallow marine and deltaic origin of Pre-Upper Creataceous age, unconformably overlying the crystalline Proterozoic basement complex which has a regional gentle northward dip (Hesse et al., 1987). The sandstone formations vary from continental sandy facies in the south to marine facies in the north (above latitude 25°N). The marine beds are dominated by limestone, dolomite and shale (Shata, 1982).

The sandstone formations vary in thickness from a few tens of meters in the northern areas of Sudan to ~250 meters in the southern regions of the Kharga Oasis and ~900 meters at its northern localities. A thickness of ~1800 meters is recorded in the Bahariya Oasis and ~3500 meters in the northern localities of the Dakhla Basin (Shata, 1982). The maximum thickness is found to be ~4500 meters in the northwestern of the Kufra basin (Hermina, 1990).

3.1.3 Tertiary-Upper Cretaceous Carbonates

The Nubian Sandstone formations are covered by carbonates and shales of Upper Cretaceous age north of latitude 25°N and north of the El-Kharga and El-

Dakhla Oases. Their thicknesses vary from 126 meter in El-Dakhla Oasis to 265 meter in the El-Kharga Oasis. Tertiary formations conformably overlie the Upper Cretaceous formations, where the carbonate deposits of Eocene age cover the plateau area surrounding the depressions areas within the Western Desert of Egypt (Wycisk, 1993).

3.1.4 Quaternary Alluvial Deposits

The Pleistocene and Quaternary deposits represent the topmost layers in the stratigraphic column and are represented by alluvium, lacustrine, and eolian sediments (sand dunes). The lacustrine deposits can be found at El-Kharga Oasis and the sand accumulations are usually located within topographic depressions at several locations, particularly the Great Sand Sea in Western Desert of Egypt.

3.2 Hydrogeologic Setting

The immense groundwater storage within the NSAS is considered one of the most important fresh groundwater reservoirs in the world for drinking and irrigation purposes. Therefore, It has been subjected to several intensive hydrogeological studies, for example the works of Ball (1927), Ambroggi (1966), Ezzat (1974), Burdon (1982), Shata (1982), Thorweihe and Heinl (2002) and CEDARE (2002). The aquifer system rocks have been deposited in large scale continental geosynclinal sub-basins separated by uplifted structural barriers which permit a hydraulic interconnection between those sub-basins (Shata, 1991). However, the NSAS has two

major basins: (1) the Kufra Basin of Libya, northeastern Chad, and northwestern Sudan and (2) the Dakhla Basin of Egypt (Fig. 7). The estimated stored fresh groundwater volume in the NSAS aquifer is approximately ~373,000–780,000 km^3 which is equivalent to approximately 500 years worth of Nile River discharge (Thorweihe, 1990; Thorweihe and Heinl, 2002; CEDARE, 2001; Salem and Pallas, 2002). Additionally, the NSAS occurs under two distinct hydrogeologic conditions, unconfined condition where the sandstones are exposed in northeast Chad, southeast Libya, northern Sudan and southwestern Egypt and confined condition to the north above latitude 25°N under thick marine carbonates and shales of Upper Cretaceous age (Thorweihe, 1982). The Upper Cretaceous carbonates form an upper impervious confining layer over the Nubian Sandstone sequence (Bakhbakhi, 2006). The NSAS can be classified into two aquifer sub-systems (Fig. 8):

(1) The older and most extensive unconfined Nubian Aquifer

(2) The younger and limited Confined Nubian Aquifer

The two aquifer subsystems are separated by lenticular and discontinuous low permeability layers (aquitards) belonging to the Upper Cretaceous and to the Lower Tertiary (Thorweihe and Heinl, 2002).

3.2.1 Unconfined Nubian Aquifer

The unconfined aquifer is composed of Paleozoic-Mesozoic continental clastic sediments mainly sandstones, which underlie most of the Egyptian Deserts, Eastern Libya, northern Chad and northern Sudan. It overlies the Precambrian

crystalline rocks (Fig. 8) and its thickness ranges from less than 500 meters in the south to about 5,000 meters northward. Despite, there was a change in the prevailing climatic condition over the NSAS from humid into arid regimes that could affect the recharge rate to the aquifer; the hydraulic properties remain unchanged over time (Issar et al., 1972).

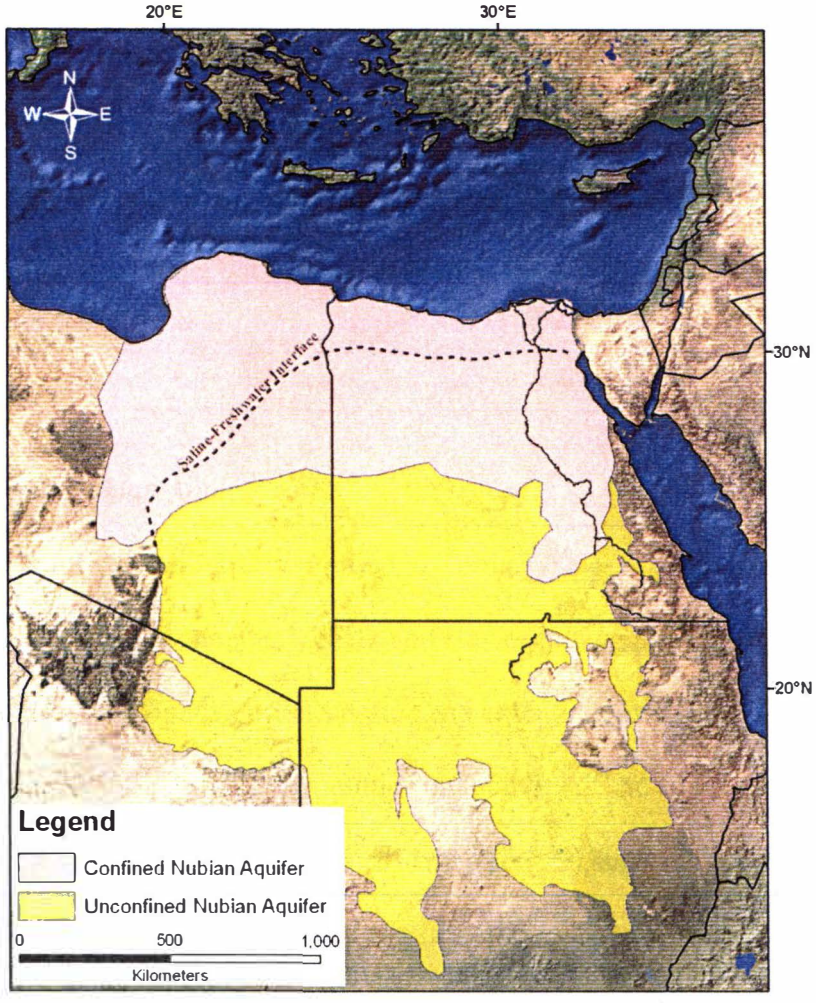

Figure 8: Regional hydrogeology map of the NSAS (After CEDARE, 2002; Salem and Pallas, 2002; Bakhbakhi, 2006; Sefelnasr, 2007).

The hydraulic conductivity of the lower part of the aquifer ranges from 10^{-5} to 10^{-6} m/s, while it varies in the upper part from 4 x 10^{-6} to >10^{-3} m/s. The storativity has been estimated to vary from 7 x 10^{-5} in the El-Kharga Oasis to 2.7 x 10^{-2} in the El Kufra over southeastern Libya. Accordingly, the aquifer transmissivity is generally medium to low, varying from 1,000 to 4,000 m^2/day (Thorweihe and Heinl, 2002). The groundwater quality is generally good to excellent in the southern unconfined aquifer (500>TDS<1000 ppm), while it is poor (hyper saline) in the northern confined aquifer (Bakhbakhi, 2006). The northward groundwater flow is limited by a saline-freshwater interface which occurs north of latitude 29°N (Fig. 8). Its location is considered spatially stable, but is vulnerable to north-south shifting (Thorweihe and Heinl, 2000).

3.2.2 Confined Nubian Aquifer

The confined aquifer is composed of Tertiary-Upper Cretaceous marine sediments mainly limestone, marl, chalk and clay occurring above latitude 25°N overlying the Nubian Sandstone succession and extending over the WD of Egypt and northeastern Libya (Fig. 8). The hydraulic conductivity of the aquifer ranges from 3.6 x 10^{-5} to 3.1 x 10^{-4} m/s. The potentiometric map (Fig. 9) shows that the regional groundwater flow in the Kufra basin flows from the south to northwest and in the Dakhla basin from the south to NNE with average gradient about 0.5 m km^{-1} (Thorweihe and Heinl, 2002).

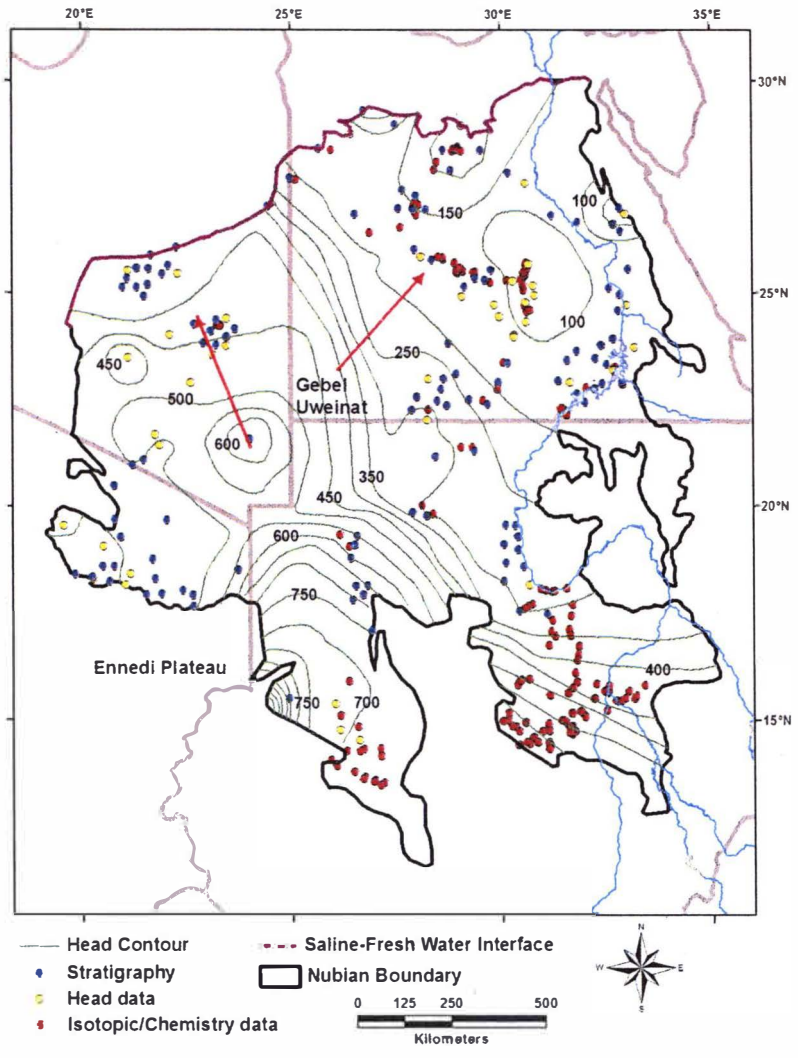

Figure 9: Potentiometric surface map of the NSAS (After Sultan et al., 2012).

The water in the NSAS discharges naturally in the oases, such as Farafra Oasis but the extensive and unmanaged extraction that commenced in the 1960s has decreased the water levels in those areas (Sultan et al., 2012).

3.2.3 Groundwater Origin

There are two conceptual models that have been proposed to describe the origin and genesis of the Nubian groundwater. The first model is the oldest and it attributes the origin of groundwater to the recharge from the precipitation that falls on the southern highlands in Chad and northern Sudan. The hypothesis is supported by the northward regional gradient in groundwater surface and the general groundwater flow from southwest to northeast of the aquifer (Ball, 1927; Sandford, 1935a). Moreover, this hypothesis supports the "renewable" nature of the groundwater as it assumes the aquifer is still receiving modern recharge estimated at ~1.6 km^3/year (Sefelnasr, 2007).

On the other hand, the second hypothesis is supported by stable isotopic and geochronologic data from the Nubian groundwater that suggests an age range from thousands to hundred thousands of years (Sturchio et al., 2004; Patterson et al., 2005). It attributes the formation of the groundwater to in situ recharge (autochthonous) in the Nubian basin during past wet pluvial periods of the Pleistocene and Holocene (Thorweihe, 1982; Sonntag, 1986; Sultan et al., 1997). According to this hypothesis, the groundwater is non-renewable and modern recharge is minimal.

The second model assumes that the NSAS was recharged only in previous wet climatic periods, which is inconsistent with meteorological data and inferences from stable isotopic data and radiocarbon age dating that indicates the Nubian aquifer is being recharged locally by modern water in some locations (Sultan et al., 2012). Using Sinai Peninsula as a test site, Sultan et al. (2011) showed that the NSAS is still

receiving modern recharge locally at the foothills of the crystalline basement terrains under the current dry climatic conditions. Furthermore, the average annual modern recharge to the NSAS was estimated to be ~13 million m^3/yr using the SWAT (Soil Water Assessment Tool) model.

CHAPTER IV

STABLE ISOTOPE DATA ANALYSIS

This chapter involves study of stable oxygen and hydrogen isotopes in both fossil groundwaters and modern precipitation that falls over North African countries. Isotopic values of the fossil waters were collected from the available database of deep wells tapping the main fossil aquifers that underlie Sahara Desert, while the modern precipitation were collected from the monthly records of the IAEA weather stations over North Africa. The comparison between both types of waters shows different wind-regime propagation and accordingly a different source of precipitation. Though, to infer the dominant wind regimes that prevailed hundred thousand of years ago and that of present day, a stable isotopic data analysis of both types of waters will be discussed in detail through the following sections.

4.1 Isotopic Composition of Fossil Groundwater

The stable oxygen and hydrogen isotopic composition of fossil groundwater (>30k yrs B.P.) determined from 65 deep wells tapping the main fossil aquifers beneath the North Africa Sahara Desert is progressively depleted from west to east (e.g., mean $\delta^{18}O$: Morocco: –6.40‰; Algeria: –8.01‰; Tunisia: –8.38‰; Libya: –8.56‰; and Egypt: –10.83‰) compared to the modern precipitation collected from IAEA stations over North Africa (e.g., mean $\delta^{18}O$: Morocco: –5.46‰ ± 1.22‰; Algeria: –3.9‰ ± 1.19‰; Tunisia: –4.67‰ ± 0.54‰; Libya: –3.8‰ ± 0.44‰; and

Egypt: –3.96‰ ± 0.54‰) suggesting that the precipitation during the previous wet climatic periods resulted from wind regimes different from those prevailing today. The west-east depletion of the stable isotopic compositions in the fossil Sahara groundwater can be attributed to the "continental effect" in groundwater and leads to the conclusion that North Africa must have been influenced by intensification of paleowesterly winds. These types of winds were responsible for carrying wet Atlantic air masses across the Sahara causing intensive rainfall that recharged the fossil groundwater aquifers that underlie the Sahara Desert (Münich and Vogel, 1962; Sonntag et al. 1978; Sultan et al., 1997; Smith et al., 2004; Abouelmagd et al., 2012).

The Rayleigh Distillation Model has been successfully adopted in previous studies such as the seasonal and spatial variations of stable isotope ratios in the contemporaneous European precipitation (Rozanski et al., 1982) and investigation of the isotopic composition trend under the direct influence of the Indian monsoons (Krishnamurthy and Bhattacharya, 1991). Similarly, it can be applied in this study to investigate the progressive isotopic depletion under the direct influence of westerly winds in a west-east traverse. In order to investigate the paleo-precipitation events over North Africa that were powered by paleo-wind regimes and determine their source origins, the stable isotopic composition of the fossil ground water ($\delta^{18}O$ & $\delta^{2}H$) can be used. Based on this premise, a simple box model was adopted to model the paleo-precipitation events that prevailed during previous wet climatic periods.

4.1.1 Data Collection

Data of stable isotopic composition of fossil ground water ($\delta^{18}O$ & $\delta^{2}H$) with ^{14}C ages over five northern African countries were collected from; (1) 10 deep wells tapping the Tadla basin, Morocco (Bouchaou, 2009); (2) 35 wells tapping the Northwestern Sahara (Continental Intercalaire) transboundary aquifer underneath Algeria, Tunisia and western Libya (Gonfiantini, 1974; Srdoč et al., 1982); (3) 11 wells tapping the Sirte basin over northeastern Libya (Edmunds and Wright, 1979); and (4) nine wells tapping the Nubian Sandstone Aquifer System beneath the WD of Egypt and SE Libya (Thorweihe, 1982; Sultan et al., 1997). The ^{14}C ages of the collected groundwater ranges from 11,701 yr BP to 51,550 yr BP. A description covering the extent and geology of the studied fossil aquifers/basins will be briefly discussed below.

4.1.1.1 Tadla Basin

The Tadla basin is one of the most important groundwater aquifers in Morocco, forming a multilayer aquifer system (Bouchaou, 2009). It is located in central Morocco with an area of 10,000 km^2 and the major source of recharge to the aquifer is the High Atlas Mountains in the southeast. The basin receives annual precipitation varying from 400 mm/year in the northern regions to 600 mm/year in the southern regions. The basin has an unconfined aquifer in the north and a multilayer confined aquifer of Lower Jurassic to Turonian age in the south (Tedla Plain). The geologic formations are mainly composed of limestone, marls and sandstone.

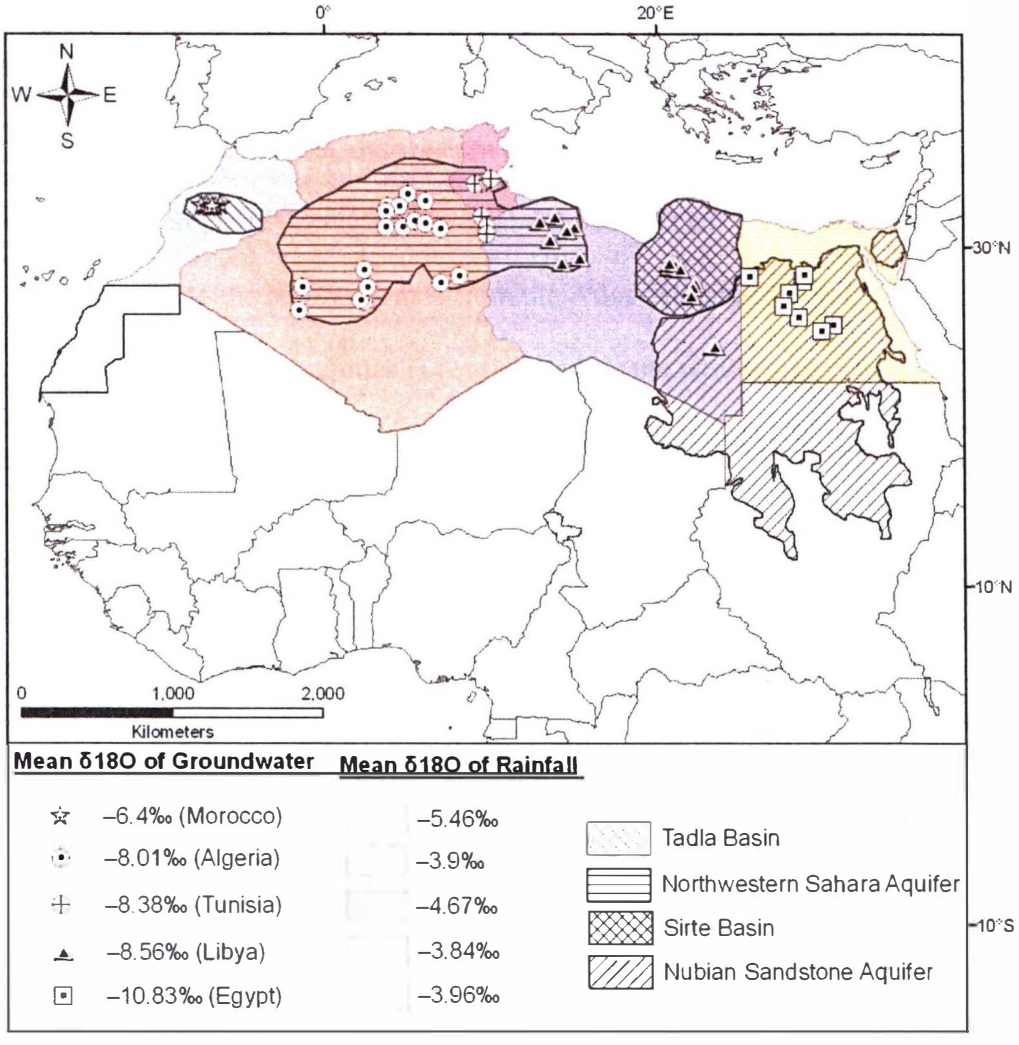

Figure 10: Spatial distribution of the fossil groundwater wells across North Africa.

The aquifers get replenished from the high precipitation that falls on the High Atlas Mountains, in addition to minor contributions from different groundwater inflows. The 10 wells tapping the confined aquifer in the Tedla basin were chosen with depths varying from 110 to 604 meter and ^{14}C ages that vary from 12,793 to 35,175 yr BP.

4.1.1.2 Northwestern Sahara Aquifer

The Northwestern Sahara Aquifer is a fossil transboundary reservoir covering large regions of Algeria, Tunisia and western Libya (Fig. 10). The principal aquifer is the Continental Intercalaire covering an area about 600,000 km^2. Approximately 80% of the total recharge to the aquifer comes from the Atlas Mountains (Wallin et al., 2005). The eastern part of the aquifer is confined while the western part is unconfined and consists mainly of detrital sediments of Mesozoic age (Gonfiantini, 1974). The eight wells that have been selected from the aquifer in the western Libya tap the Lower Cretaceous sandstone (Srdoč et al., 1982). Generally, the 35 wells tapping the Intercalaire aquifer have ^{14}C ages varying from 11,701 to 51,550 yr BP.

4.1.1.3 Sirte Basin

The Sirte basin is a sediment-filled trough located in northeastern Libya (Fig. 10). It includes Mesozoic and Tertiary formations with thicknesses exceeding 3000 meters. The Post-Eocene sequence of the Sirte basin is composed of sands and clays of continental origin to the south and intercalation of sands, clays and carbonates of marine origin to the north. Although the northwards groundwater flow direction is similar to that in the NSAS, the two aquifers appear independent even in the overlaping areas (Edmunds and Wright, 1979). The 11 wells that tap the Sirte basin have radiocarbon ages varying from 25,188 to 40,360 yr BP.

4.1.1.4 Nubian Sandstone Aquifer System (NSAS)

A total of nine wells were selected to represent the fossil groundwater in the NSAS including eight wells from the WD of Egypt and one well from the Kufra area, southeastern Libya (Thorweihe, 1982; Sultan et al., 1997). The nine wells that tap the NSAS vary in depth from 600 meters to more than 1000 meters and radiocarbon ages range from 15,100 to 48,500 yr BP. The geological and hydrogeological settings of the aquifer were already discussed in Chapter III.

4.1.2 Rayleigh Distillation Model

The Rayleigh distillation model basically describes air masses that follow a definite trajectory from a vapor source area to higher latitudes and over continents. Along the trajectory, the air masses are subject to a rainout process where the heavy isotopes distill from the water vapor and the vapor then becomes progressively depleted in their isotopic composition (Clark and Fritz, 1997).

A total of 65 groundwater deep wells were selected to spatially distribute over North Africa covering a distance of approximately 4000 km and forming a longitudinal track between the Atlantic Ocean and Red Sea Hills. A simple box model was constructed to encompass most of the area between the Atlantic Ocean and the Red Sea. The model was divided into eight irregular boxes in which each box encompasses a certain number of groundwater wells (Appendix A) and the box numbers are progressively increasing eastward (Fig. 11).

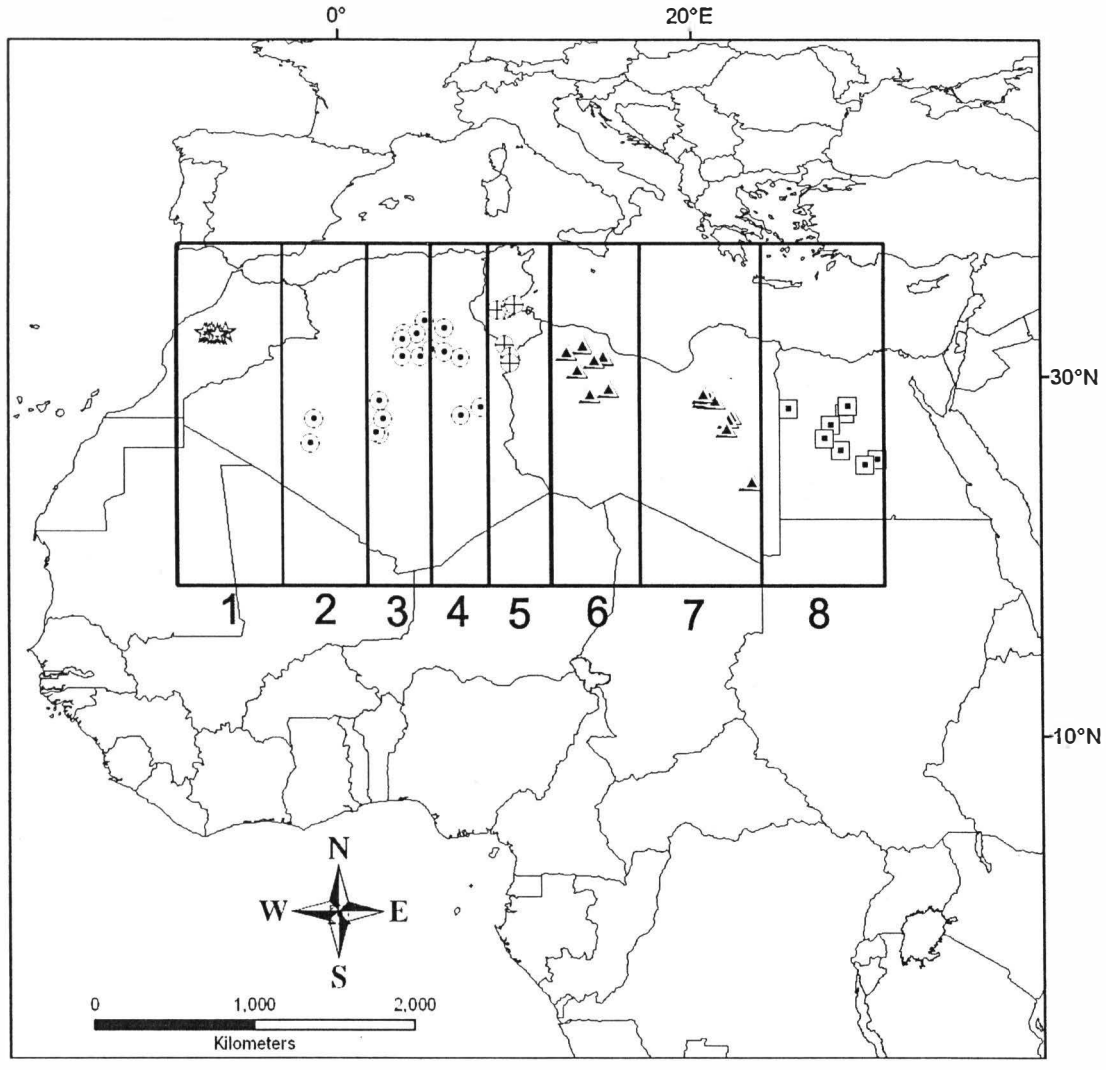

Figure 11: Rayleigh distillation box model constructed over North Africa.

The use of irregular boxes (Box No. 3, 4 and 5) was preferred over these of uniform size because the selected wells are not evenly distributed over the investigated area and it is appropriate to distribute the wells as uniformly as possible inside each box. The mean value of $\delta^{18}O$ from all wells in a certain box was calculated and assigned to that box. In each box, a sequence of equations was applied as described in Chapter II.

4.1.3 Results and Discussion

The $\delta^{18}O$ values of fossil groundwaters as function of distance from the Atlantic Ocean are plotted in (Fig. 12). The progressive depletion of the $\delta^{18}O$ values with distance due to the continental effect can be easily seen. Thus, this phenomenon indicates the intensification of paleowesterlies during the previous wet climatic periods during which the air masses collect moisture from the Atlantic Ocean and release it as rain when they are carried by the prevailing winds inland in a west-east direction. The average $\delta^{18}O$ in each box was plotted against the distance from the Atlantic coast measured to estimate the $\delta^{18}O$ inland gradient (Fig. 13). Distances were calculated using the mid point of each box. The inland gradient in $\delta^{18}O$ was estimated to be approximately –1‰ per 1000 km between the Atlantic Ocean (west) to the Red Sea (east).

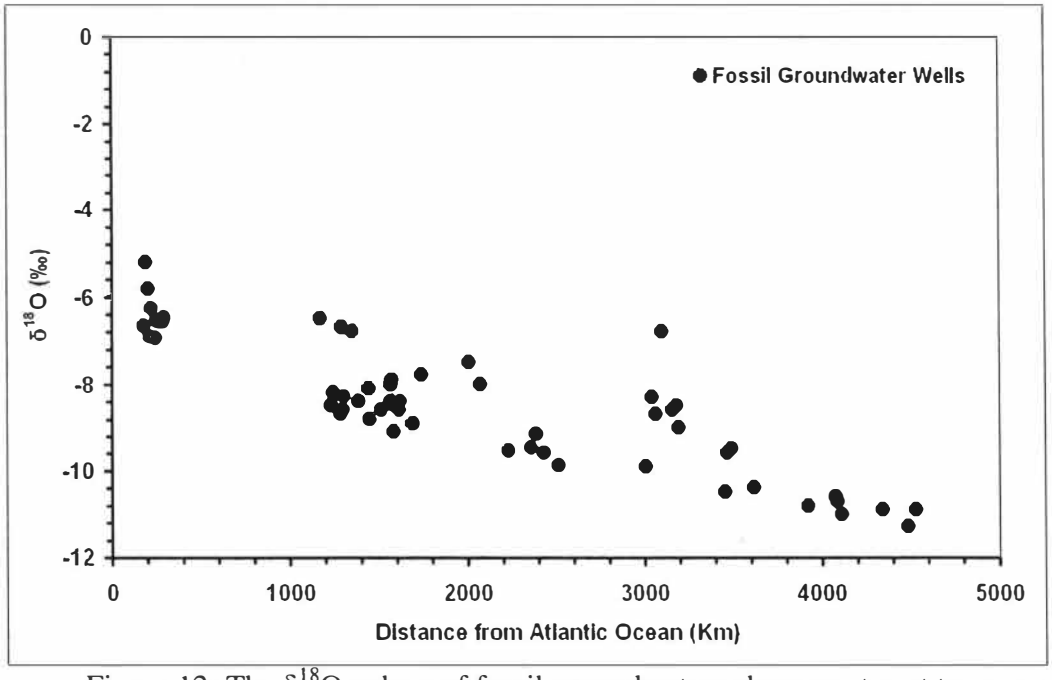

Figure 12: The $\delta^{18}O$ values of fossil groundwaters along west-east traverse.

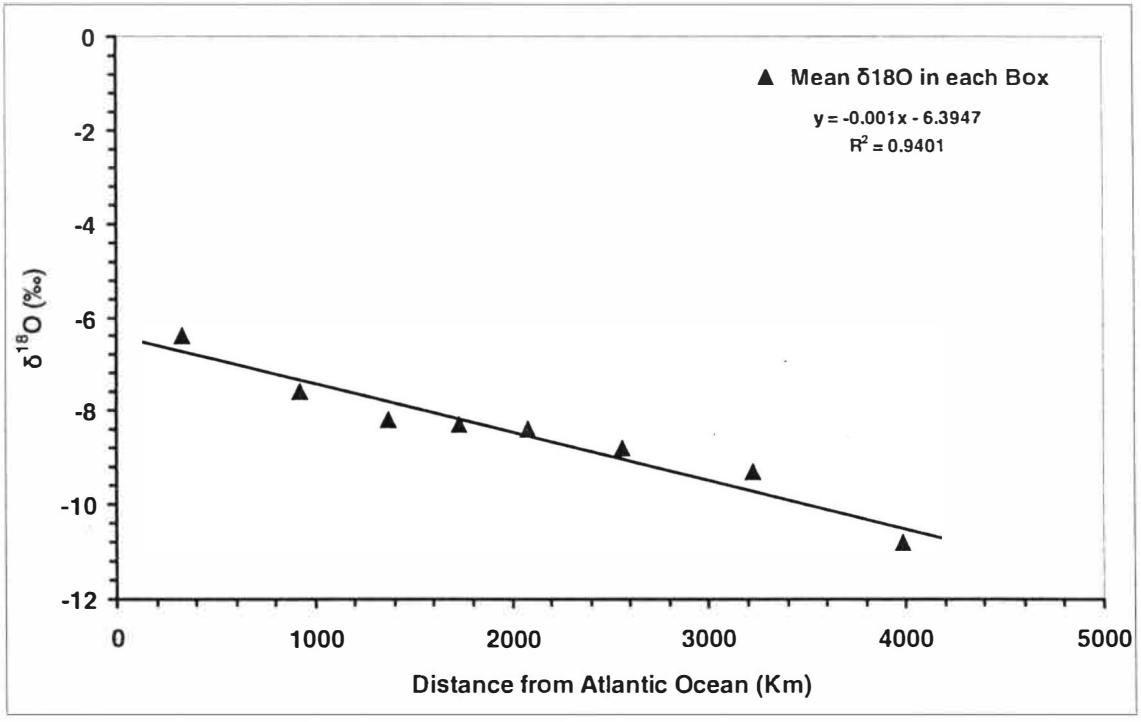

Figure 13: The mean $\delta^{18}O$ in each box vs. the distance from the Atlantic Ocean plot for measuring the $\delta^{18}O$ inland gradient.

In comparison, gradient of –2.8‰ per 1000 km has been reported over West Germany (Forstel and Hutzen, 1983) and that of –3‰ per 1000 km has been reported for the precipitation in the European continent (Sonntag et al., 1976). The calculated value over North Africa is somewhat lower than globally measured values and this reduction can be attributed to the recycling of the vapor mass through processes such as evapotranspiration (Salati et al., 1979; Krishnamurthy and Bhattacharya, 1991).

A linear relationship between the isotopic signature of $\delta^{2}H$ and of $\delta^{18}O$ in the fossil groundwater and precipitation waters can be observed in (Fig. 14).

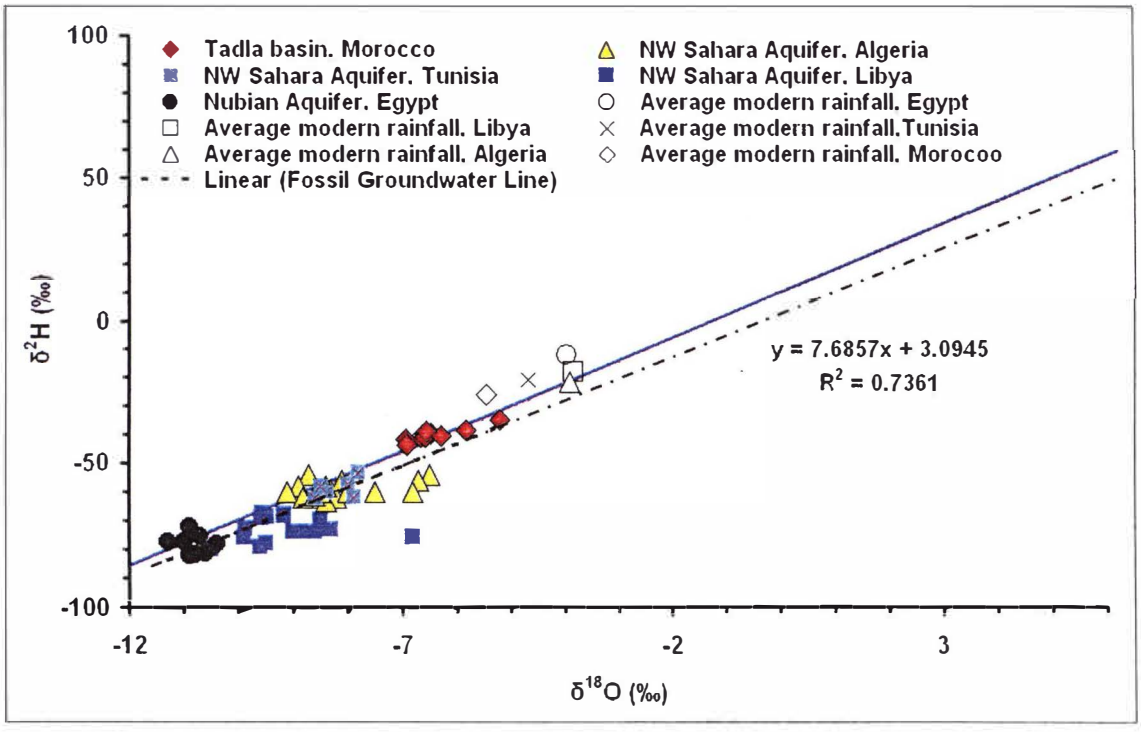

Figure 14: The $\delta^2H - \delta^{18}O$ plot f fossil groundwaters over North Africa.

The constructed $\delta^2H - \delta^{18}O$ line of the deep fossil groundwaters along the west-east traverse can be expressed by the following equation:

$$\delta^2H = 7.7\ \delta^{18}O + 3.1\ ‰ \quad (r^2 = 0.74,\ n = 65)$$

This line is close to the Global Meteoric Water Line (GMWL) by (Craig, 1961):

$$\delta^2H = 8\ \delta^{18}O + 10\ ‰$$

The observed displacement of the constructed line from the GMWL can give indication of evaporation process during the recharge. However, the evaporation was minimal as indicated from the slope of the line which is very close to 8. Furthermore, the slope of 8 results from an equilibrium condensation process indicating that the precipitation over Sahara Desert occurred under equilibrium conditions without interference with other secondary processes such as evaporation of falling raindrops.

Additionally, the hydrogen and oxygen isotopes in water provide a significant parameter called deuterium excess (*d*) that can be used as an index for non-equilibrium conditions to infer the vapor source origin as well the variation in humidity, wind speed and sea surface temperature during the primary evaporation (Dansgaard, 1964). It is defined as:

$$d = \delta^2H - 8\,\delta^{18}O$$

The low (*d*) value of the plotted fossil groundwaters (3.09) reflects high humidity (h > 95%) during the formation of the Atlantic air masses (Merlivat and Jouzel, 1979). Additionally, this low value greatly differs from that value (22) noted for the Eastern Mediterranean Meteoric Water Line (EMWL):

$$\delta^2H = 8\,\delta^{18}O + 22\ ‰$$

The winter precipitation that originated from the Mediterranean Sea is characterized by distinctly higher excess values and reflects the specific source conditions during water vapor formation (Gat and Carmi, 1970).

Rayleigh-type distillation can be interpreted from (Table 2 and Fig. 15) as the condensation occurred in each box by successive removal of the initial vapor mass and the "continental effect" becomes evident. Although the precipitated rainfall is enriched in the isotopic composition compared to the parent water vapors, the latter still shows a similar progressive depletion of the heavy isotopes with distance from the ocean (Fig. 15).

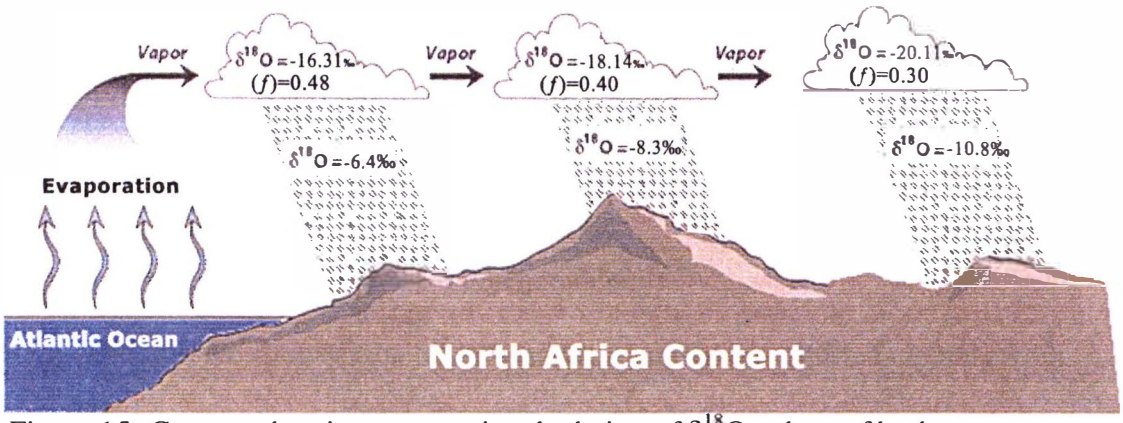

Figure 15: Cartoon showing progressive depletion of $\delta^{18}O$ values of both condensates and vapor flux across eastward trajectory over North Africa.

Table 2: Calculated $\delta^{18}O_v$ and fraction of the remaining vapor (f) over North Africa.

Box No.	$\delta^{18}O_L$ (‰)	T(°F)	T(°K)	α	$\delta^{18}O_v$ (‰)	f
1	–6.4	62	290	1.010070	–16.31	0.48
2	–7.6	62	290	1.010070	–17.49	0.42
3	–8.2	62	290	1.010070	–18.08	0.40
4	–8.3	62	290	1.010070	–18.14	0.40
5	–8.4	75	297	1.010070	–18.27	0.39
6	–8.8	75	297	1.009468	–18.12	0.38
7	–9.3	75	297	1.009468	–18.58	0.36
8	–10.8	75	297	1.009468	–20.11	0.30

It is also concluded that the Atlantic Ocean was the main source of moisture for recharging the Sahara groundwater aquifers during the previous wet climatic periods. The Rayleigh distillation box model shows that significant amount of precipitation occurred prior to the arrival of the air masses on the west coast of northern Africa (see box 1 vapor reduction factor). Similar effects have been reported

over the Pacific Ocean in a study of precipitation across west-east traverse along northern California coast (Ingraham and Taylor, 1986). Furthermore, the reduction of the water vapor was up to 70% through the eastward trajectory.

4.2 Isotopic Composition of Modern Precipitation

The isotopic composition of the modern precipitation collected monthly from the International Atomic Energy Agency (IAEA) stations over North Africa is enriched (average $\delta^2H \pm 1\sigma$: Algeria: –17.05‰ ± 8.81‰; Tunisia: –24.2‰ ± 4.23‰; Libya: –17.7‰ ± 2.72‰; Egypt: –15.46‰ ± 3.45‰) compared to the fossil groundwater across North Africa, which shows progressive west-to-east depletion.

This indicates that the precipitation from paleo-wind regimes was different from those prevailing in the present day. Over 600 monthly records for isotopic compositions for precipitation, collected from 10 stations distributed over four countries (Morocco, Algeria, Tunisia and Egypt) in North Africa and in neighboring Jordan (Fig. 16) were examined. The locations, elevations, and time periods of the data availability for each of these stations are listed in (Table 3).

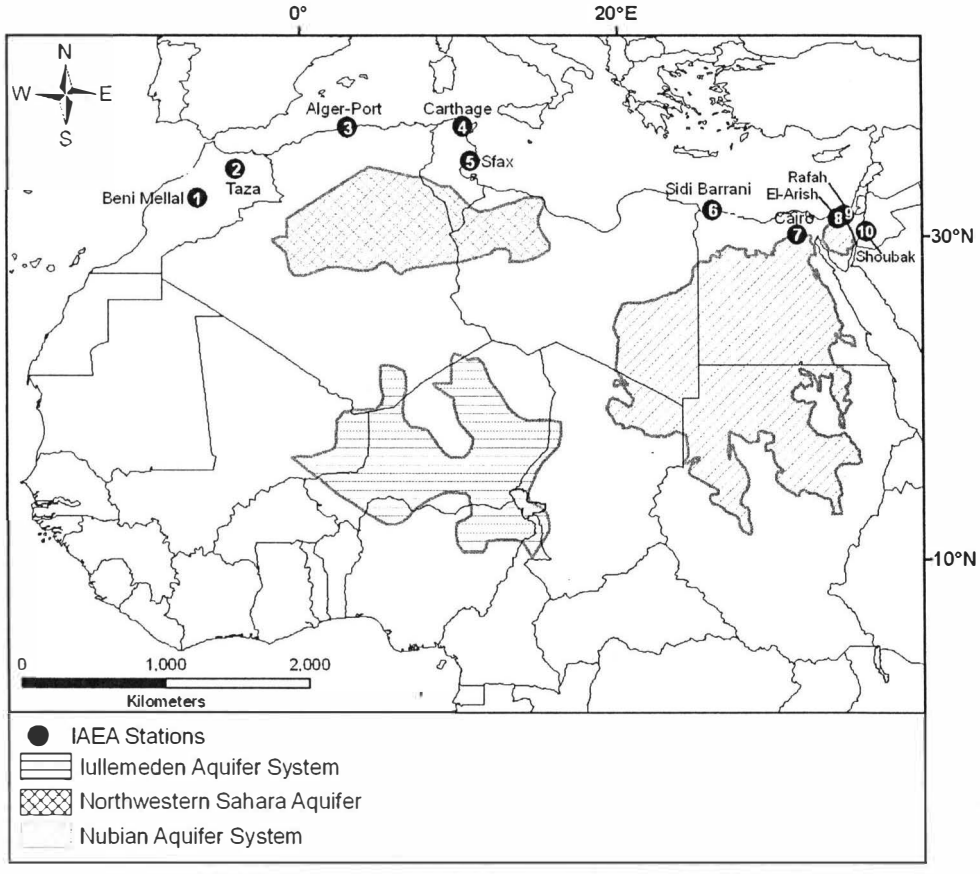

Figure 16: The location of IAEA meteorological stations from which precipitation amounts and isotopic compositions were derived.

Table 3: IAEA meteorological stations parameters over North Africa and Levant.

St. No.	Station Name, Country	Longitude	Latitude	Altitude (m+MSL)	Period of Data Availability	NDR*
1	Beni Melal, Morocco	–6.4	32.36	468	2001–2002	7
2	Taza, Morocco	–4.0	34.21	1500	2001–2002	13
3	Alger-Port, Algeria	3.05	36.78	180	1998–2006	69
4	Carthage, Tunisia	10.23	36.83	4	1967–2006	208
5	Sfax, Tunisia	10.68	34.71	23	1992–2006	129
6	Sidi Barrani, Egypt	25.95	31.62	24	1978–2003	111
7	Cairo, Egypt	31.28	30.08	34	1968–2003	19
8	El-Arish, Egypt	33.83	31.08	31	1979–2003	17
9	Rafah, Egypt	34.23	31.28	73	2000–2003	18
10	Shoubak, Jordan	35.58	30.27	1300	1965–2003	17

*Number of Data Records

For each of the individual stations in North Africa, I reported an average isotopic composition that was extracted from all available records for all the precipitation events as early as 1965 and as late as 2006 (Table 3). For comparison, the isotopic composition of fossil aquifers across North Africa is plotted as isolines joining locations with similar composition (Fig. 17) (Sonntag et al., 1978). Firstly, I examined the precipitation records (IAEA) over Egypt to identify the most isotopically depleted precipitation events. Then I used temporal satellite data to track the progression of clouds that produced each of these events in neighboring countries.

For each of the identified events, the variations in the isotopic composition of precipitation were investigated as clouds moved long distances laterally. For comparison purposes, the same approach was applied to identify the nature of wind regimes that produced precipitation having intermediate to enriched isotopic compositions. The precipitation records over Egypt were chosen to examine because: (1) the Egyptian precipitation records are the most comprehensive (4 of 10 examined stations), and (2) modern precipitation with isotopic affinities similar to those of fossil groundwater are the easiest to identify in Egypt, given that they show the largest deviation from average modern isotopic compositions. The isotopic depletion was not the only criterion I used in the selection of the anomalous records.

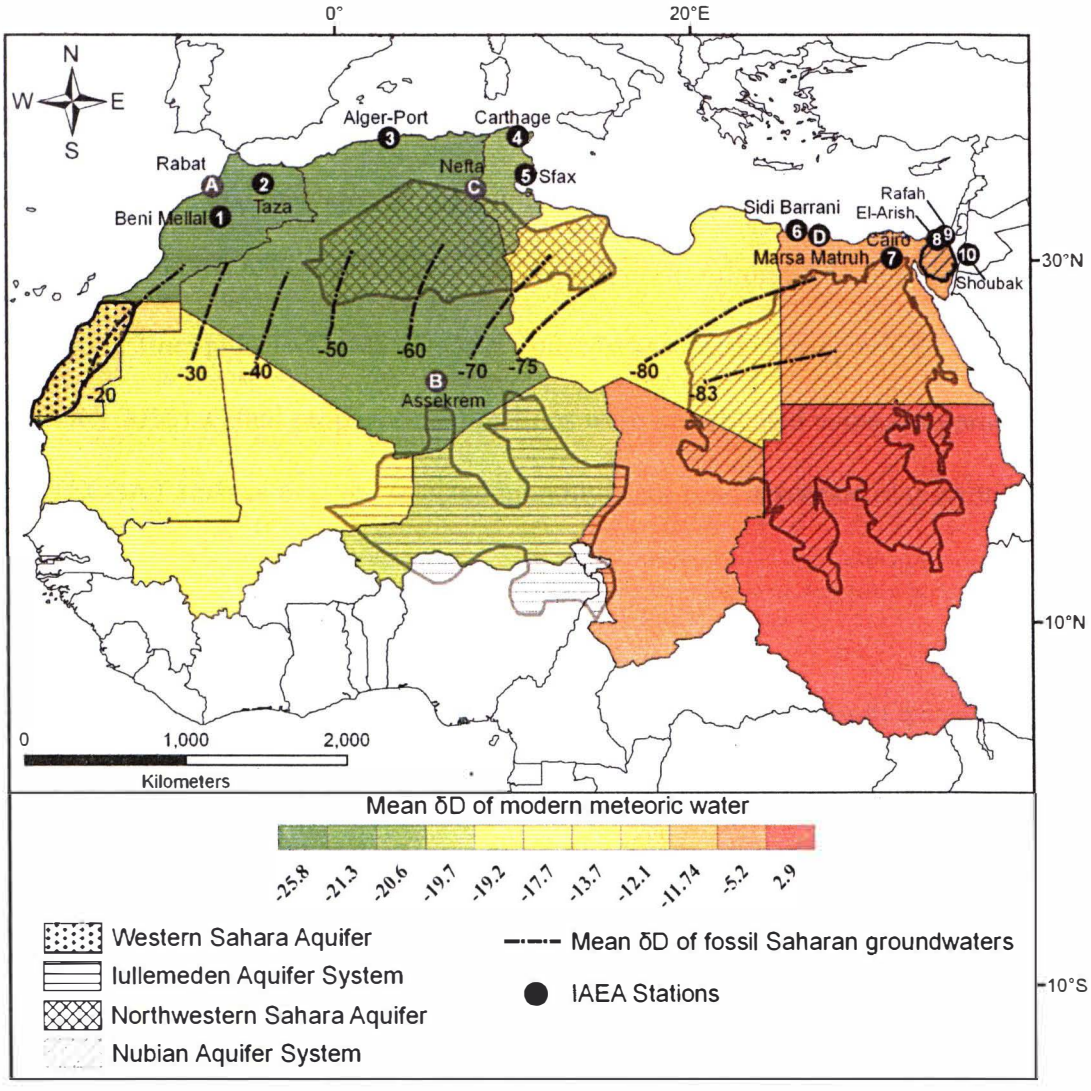

Figure 17: Regional variation of the mean $\delta^2H‰$ values of modern precipitation (Bowen and Revenaugh, 2003; WISER/IAEA, 2010) and mean $\delta^2H‰$ values for fossil Sahara groundwaters (Sonntag et al., 1978).

The initial 165 records were refined for the selected four stations to include only the months in which a single precipitation event accounted for the total or near-total (>80%) monthly precipitation and/or the records where the cloud propagation directions remained constant throughout the month. The latter selection criteria were designed to exclude the records in which the monthly compositions could be related

to contributions from varying cloud propagation directions throughout the selected months. Precipitation-related data, such as the number of rainy days within the selected month, and the date and the amount of precipitation (Appendix B), were extracted from the National Oceanic and Atmospheric Administration's (NOAA's) National Climatic Data Center database <http://www7.ncdc.noaa.gov/CDO/cdo> (NCDC, 2010). Cloud propagation directions were investigated using temporal METEOSAT images over the selected monthly records as described in (Chapter V).

4.2.1 Data Analysis

Examination of Figure 17 shows that the composition of fossil water in each of the investigated countries is depleted compared to modern precipitation. From west to east, the δ^2H values in fossil water (F) and modern precipitation (M) are (Table 3 and Fig. 17): Morocco: (M): –25.8 ‰, F: –20‰ to –40‰; Algeria: (M): –21.3 ‰, F: –30 ‰ to –70 ‰; Tunisia: (M): –20.6 ‰, F: –60 ‰ to –70 ‰; Libya: (M): –17.7 ‰, F: –70 ‰ to –80 ‰; and Egypt: (M): –11.7 ‰, F: –80 ‰ to –83 ‰. Such depletions are expected if the groundwater residing in the fossil aquifers of North Africa resulted from precipitation during (1) cooler glacial periods (2) had a different air mass history than what is normal today. Examination of the isotopic compositions of modern precipitation (Bowen and Revenaugh, 2003; WISER/IAEA, 2010) and fossil groundwater (Sonntag et al., 1978; Sultan et al., 1997) in North Africa showed that the fossil water, but not the modern precipitation, exhibits progressive isotopic depletion from west to east (Fig. 17). This comparison suggests that precipitation

during previous wet climatic periods (450,000–10,000 years B.P.) resulted from wind regimes different from those prevailing in the present day. However, I found that a small number of the investigated modern rainfall events have isotopic compositions similar to those of the fossil groundwaters of North Africa. By identifying these precipitation events and deciphering the wind patterns that gave rise to these events, I sought to gain insight into the prevailing wind regimes during the recharge of the fossil aquifers of North Africa. I examined rainfall events that were reported over Egypt for the period from April 1979 to March 2003 to determine the dominant wind directions during measureable precipitation events. Figure 18 compares the isotopic compositions for all of the monthly composite precipitation samples (165 samples) collected (1979 to 2003) from the four IAEA stations (Sidi Barrani, Cairo, Rafah, and El-Arish) in Egypt to those of fossil groundwater from the Nubian Sandstone Aquifer in the Western Desert of Egypt and Sinai Peninsula (Sultan et al., 1997; JICA, 1999).

Three of these stations are located along the Mediterranean coast and the fourth is located in Cairo, about 150 km inland south of the coast. Inspection of Figure 18 shows that modern precipitation over Egypt is generally isotopically enriched relative to the fossil groundwater. Modern precipitation plots along the Global Meteoric Water Line (GMWL) with isotopic compositions ranging from δ^2H – 56.9‰ to +34.6‰.

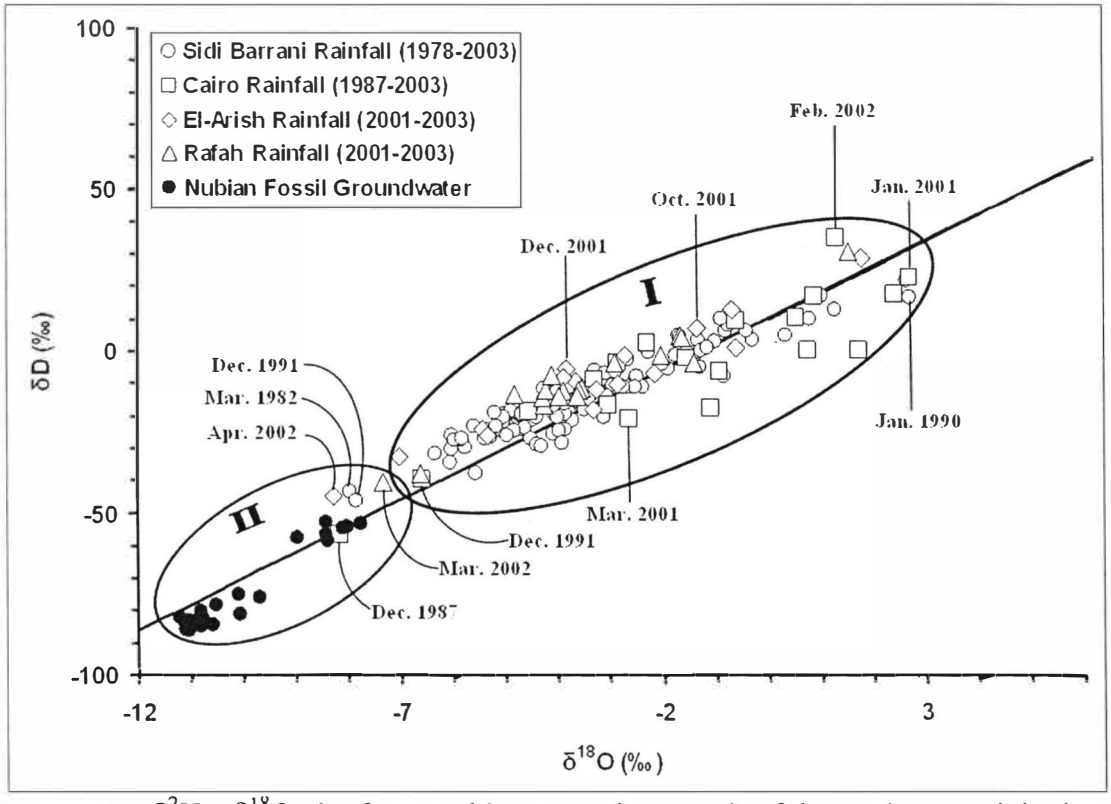

Figure 18: $\delta^2H - \delta^{18}O$ plot for monthly composite records of the modern precipitation (1978 to 2003) collected from Sidi Barrani, Cairo, El-Arish, and Rafah IAEA stations in Egypt.

The five most depleted of these samples (March 1982, December 1987, December 1991, March 2002, and April 2002) have isotopic compositions (δ^2H: –56.9‰ to –43.7‰) that are similar to, yet slightly more enriched than, those of the Nubian aquifer in Egypt (δ^2H: –86.3‰ to –53‰; Sultan et al., 1997, 2007, 2011; JICA, 1999). One explanation for the observed modest enrichments in the selected modern precipitation records compared to the fossil groundwater of the Nubian Aquifer in Egypt is that the Egyptian IAEA stations are on or proximal to the Mediterranean Sea, a source of moisture that can enrich the isotopic compositions of precipitation, whereas the reported Nubian aquifer compositions are for samples

located hundreds of kilometers (500 to 1000 km) from the Mediterranean. This suggestion is supported by the observed enrichment in the isotopic compositions of modern precipitation from stations on the Mediterranean Sea (Rabat, Alger-Port, Carthage) compared to those reported from stations located further inland (Beni Mellal, Assekrem, Nefta), and to the south of the coastal stations (Morocco, Algeria, Tunisia) (Fig. 19). The figure shows that three precipitation events, in January 2001, February 2002, and April 2003, reported from the coastal Rabat station in Morocco were enriched (δ^2H: –25.64‰, –15.32‰, and –12.35 ‰) compared with precipitation from the same events reported from Beni Mellal station (δ^2H: –43.82‰, –35.7‰, and –34.5‰), about 200 km to the south. The figure also shows similar enrichments from other coastal stations (Alger-Port, Carthage) compared to inland stations (Assekrem, Nefta) (Fig. 19).

Though, a subset (12 samples) of the entire data set (165 samples) were selected from (Fig. 18) that encompasses the entire range of observed isotopic variations, all of which were produced from a single precipitation event or from multiple events with a unified cloud propagation direction. Using the temporal satellite data (MFG) that will be discussed in (Chapter V), I searched for relationships between the observed isotopic compositions of the 12 precipitation samples and the wind regimes that produced them.

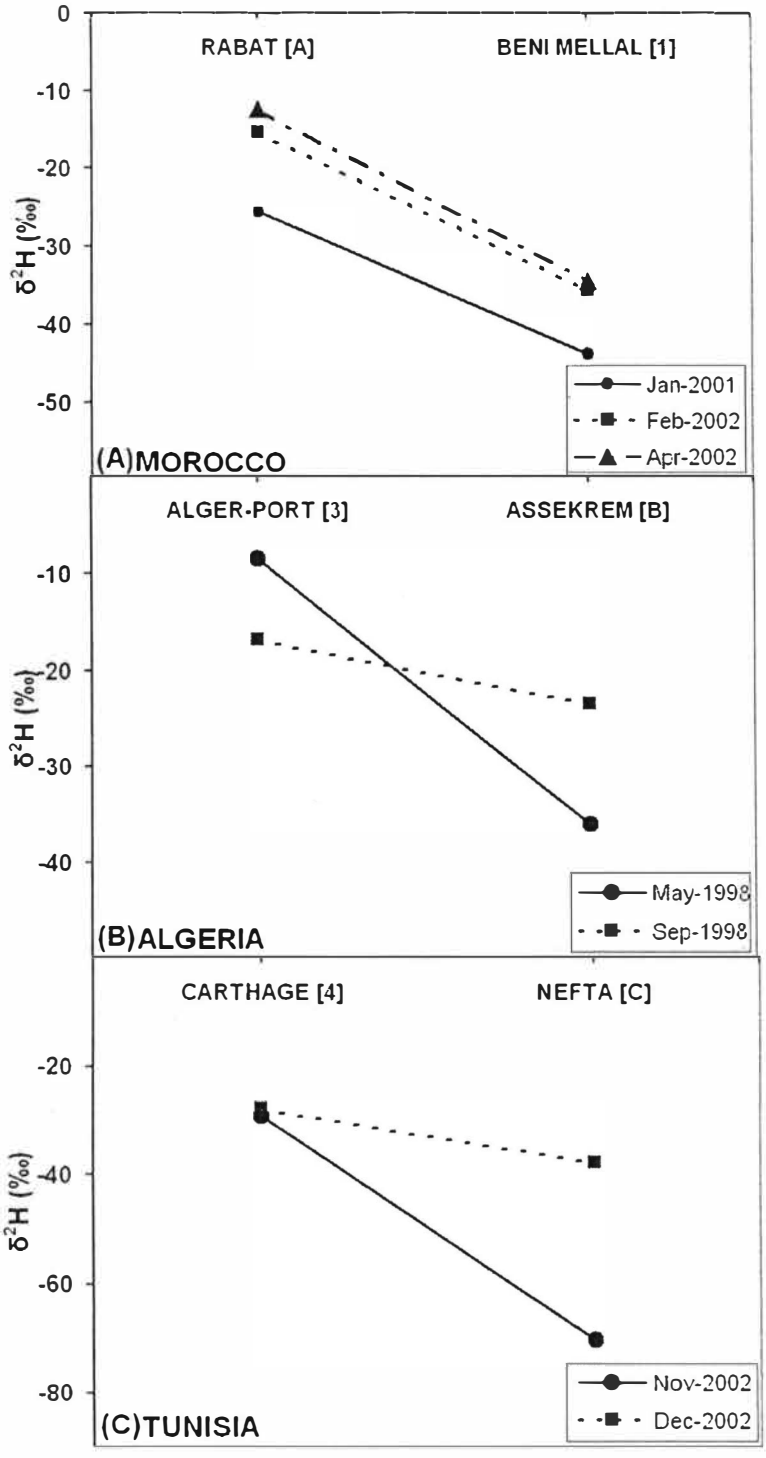

Figure 19: Comparison between the isotopic compositions of individual precipitation events that were reported from IAEA stations on or proximal to the Mediterranean coastline and from inland stations located south of the Mediterranean stations.

The enriched samples reported from the Cairo station in January 2001 and February 2002 (δ^2H: 22.4‰ and 34.6 ‰, respectively), and samples with intermediate compositions (δ^2H: –39.7‰ to +34.6‰) that were collected from the Sidi Barrani, Cairo, El-Arish, and Rafah stations in January 1990, December 1991, March 2001, October 2001, and December 2001 were all found to have been precipitated from northerly to northwesterly wind regimes. The wind regimes that produced these precipitation events traveled over the Mediterranean Sea and across varying distances of the North African continent toward Egypt, in the case of the northwesterlies.

On the other hand, four of the five most depleted (δ^2H: –46.4‰ to –40.8‰) samples that were collected from Sidi Barrani, El-Arish, and Rafah stations in March 1982, December 1991, March 2002, and April 2002 were found to have been precipitated from westerly wind regimes that traveled across the entire North African landscape. Additionally, the fifth sample (δ^2H: –56.9‰) that collected (December 1987) from the Cairo station, precipitated from a cyclonic event that started on December 21 and lasted for three days centered over Cairo.

CHAPTER V

REMOTE SENSING AND GIS

This chapter devoted to identify the modern precipitation events that have isotopic compositions similar to those of the fossil groundwaters of North Africa. Consequently, the wind patterns that gave rise to these events will be easily deciphered which would mimic the prevailing wind regimes during the recharge of the fossil aquifers of North Africa Sahara Desert using the methodologies described in Chapter II and the findings in Chapter IV.

Guided by the above synthesis and data analysis from (Fig. 18), I demonstrate specific examples of precipitation events from northerly to northwesterly wind regimes that are represented as group I (enriched and intermediate isotopic composition) and from westerly wind regimes that are represented as group II (depleted isotopic composition), respectively, with an emphasis on the latter. For each of these events, I investigate the direction of cloud propagation in relation to the isotopic composition of precipitation as it travels over the African continent and surroundings. Cloud propagation directions and air parcel flow paths were extracted from: (1) temporal (every 30 minutes) Infra-red METEOSAT First Generation (MFG) products; (2) Cloud Motion Winds (CMW); and (3) Back Trajectory Models (BTM).

5.1 Precipitation Events from Northerlies to Northwesterlies

Two examples were selected from the first-order groupings for precipitation events resulting from northerly to northwesterly wind regimes (Fig. 18). The first example is for isotopically enriched compositions from a rainfall event recorded on February 10, 2002, in Egypt. The second example was reported from a weaker system in the month of October 2001 from El-Arish station (2.03 mm; δ^2H: 7.1‰) in Egypt. The results from analyzing the MFG, the CMW and the BTM will be presented in the following sections.

5.1.1 February 2002 Precipitation Event

Isotopically enriched compositions from a rainfall event reported from the Cairo station (5.08 mm; δ^2H: 34.6‰), the El-Arish station (13.9 mm; δ^2H: 28.7‰), and the Rafah station (10.3 mm; δ^2H: 30.7‰) on February 10, 2002, in Egypt (Table 4). The precipitation amounts are those reported for the entire month, whether they resulted from a single event, as is the case for the Cairo station, or from multiple events, as is the case with the precipitation from the El-Arish and Rafah stations.

Examination of temporal Meteosat data (1339 scenes) showed that by February 10, 2002 (0000 UTC), clouds that originated over the Atlantic Ocean propagated eastward to cover large sectors of the European continent and northern parts of the Mediterranean Sea. By 0600 UTC, these clouds had moved southeast, crossed the Mediterranean, and reached the northern parts of Egypt and Libya. These patterns intensified by 1200 UTC and weakened by 1800 UTC (Fig. 20 A–D).

Table 4: Data pertaining to modern precipitation events resulting from northerlies to northwesterlies, westerlies, and cyclones.

Station No. & Name	March-1982'				December-1987'				December-1991'				October-2001'				Feburary-2002'				March-2002'				April-2002'			
		PPT				PPT				PPT				PPT				PPT				PPT				PPT		
	δ^2H	Total	Daily		δ^2H	Total	Daily		δ^2H	Total	Daily		δ^2H	Total	Daily		δ^2H	Total	Daily		δ^2H	Total	Daily		δ^2H	Total	Daily	
	‰	mm	Day	mm	‰	mm	Day	mm	‰	mm	Day	mm	‰	mm	Day	mm	‰	mm	Day	mm	‰	mm	Day	mm	‰	mm	Day	mm
1. Beni Mellal	x	x	x	x	x	x	x	x	x	x	x	x	x	x	x	x	x	x	x	x	-19.5	142.7	x	x	x	x	x	x
2. Taza	x	x	x	x	x	x	x	x	x	x	x	x	x	x	x	x	x	x	x	x	x	x	x	x	-12.3	154.4	1	11.9
3. Alger Port	x	x	x	x	x	x	x	x	x	x	x	x	x	x	x	x	x	x	x	x	-27.3	150.6	28	0.8	-32.9	46.4	3	4.1
4. Carthage	-13.9	41	x	x	x	x	x	x	-35.3	91	7	2.03	x	x	x	x	x	x	x	x	x	x	x	x	x	x	x	x
5. Sfax	x	x	x	x	x	x	x	x	x	x	x	x	22.3	1.3	x	x	x	x	x	x	-21.9	110	29	0.8	-20.2	42	1	0.5
6. Sidi Barrani	-43.7	6.9	13	1.02	x	x	x	x	-46.4	73.7	11	1.02	x	x	x	x	x	x	x	x	x	x	x	x	x	x	x	x
7. Cairo	x	x	x	x	-56.9	34.7	23	5.1	x	x	x	x	x	x	x	x	34.6	5.1	10	5.1	x	x	x	x	x	x	x	x
8. El-Arish	x	x	x	x	x	x	x	x	x	x	x	x	7.1	2.03	28	2.03	28.7	13.9	10	0.8	x	x	x	x	-44.9	2.7	2	2.03
9. Rafah	x	x	x	x	x	x	x	x	x	x	x	x	x	x	x	x	30.7	10.3	x	x	-40.8	29.4	29	7.9	x	x	x	x
10. Shoubak	x	x	x	x	x	x	x	x	x	x	x	x	x	x	x	x	x	x	x	x	x	x	x	x	-58.1	22	x	x
	Westerly				Cyclonic				Westerly				Northerly-Northwesterly								Westerly				Westerly			

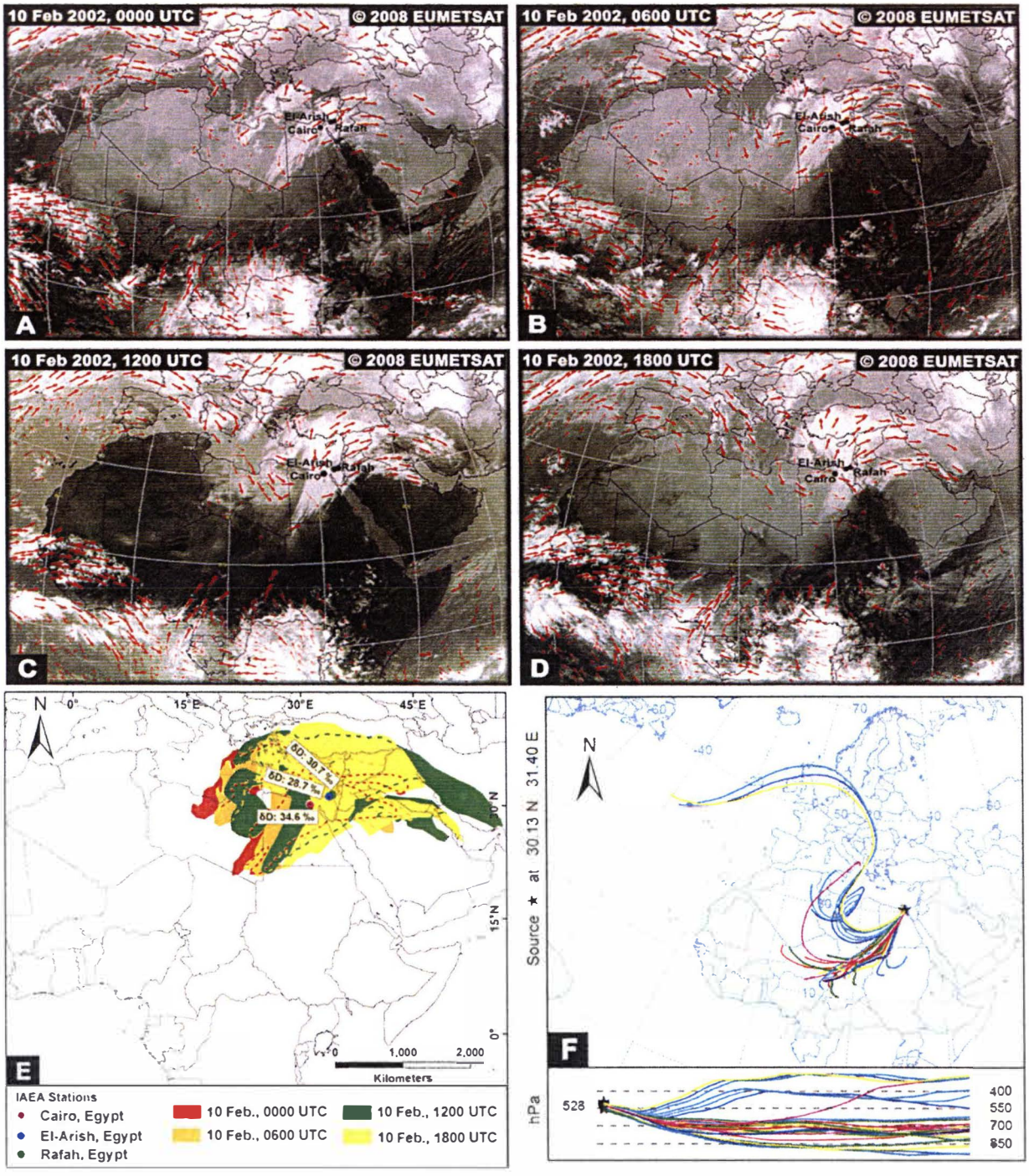

Figure 20: Cloud distribution extracted from Meteosat-7 and wind vectors for a precipitation event resulting from a northwesterly event reported on Feb. 10, 2002.

The spatial distribution of clouds that showing in (Fig. 20 A–D) was portrayed as overlapping polygons using GIS methodology (Fig. 20 E). Additionally, the backward trajectories of the clouds were calculated 72 hours backwards in time starting from Cairo, on Feb 10, 2002 at 1800 UTC (Fig. 20 F).

5.1.2 October 2001 Precipitation Event

The second example was reported from a weaker system in the month of October 2001 from El- Arish station (2.03 mm; δ^2H: 7.1‰) in Egypt. This rainfall event was the only event recorded for the month. Temporal Meteosat data (1445 scenes) showed that clouds originated over the Atlantic Ocean and followed trajectories similar to those in the previous example (Feb. 2002). By 0600 UTC, clouds covering areas in southern Europe had propagated southeast and crossed the Mediterranean to cover patchy areas in Libya and Egypt. The wind patterns dissipated by 1800 UTC (Fig. 21 A-D).

The spatial distribution of clouds that showing in (Fig. 21 A–D) was portrayed as overlapping polygons using GIS methodology (Fig. 21 E). Additionally, the backward trajectories of the clouds were calculated 72 hours backwards in time starting from El-Arish, on October 28, 2001 at 1800 UTC (Fig. 21 F).

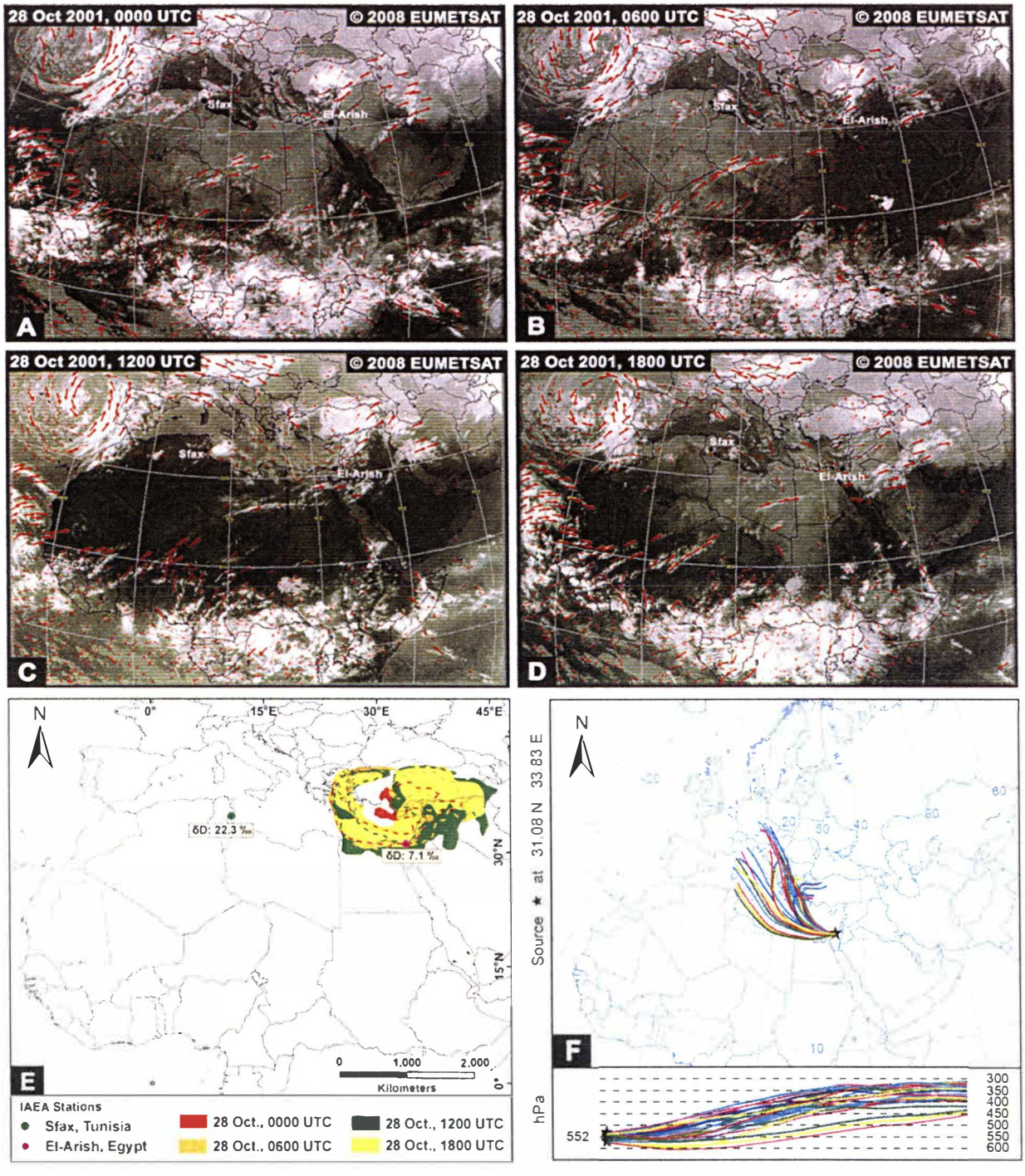

Figure 21: Cloud distribution extracted from Meteosat-7 and wind vectors for a precipitation event resulting from a northwesterly event reported on Oct. 28, 2001.

5.2 Precipitation Events from Westerlies

Four of the five most depleted (δ^2H: –46.4‰ to –40.8‰) samples that were collected from Sidi Barrani, El-Arish, and Rafah stations in March 1982, December 1991, March 2002, and April 2002 were found to have been precipitated from westerly wind regimes that traveled across the entire North African landscape. The fifth sample (δ^2H: –56.9‰), collected (December 1987) from the Cairo station, precipitated from a cyclonic event that started on December 21 and lasted for three days centered over Cairo. The results from analyzing the MFG, the CMW and the BTM will be presented in the following sections.

5.2.1 March 1982 Precipitation Event

Available isotopic compositions for March 1982 from the Carthage station (41 mm; δ^2H: –13.9‰) in Tunisia and the Sidi Barrani station (6.9 mm; δ^2H: –43.7‰) in Egypt showed progressive west-to-east depletion. Multiple precipitation events were reported from both stations. Examination of temporal Meteosat data (652 scenes) and the animations produced from such datasets indicated that the direction of cloud propagation for these multiple events remained uniform throughout the month. The images also showed that by March 11 (1300 UTC), clouds that originated over the Atlantic Ocean had progressed inland over western Morocco and central Algeria, and by March 13 (0500 UTC), clouds covered areas to the west in Tunisia and eastern Algeria (Fig. 22 A-D).

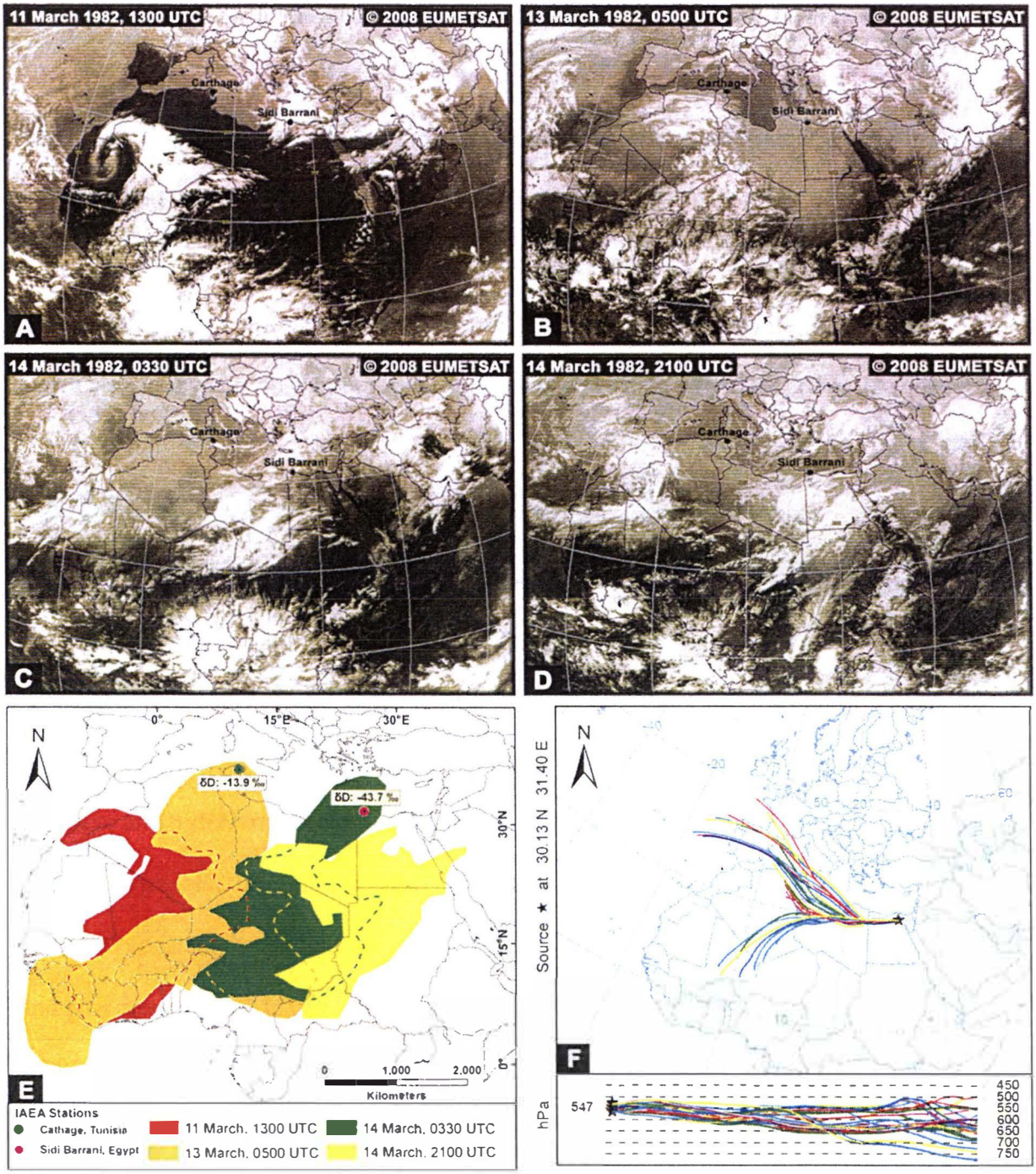

Figure 22: Cloud distribution extracted from Meteosat-2 for a precipitation event resulting from a westerly event reported on March 11–14, 1982.

On the following day, March 14, clouds covered most of western and central Libya by 0330 UTC, and by 2100 UTC clouds covered most of the Egyptian landscape. Available daily precipitation data show precipitation on March 13 over the Marsa Matruh station (1.02 mm). The spatial distribution of clouds that showing in (Fig. 22 A–D) was portrayed as overlapping polygons using GIS methodology (Fig. 22 E). Additionally, the backward trajectories of the clouds were calculated 72 hours backwards in time starting from Cairo, on March 14, 1982 at 2100 UTC (Fig. 22 F).

5.2.2 December 1991 Precipitation Event

A similar event was reported from the same two stations for the month of December 1991. A progressive west-to-east depletion can be recognized for rainfall from the Carthage station (91 mm; δ^2H: –35.3‰) and from the Sidi Barrani station (73.7 mm; δ^2H:–46.4‰). Multiple precipitation events were recorded from the Carthage and Sidi Barrani stations during that month, but again, examination of temporal Meteosat data (1482 scenes) revealed that the direction of cloud propagation remained constant throughout the month. Clouds originated over the Atlantic Ocean and progressed inland to cover Saharan Morocco and western Algeria by December 7 (2000 UTC). The clouds moved eastward, and by December 9 they covered eastern Algeria, Tunisia, and western and northern Libya. By December 10 (1200 UTC), the clouds covered northern Egypt, the Levant, and northern parts of the Arabian Peninsula (Fig. 23 A-D). Precipitation occurred over the Carthage station (2.03 mm) on December 7 and over the Marsa Matruh station (1.02 mm) on December 11.

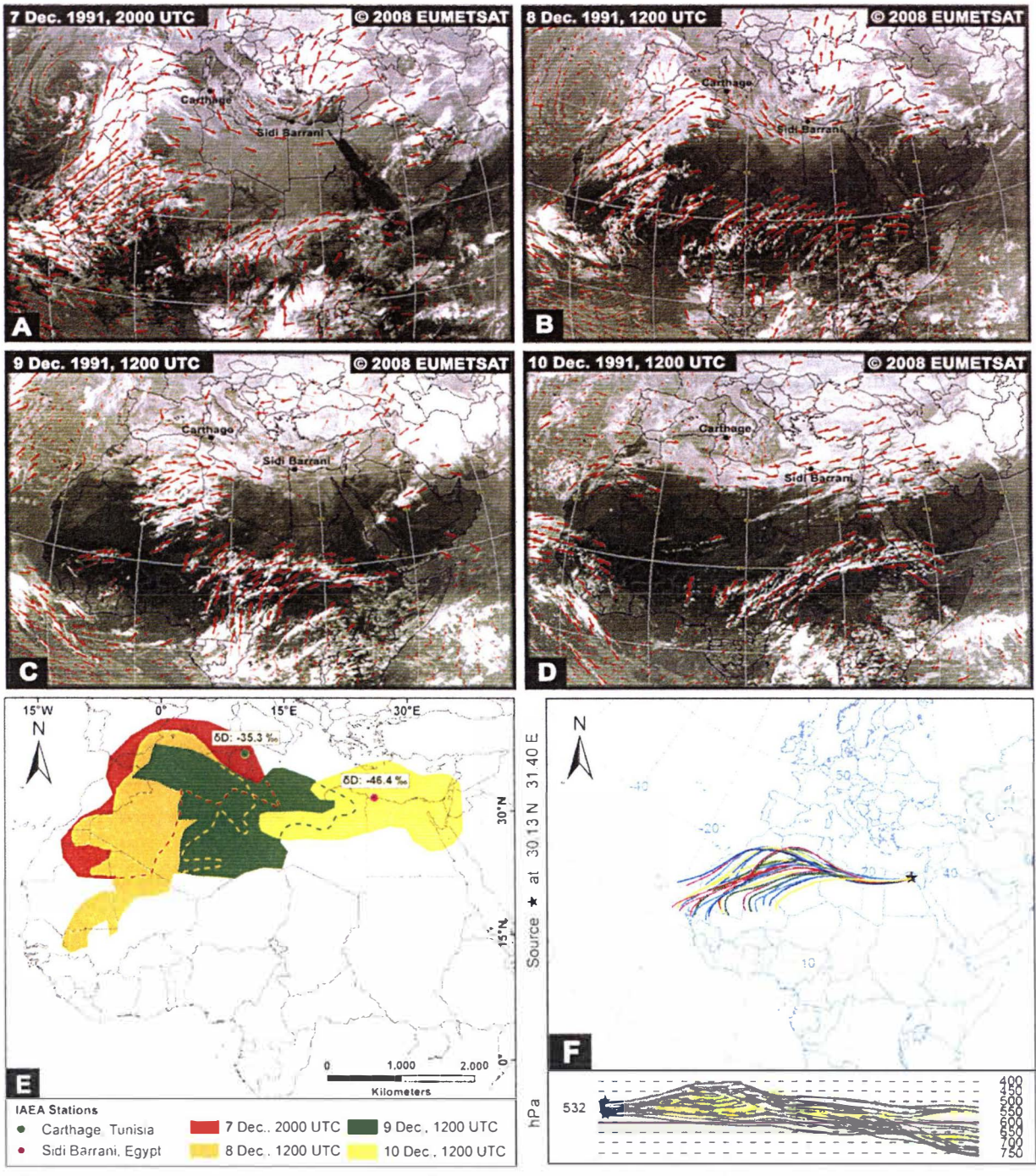

Figure 23: Cloud distribution extracted from Meteosat-4 and wind vectors for a precipitation event resulting from a westerly event reported on Dec. 7–10, 1991.

The spatial distribution of clouds that showing in (Fig. 23 A–D) was portrayed as overlapping polygons using GIS methodology (Fig. 23 E). Additionally, the backward trajectories of the clouds were calculated 72 hours backwards in time starting from Cairo, on Dec. 10, 1991 at 1200 UTC (Fig. 23 F).

5.2.3 March 2002 Precipitation Event

Similar wind patterns were apparently responsible for a precipitation event (March 28, 0400 UTC, to March 30, 2000 UTC) that was reported from the Beni Mellal station (Morocco), Alger-Port station (Algeria), Sfax station (Tunisia), and Rafah station (Egypt) for the month of March 2002. The available isotopic composition records showed progressive west-to-east depletion (Beni Mellal: 142.7 mm, δ^2H: –19.5‰; Alger-Port: 150.6 mm, δ^2H: –27.3‰; Sfax: 110 mm, δ^2H: –21.9‰; and Rafah: 29.4 mm, δ^2H: –40.8‰). Multiple precipitation events were reported from all stations; however, examination of temporal Meteosat images and animations for the entire month showed that cloud propagation directions remained consistent throughout the month. By March 28 (0400 UTC), clouds originating in the Atlantic Ocean covered northwest Morocco and North Algeria. These clouds progressed eastward and covered almost all of Tunisia and northern Libya by March 29 (400 UTC). By March 30 (2000 UTC), clouds moved eastward to cover northern Egypt, the Sinai Peninsula, and areas to the east (Fig. 24 A-D).

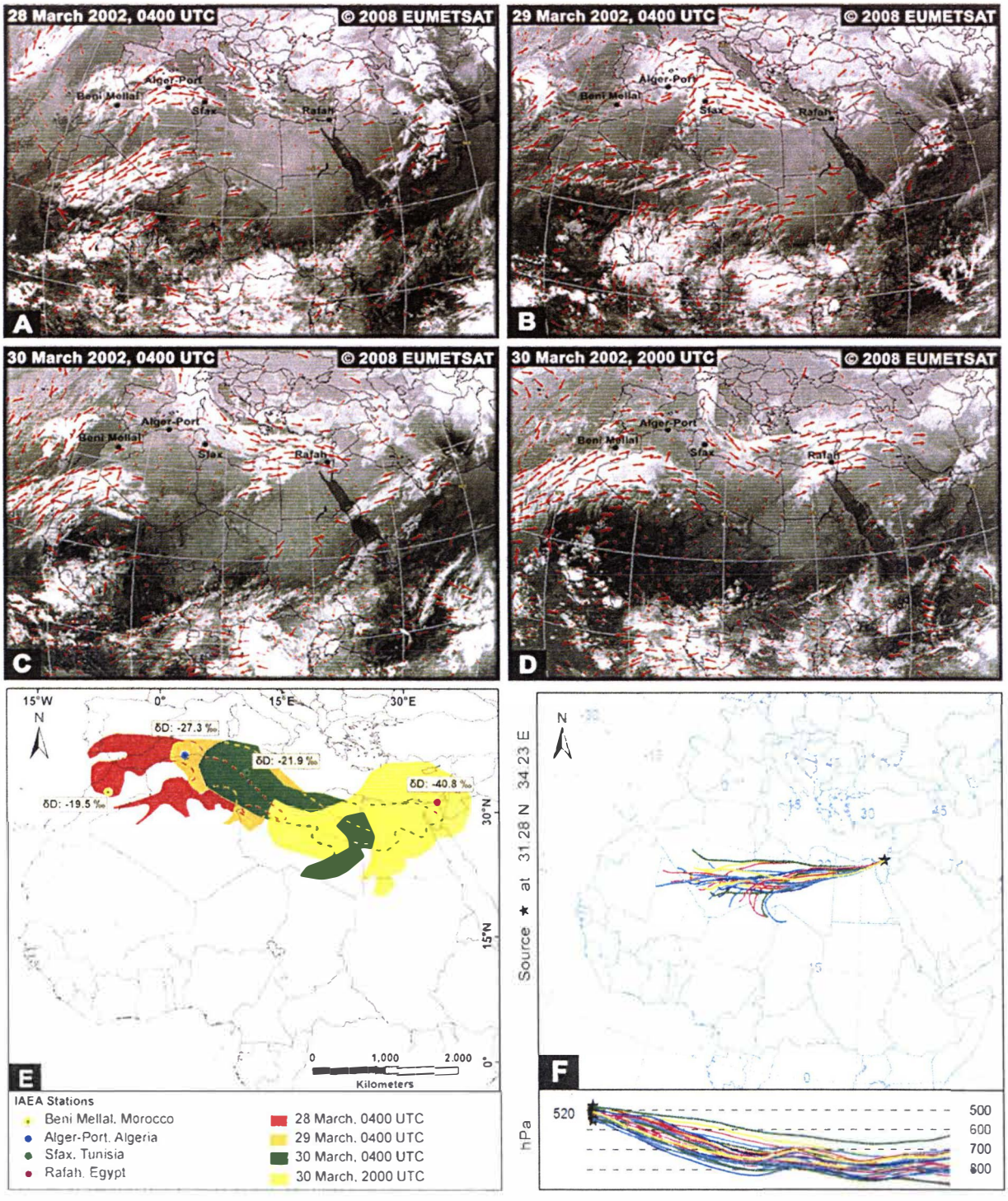

Figure 24: Cloud distribution extracted from Meteosat-7 and wind vectors for a precipitation event resulting from a westerly event reported on March 28–30, 2002.

Available daily precipitation data show precipitation on March 28 over the Alger-Port station (0.76 mm), and on March 29 over the Sfax station (0.76 mm) and the El-Arish station (7.87 mm). The spatial distribution of clouds that showing in (Fig. 24 A–D) was portrayed as overlapping polygons using GIS methodology (Fig. 24 E). Additionally, the backward trajectories of the clouds were calculated 72 hours backwards in time starting from Rafah, on March 30, 2002 at 2000 UTC (Fig. 24 F).

5.2.4 April 2002 Precipitation Event

This is the last example for a precipitation event resulting from a westerly wind regime occurred in April 2002. It started on April 1st (0400 UTC) and ended on April 4th (0400 UTC), and was reported from five stations (Morocco: Taza; Algeria: Alger-Port; Tunisia: Sfax; Egypt: El-Arish; Jordan: Shoubak). As is the case with all previous examples, a progressive west-to-east depletion in the isotopic composition of precipitation was observed: (Taza: 154.5 mm; δ^2H: –12.3‰; Alger-Port: 46.4 mm; δ^2H: –32.9‰; Sfax: 42 mm; δ^2H: –20.2‰; Shoubak: 22 mm; δ^2H: –58.1‰; El-Arish 2.7 mm; δ^2H: –44.9‰). Multiple precipitation events were reported from all stations except for the El-Arish station, where a single event was identified. Examination of temporal Meteosat images (1459) and animations produced from these scenes for the entire period showed that the cloud propagation direction remained consistent during the entire month (Fig. 25 A-D). Clouds that originated over the Atlantic Ocean progressed inland in a northeasterly direction, covering areas in Morocco, western and central Algeria, and Tunisia by April 1 (0400).

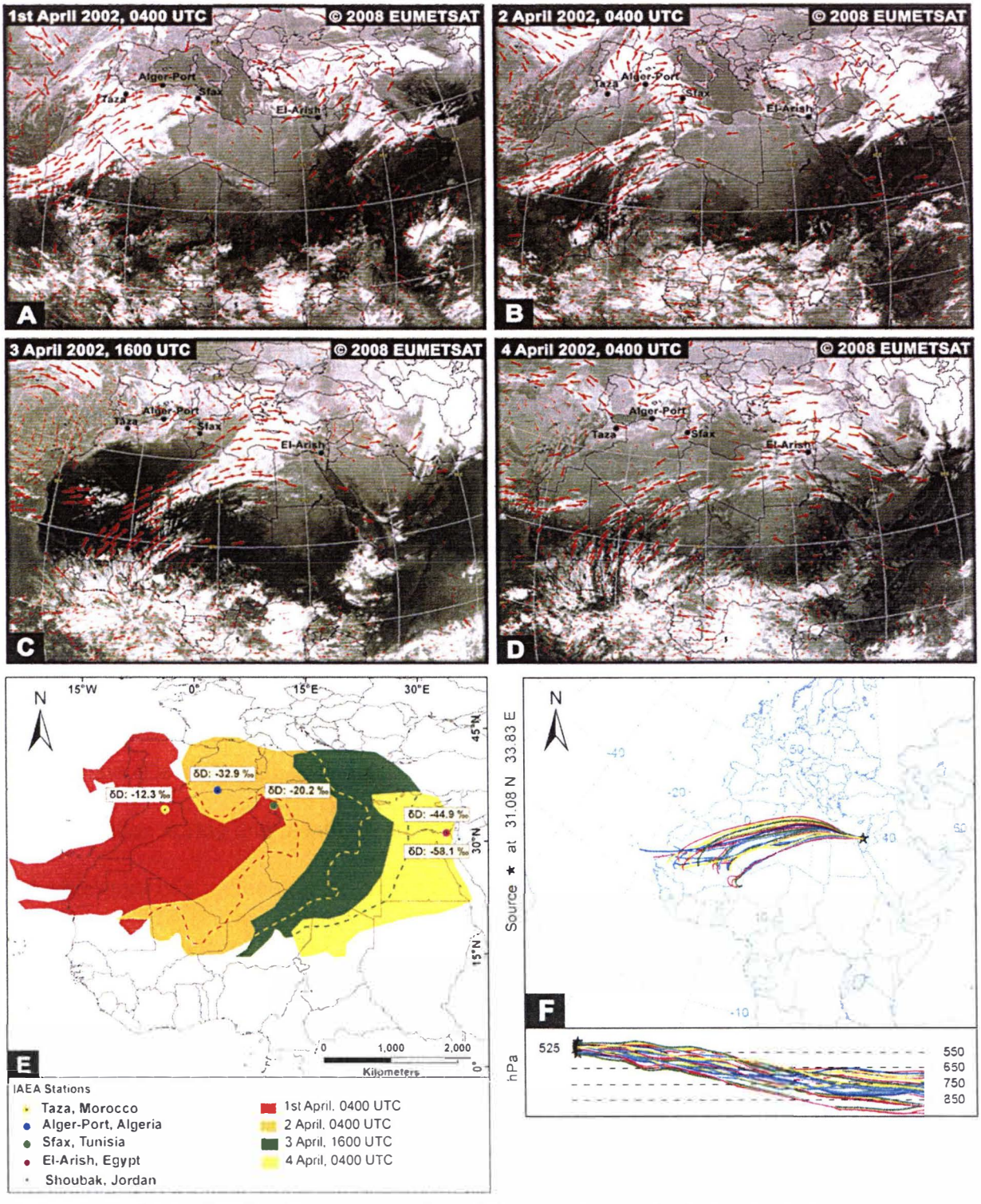

Figure 25: Cloud distribution extracted from Meteosat-7 and wind vectors for a precipitation event resulting from a westerly event reported on April 1–4, 2002.

The clouds continued along a northeast-trending trajectory, crossing Libya by April 3 (1600 UTC). Finally, by April 4 the clouds progressed to cover most of northern Egypt and Jordan (Fig. 25 D). Precipitation occurred on April 1 over the Taza (11.94 mm) and Sfax (0.51 mm) stations, on April 2 over the El-Arish station (2.03 mm), and on April 3 over the Alger-Port station (4.06 mm). The spatial distribution of clouds that showing in (Fig. 25 A–D) was portrayed as overlapping polygons using GIS methodology (Fig. 25 E). Additionally, the backward trajectories of the clouds were calculated 72 hours backwards in time starting from El-Arish, on April 4th, 2002 at 0400 UTC (Fig. 25 F).

5.3 Precipitation Events from Cyclones

The most depleted ($\delta^2H = -56.85‰$) of all the examined isotopic records in Egypt was reported from the Cairo station for the month of December 1987. Only two rainy days (December 20: 2.03 mm; December 23: 5.08 mm) were recorded from the Cairo station during that month. Examination of temporal Meteosat images revealed the presence of a cyclone centered over Cairo starting on December 20, 1987, and ending on December 23, 1987 (Fig. 26 A-D). The spatial distribution of clouds that showing in (Fig. 26 A–D) was portrayed as overlapping polygons using GIS methodology (Fig. 26 E). Additionally, the backward trajectories of the clouds were calculated 72 hours backwards in time starting from Cairo, on December 24, 1987 at 1000 UTC (Fig. 26 F)

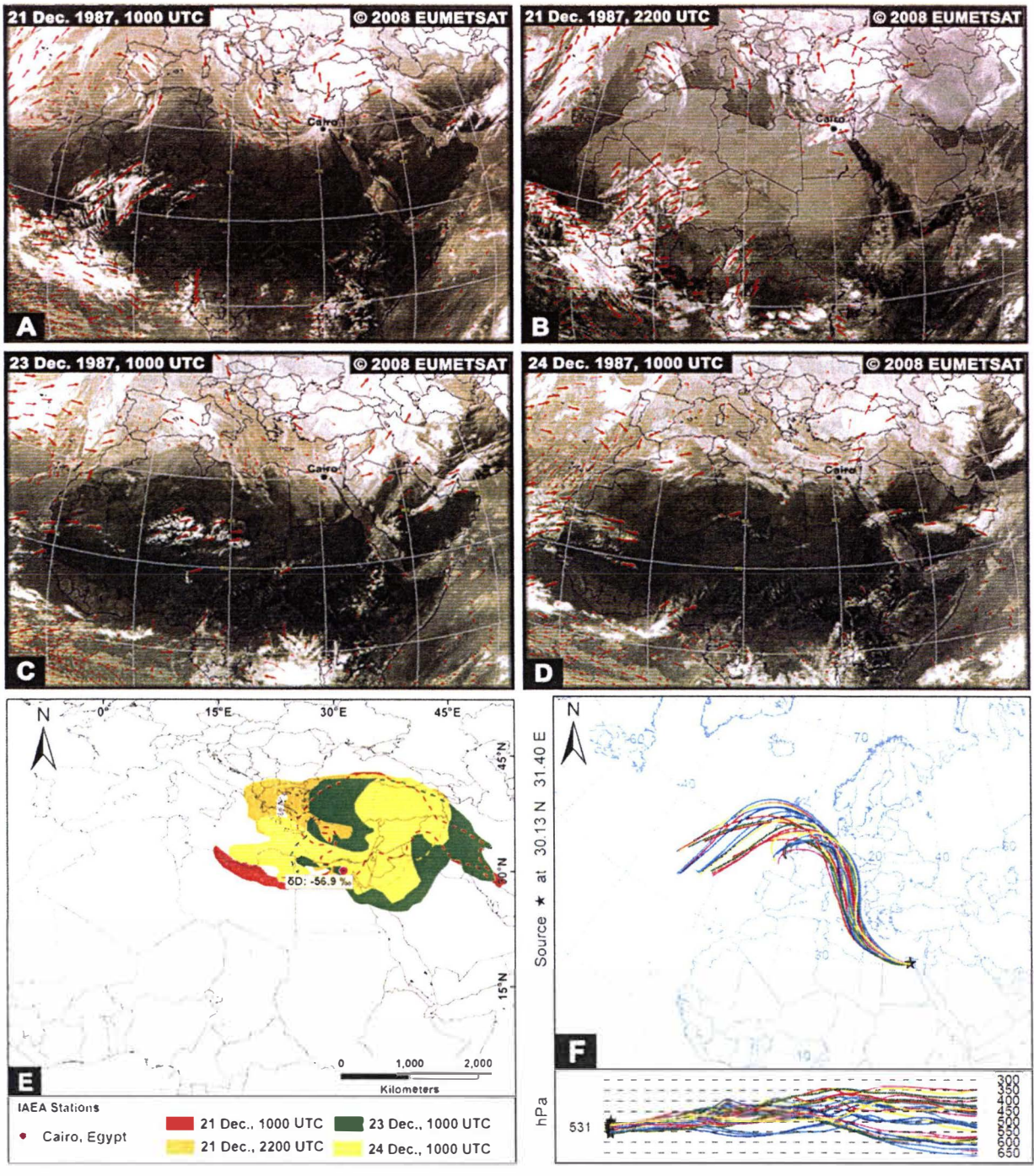

Figure 26: Cloud distribution extracted from Meteosat-2 and wind vectors for a precipitation event resulting from a cyclonic event reported on Dec. 21–24, 1987.

CHAPTER VI

NOBLE GASES PALEOTHERMOMETER

6.1 Overview

To substantiate the findings from the previous two stages, this stage of study was applied to investigate the paleo-recharge temperatures of the groundwater in the Nubian Aquifer. If the fossil groundwater were precipitated during cool glacial periods through intensification of paleowesterlies, one would expect (1) groundwater ages indicative of deposition during glacial Pleistocene periods; (2) depleted isotopic compositions and (3) lower recharge temperatures compared to the modern Mean Annual Air Temperature (MAAT). Therefore, a field trip was performed in June 2010 to sample groundwater from deep wells that tap the Nubian Aquifer beneath the Egyptian Sinai Peninsula (SP). Although, the NSAS is considered as non-renewable (fossil), the recent findings from the Nubian Aquifer that underlies SP showed that the aquifer is still receiving modern recharge locally at the foothills of the crystalline basement terrains under the current dry climatic conditions (Sultan et al., 2011). Thus, SP has been selected as a test site due to its accessibility and the proximity of the sampling wells to the elevated recharge areas, so the hydraulic connection between fossil groundwater and modern rainfall can be well addressed. In this chapter, a robust three-fold analysis was used to: (1) determine the routes of the general groundwater flow from the recharge areas at the foothills of the basement mountainous terrain in the SP using the available well data and the measured stable isotopic compositions of

the fossil groundwater; (2) age date the fossil groundwater using radiocarbon ^{14}C analysis to identify the paleorecharge periods; and (3) determine the paleotemperatures over the recharge areas using dissolved noble gas concentrations and through comparison to the modern MAAT.

6.2 Description of Study Area

Sinai Peninsula is located northeastern Egypt and constitutes 6% (about 61,000 km^2) of the total area of Egypt and it acts as a bridge connecting Asia and Africa continents. It is an arid desert with an average annual rainfall of 40 mm/yr, however the northern territory along the Mediterranean coast can receive 100 mm/yr and the southern mountainous highlands can receive up to 76 mm/year. The rainfall usually occurs in winter during short periods, sometimes causing flash floods caused mainly by cyclonic winter storms tracking southeast passing over the Mediterranean depressions (EMA, 1996; Geb, 2000). The amount of rainfall that is necessary to produce flash flood between 1320 m^3/s and 1660 m^3/s was estimated in Wadi Isla, southern SP to equal ~102-125 mm using a calibrated rainfall-runoff SWAT model (Kehew et al., 2010). Geomorphologically, SP is divided into three distinct regions; the southern elevated Precambrian mountainous terrains, the central high plateau area which is composed of Upper Cretaceous limestone and the northern large mountain and hilly blocks of the Syrian Arc Zone bordered by sand dunes and coastal plain lowlands (Said, 1962; JICA, 1992). The general gradient of the three regions slopes northward towards the Mediterranean Sea. Geologically, there are two main groups of

rock units that crop out over the SP: (1) Neoproterozoic (550-900 Ma) volcano-sedimentary basement rocks are located in southern SP and can be considered part of the Arabian-Nubian Shield Massif, and (2) overlying thick Phanerozoic cover (Sultan et al., 1988; Stern and Kroner, 1993). The latter unit can be divided into three formations exposed from south to north as follows (JICA, 1999): (a) gently inclined sedimentary rocks from Paleozoic to Eocene covering central Sinai, (b) strongly folded Triassic to Cretaceous Formations and unfolded Paleocene and Eocene formations covering North Sinai folded belt, and (c) Quaternary deposits particularly sand dunes covering the North Sinai foreshore region. The Nubian Aquifer is composed of unfossiliferous continental sandstones of Lower Cretaceous age intercalated with shales of shallow marine and deltaic origin resting unconformably on the Precambrian basement rocks (Shata, 1982). The aquifer is overlain by a calcareous sequence of limestones, dolostones, chalks and marls which belong to the Middle Calcareous Division of Cenomanian to Upper Eocene age (Said, 1962). The lower Cretaceous sandstones in SP are represented by the Malha Formation (Abdallah and Adidani, 1963), which crops out at two locations (Fig. 27): (1) the foot hills of the southern fractured basement terrains where the fracture networks enhance transmission loss of the modern meteoric water to recharge the groundwater of Nubian Aquifer; and (2) marine Lower Cretaceous sediments which are exposed in northern Sinai where they are known as the Risan Aneiza Formation (Said, 1971).

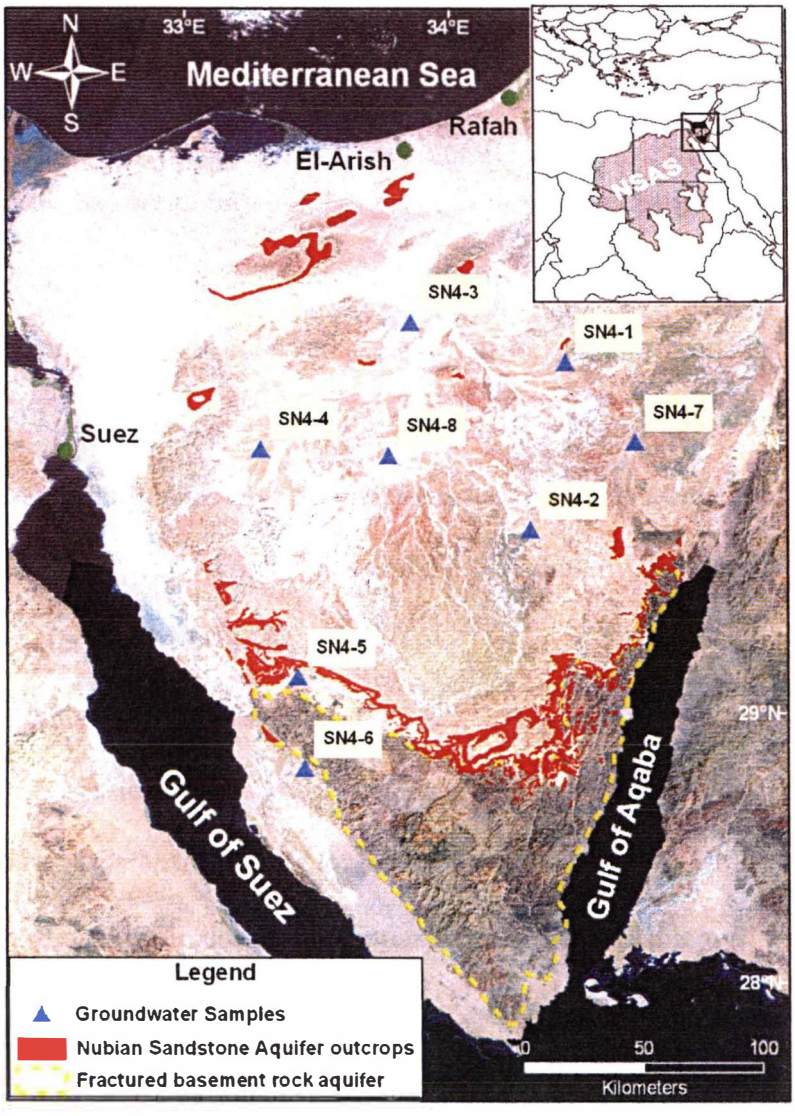

Figure 27: Well location map of Sinai Peninsula, Egypt showing the boundary of the fractured basement rocks, the Nubian Aquifer outcrops and deep groundwater wells on LANDSAT-TM image (USGS, 2003). Sample names are given in (Table 5).

6.3 Groundwater Sampling

Groundwater samples from eight locations were collected from deep productive pumping wells evenly distributed over the south central part of SP (Fig. 27). Based on penetration depth, the collected samples can be divided into two main groups, Group I and Group II. Wells from the former group are collected from deep

(700 - 1200 m) groundwater wells (e.g., Arif El Naqa 2, El Themed 2, El Hasana 3, Sudr El Hetan 3, El Kuntella 3 and Nekhel 5), while the latter group have shallower depths (~400 m) as they are in proximity to the high elevated recharge area (e.g., El-Rueikna 3 and Feiran 3). The discharge temperatures for all well waters range from 27 to 39 °C. Four samples were collected at each well for: 1) cations, anions and total alkalinity; 2) stable isotope ratio analysis for hydrogen and oxygen; 3) radiocarbon for age dating analysis; and 4) dissolved noble gas concentrations to extract the recharge temperatures. The analytical method and sampling procedure for each analysis were explained in Chapter II.

6.4 Results and Discussion

6.4.1 Stable Isotope Compositions and Radiocarbon Ages

Groundwater flow directions were inferred from the available well data (Table 5 and Fig. 28). The groundwater heads show a remarkable decrease from > 400 m (AMSL) at the southwestern part of SP to < 50 m (AMSL) in the northern parts indicating that the general groundwater flow in the Nubian Aquifer is occurring from the southern outcrops at the foothills of the basement rocks towards the northern regions, the northeastward towards Gulf of Aqaba, and the northwest towards the Gulf of Suez. This pattern of flow mimics the northward dip of the paleosurface of the Arabo-Nubian shield with the overlying sediments (Jenkins, 1990) and is similar to the regional groundwater flow in the NSAS underlying the WD of Egypt (Thorweihe, 1990).

Table 5: Sample locations, isotopic data for the deep groundwater wells collected from Sinai Peninsula, and conventional ^{14}C ages.

ID	Name	Latitude (N)	Longitude (E)	Altitude (m)	TD[a] (m)	DTW[b] (m)	δ^2H ‰	$\delta^{18}O$ ‰	^{14}C (pmC)	^{14}C yr BP/± (UGAMS#)[c]
SN4-1	Arif El Naqa 2	30° 18.21`	34° 26.30`	443	870	271	–49.3	–7.62	2.42 ± 0.03	29,910 ± 90 (7643)
SN4-2	El Themd 2	29° 40.80`	34° 18.20`	628	747	377	–52.3	–7.7	3.90 ± 0.03	26,060 ± 70 (7342)
SN4-3	El Hasana 3	30° 26.99`	33° 51.06`	236	1200	200	–51.6	–7.19	2.70 ± 0.03	29,000 ± 80 (7644)
SN4-4	Sudr El Hetan 3	29° 58.70`	33° 16.95`	447	1040	270	–53	–7.85	1.82 ± 0.02	32,190 ± 100 (7645)
SN4-5	El Rueikna 3	29° 08.06`	33° 25.35`	490	–	56	–33.3	–5.89	46.30 ± 0.15	6,180 ± 30 (7646)
SN4-6	Feiran 3	28° 47.72`	33° 26.91`	325	366	50	–25.1	–4.88	–	1,740 ± 40 (178926)
SN4-7	El Kuntella 3	30° 00.38`	34° 42.04`	510	1121	353	–63.1	–8.85	2.03 ± 0.02	31,300 ± 100 (7647)
SN4-8	Nekhel 5	29° 57.27`	33° 46.08`	398	1200	201	–61.2	–8.81	2.49 ± 0.03	29,670 ± 90 (7648)

[a] Total depth data are collected from (JICA, 1999).
[b] Depth to water table data are collected from (JICA, 1999).
[c] Samples are analyzed at Center for Applied Isotopic Studies (CAIS), University of Georgia except SN4-6 (Feiran 3) is analyzed at Isotech Lab.

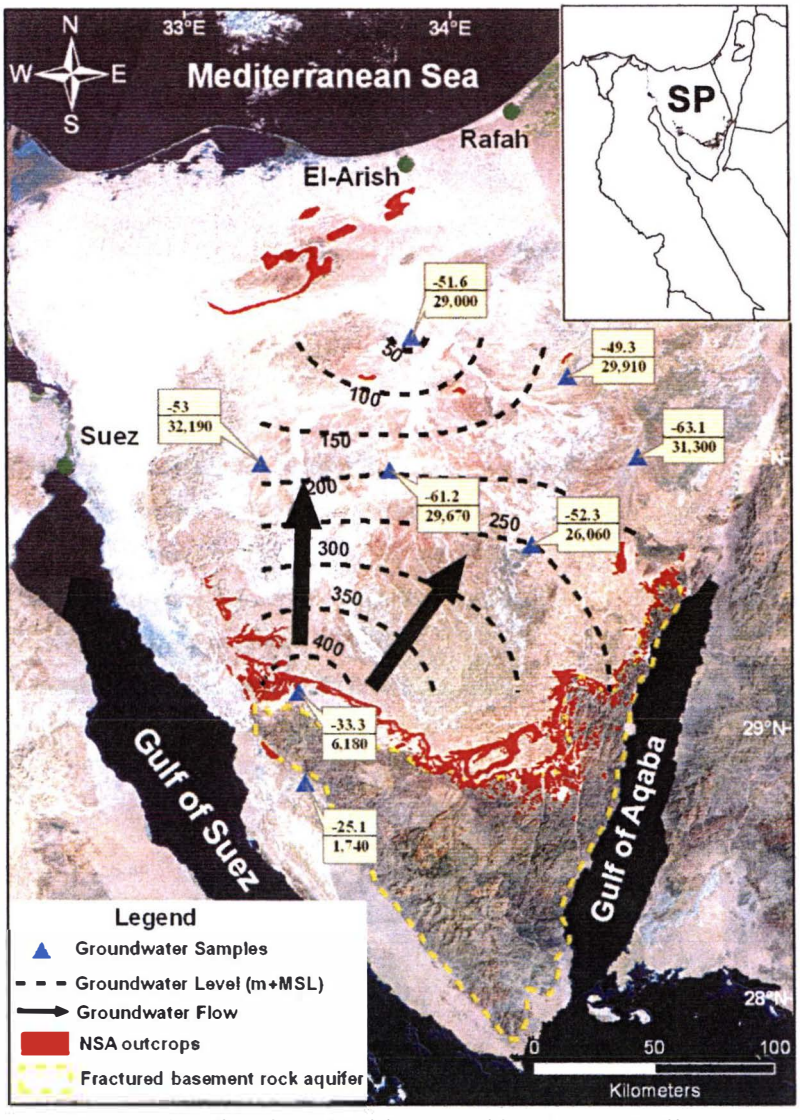

Figure 28: Groundwater levels of the Nubian Aquifer that underlies the central part of Sinai Peninsula. The groundwater flow directions are shown by the black arrows. The numerator indicates the δ^2H isotopic ratio and the denominator indicates the ^{14}C ages.

Insights into the origin and the timing of groundwater recharge were acquired from the analysis of stable isotopic compositions and radiocarbon ages (Table 5 and Fig. 28). The two group of waters that were collected from the Nubian Aquifer of the SP are plotted on the GMWL graph (Fig. 29) in addition to three other waters,

namely: (1) groundwater samples collected from NSAS of WD (Sultan et al., 1997; Sturchio et al., 2004); (2) groundwater samples collected from fractured basement aquifer in the SP (Sultan et al., 2011); and (3) average isotopic composition of modern rainfall collected from Rafah and El-Arish meteorological stations (IAEA and WISER, 2010).

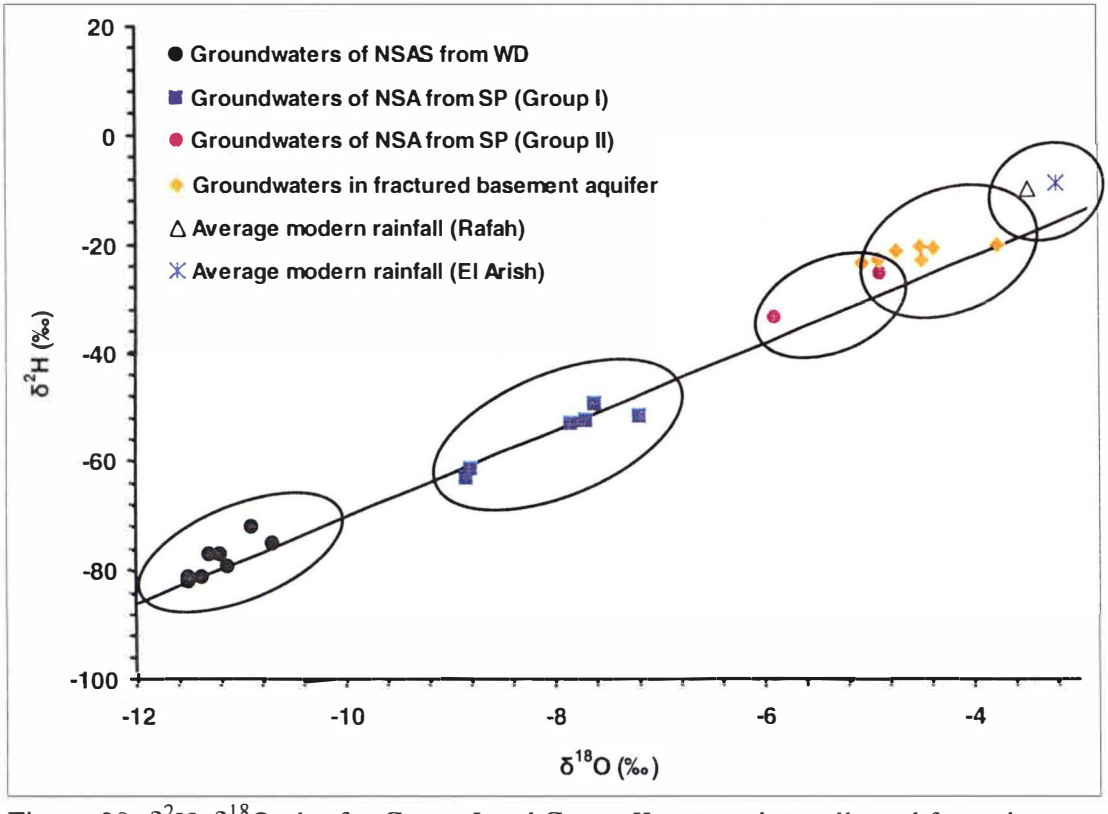

Figure 29: δ^2H–$\delta^{18}O$ plot for Group I and Group II waters that collected from the Nubian Aquifer of Sinai Peninsula. Also shown: (1) the highly depleted groundwater samples collected from NSAS of Western Desert (Sultan et al., 1997; Sturchio et al., 2004); (2) highly enriched groundwater samples from fractured basement rocks in southern SP (Sultan et al., 2011); and (3) average composition of modern rainfall from Rafah and El-Arish meteorological stations (IAEA and WISER, 2010). Also shown is the Global Meteoric Water Line ($\delta D = 8\ \delta^{18}O + 10$) of Craig (1961).

Investigation of Fig. 29 shows that Group I samples have depleted isotopic compositions ($\delta^{18}O$: –8.9 to –7.2‰; $\delta^{2}H$: –63.1 to –49.3‰) compared to Group II samples which have enriched isotopic compositions ($\delta^{18}O$: –5.9 to –4.9‰; $\delta^{2}H$: –33.3 to –25.1‰). Additionally, Group I waters are less depleted compared to those collected from the same aquifer in the WD indicating mixing of the Nubian Aquifer waters in SP with enriched modern waters. While Group II waters are very close to those collected from the fractured basement aquifer indicating that the Nubian Aquifer in SP is replenished by meteoric waters that precipitated over the recharge area that cropping out at the foothills of the basement terrains (Fig. 27).

The isotopic compositions of the two samples of Group II and those collected from the fractured basement aquifer are similar to those of average modern rainfall over the Rafah and El-Arish meteorological stations (Fig. 27). On the other hand, the depleted waters of Group I and those collected from WD were directly plotted on the same GMWL of the $\delta^{2}H$ vs. $\delta^{18}O$ plot (Fig. 29) which indicates both waters originated from meteoric waters recharged during a cooler period than the present (Gat et al., 1969). The analysis of the radiocarbon ages of the collected samples (Table 5) shows that the two groups of samples have two distinct ages. Waters of Group I are fossil and were deposited during the Late Pleistocene [ages: 26,060 ± 70 ^{14}C yr BP to 32,190 ± 100 ^{14}C yr BP], while Group II waters are younger and were deposited during the Holocene [ages: 1,740 ± 40 ^{14}C yr BP to 6,180 ± 30 ^{14}C yr BP]. The younger ages of the latter group are attributed to modern recharge to the Nubian Aquifer from the southern fractured basement rocks. Additionally, there is an obvious

progressive depletion trend in the isotopic composition of the collected samples (R^2=0.59; Fig. 30a) and an apparent gradual increase in the age of groundwater with distance from the recharge areas (R^2=0.83; Fig. 30b).

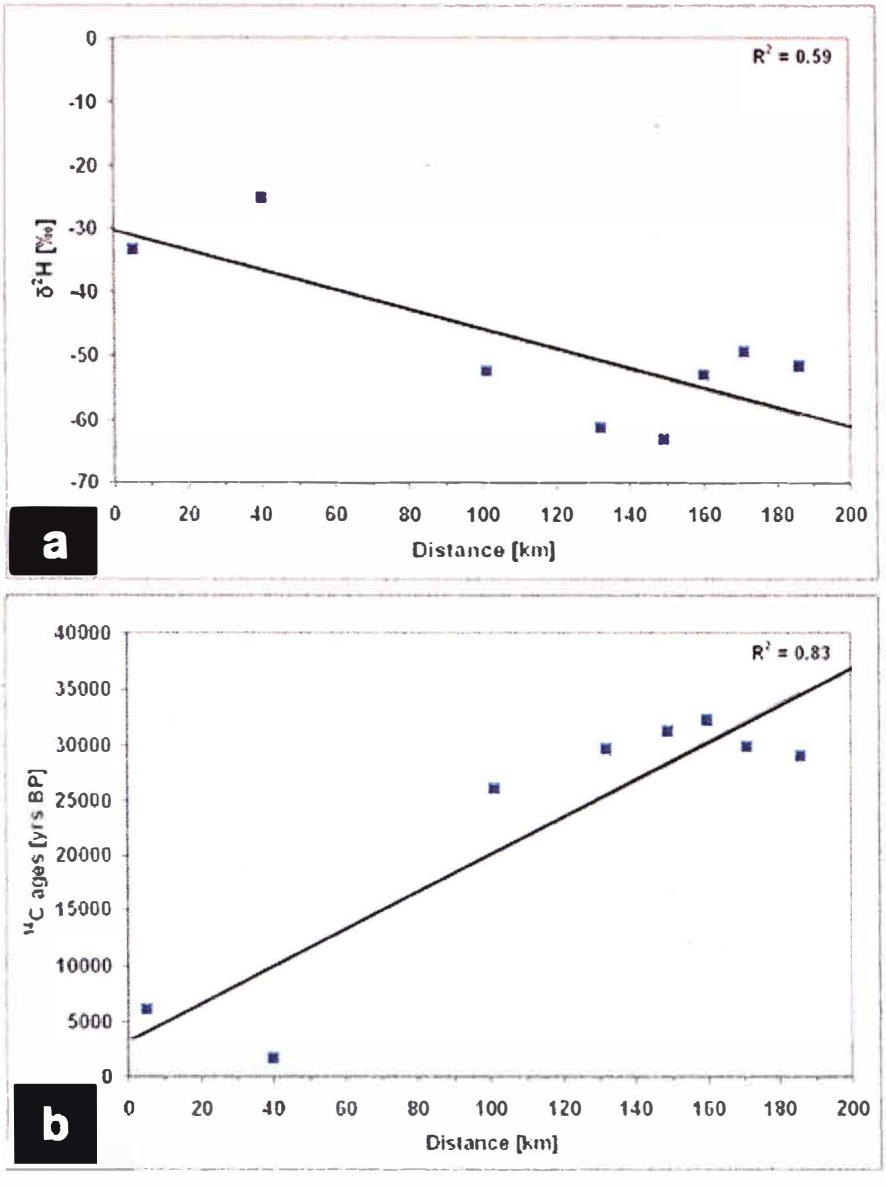

Figure 30: (a) Plot of δ^2H with horizontal distance from the Nubian Aquifer outcrops (recharge area) over the central SP. (b) Plot of ^{14}C radiocarbon ages as a function of horizontal distance from the recharge area.

6.4.2 Noble Gas Recharge Temperatures (NGTs)

Dissolved noble gas concentrations (He, Ne, Ar, Kr, and Xe) in groundwater have been used successfully in many paleoclimatic studies in conjunction with ^{14}C age dating to determine the recharge temperatures during the Quaternary (Mazor, 1972; Stute and Schlosser, 1993; Kipfer et al., 2002; Klump et al. 2007). The atmospheric noble gases are incorporated into groundwater by exchange between recharge water and soil air within the unsaturated zone. As the water enters the saturated zone, gas exchange stops and the noble gas concentrations are kept by the water as a tracer for the environmental conditions prevailing during infiltration. Because noble gases are conservative and inert, the atmospheric noble gas concentrations are preserved in groundwater. Given the fact that the solubility of the noble gases significantly depends on the water temperature during gas exchange particularly for Ar, Kr and Xe (Mazor, 1972). Hence, the dissolved noble gases in groundwater can potentially be used for temperature reconstruction. The governing equations for estimating the recharge temperatures from the noble gas concentrations are explained in (Solomon et al., 1998). The noble gas recharge temperatures (NGTs) were calculated from the measured four concentrations of (Ne, Ar, Kr, and Xe) dissolved in groundwater samples using RT-Calculator Spreadsheet Ver. 1 based on algorithms describe in (Manning and Solomon, 2003), which is used in the Dissolved and Noble Gas Laboratory, University of Utah (Table 6).

Table 6: Data of noble gas concentrations of seven deep groundwater wells collected from SP, and other well parameters measured in the field and in the Laboratory to calculate the NGTs.

ID	Name	He [10^{-7}] cc STP/g	Ne [10^{-7}] cc STP/g	Ar [10^{-4}] cc STP/g	Kr [10^{-8}] cc STP/g	Xe [10^{-8}] cc STP/g	Well Temp (°C)	TDS[a] (‰)	NGT[b] (°C)
SN4-1	Arif El Naqa 2	5.71	2.49	3.23	6.57	0.88	33.6	3.81	20.62
SN4-2	El Themd 2	7.49	7.15	5.5	10.2	1.1	30.5	1.83	21.09
SN4-3	El Hasana 3	9.14	2.11	3.13	7.58	0.94	39.1	3.26	17.51
SN4-5	El Rueikna 3	1.01	2.03	2.97	6.77	0.87	27.2	0.48	20.63
SN4-6	Feiran 3	1.82	2.03	2.72	6.04	0.74	29.5	0.85	26.21
SN4-7	El Kuntella 3	533	22.9	15.6	23.1	2.15	33.6	1.82	18.07
SN4-8	Nekhel 5	22.9	6.09	5.9	11.8	1.15	38.6	1.62	22.03

[a] Total dissolved solids are estimated from sum of total cations and anions dissolved in the sample (Appendix C)
[b] Noble gas recharge temperatures are calculated using (RT-Calculator Ver. 1) used at Dissolved and Noble Gas Laboratory, University of Utah.

The obtained values of the (NGTs) were further tested and validated using multiple algorithms and modeling spreadsheets based on a weighted least square fitting technique and excess air fractionation (Table 7).

Table 7: Comparison of the noble gas recharge temperatures (NGTs) of seven groundwater samples using four different algorithms collected from multiple sources (see table footnotes).

		NGTs (°C)			
ID	Name	RT-Calculator[1]	PALEOTEMP[2]	WNOSALT[3]	NOBLE90[4]
SN4-1	Arif El Naqa 2	20.62	21.36 ± 0.7	21.26	20.39 ± 0.42
SN4-2	El Themd 2	21.09	20.55 ± 2.51	20.58	20.33 ± 1.55
SN4-3	El Hasana 3	17.51	16.82 ± 1.9	17.49	16.74 ± 1.25
SN4-5	El Rueikna 3	20.63	20.44 ± 1	20.34	20.29 ± 0.66
SN4-6	Feiran 3	26.21	26.31 ± 1.3	25.89	25.81 ± 0.88
SN4-7	El Kuntella 3	18.07	4.14 ± 5.9	8.91	18.07 ± 2.49
SN4-8	Nekhel 5	22.03	10.57 ± 4.99	13.21	12.82 ± 3.79

[1] RT-Calculator Ver.1 is a spreadsheet used at the Dissolved and Noble Gas Laboratory, University of Utah.
[2] PALEOTEMP is an algorithm written with *MATHEMATICA*® software, based on (Pinti and Van Drom, 1998).
[3] WNOSALT is a model fitting program based on (Ballentine and Hall, 1999).
[4] NOBLE90 program Ver.9.0 developed by Frank Peeters and the ideas behind the program have been described in (Aeschback-Hertig et al., 1999).

The PALEOTEMP is an algorithm written with *MATHEMTICA*® software and described by (Pinti and Van Drom, 1998); the WNOSALT is a simple unfractionated air model to calculate (NGTs) based on mathematical methods described in (Ballentine and Hall, 1999); and the NOBLE90 program of the MATLAB-routine was

developed by (Aeschbach-Hertig et al., 1999). As the solubility of the atmosphere-derived noble gas concentrations are reduced by dissolved salts (Mazor, 1972; Pinti and Van Drom, 1998), these programs and algorithms take into account the effect of the salinity of the groundwater samples. Usually the effect of salinity can be neglected for fresh waters but the TDS values of the collected samples were incorporated as they range from 480 to 3800 mg/l (Table 6). On the other hand, the solubility of noble gases is dependent on the atmospheric pressure of each gas, so the elevation of the recharge area (altitude) was also incorporated into the program. The average elevation of the recharge area in south-central SP was estimated from the Digital Elevation Model (DEM) to be 761 m (AMSL). The NGTs derived from the three algorithms (PALEOTEMP, WNOSALT, and NOBLE90) were well matched those derived from the RT-Calculator except for two samples (SN4-7 and SN4-8), due to the high concentrations of He and Ne compared to the other samples.

The NGTs derived for the Group I waters range between 17.5° ± 1.3°C for the El-Hasana-3 well (SN4-3) to 22.03° ± 3.8°C for the Nekhel-5 well (SN4-8). The values of NGTs for Group II waters range between 20.6° ± 0.7°C for El-Rueikna-3 well (SN4-5) to 26.2° ± 0.9°C for Feiran-3 well (SN4-6). The calculated mean NGTs value of Group I waters is 19.9 °C and that for Group II is 23.9 °C. The mean value for the former group is well matched what was measured (20 °C) in the Dakhla Basin, Western Desert of Egypt (Patterson, 2003). Additionally, the two mean values were compared to the modern MAAT over the recharge area to infer whether glacial or interglacial periods prevailed during the recharge regime over the Nubian aquifer.

The modern MAAT over the recharge area was estimated (~23 °C) using the available temperatures data of five nearby meteorological stations covering south-central the SP (Ras Sudr, Nekhel, Taba, Sharm El-Sheikh and El-Tor) (Table 8). The Thiessen polygons tool that is included in the ESRI's ArcMap 9.3.1 software was used to calculate the modern MAAT value (Fig. 31). By using this tool, the study area was divided into five proximal zones that are affected by the enclosed station.

Table 8: Calculation of the modern average weighted temperature over central SP using Thiessen polygon technique in ArcMap 9.3.1.

Station Name	Latitude (N)	Longitude (E)	Temp[a] (°C)	Area[b] (km^2)	Area (%)	Temp[c] (°C)
Ras Sudr	29° 34.98`	32° 43.02`	20.6	245.72	18.24	3.76
Nekhel	29° 40.80`	34° 18.20`	17.8	47.48	3.52	0.63
Taba	30° 26.99`	33° 51.06`	25	694.56	51.56	12.89
El Tor	29° 58.70`	33° 16.95`	21.7	215.78	16.02	3.48
Sharm El Sheikh	29° 08.06`	33° 25.35`	21.7	143.43	10.65	2.31
T O T A L				1346.97	100	23.06

[a] Average temperature recorded over the past 35 years (WeatherReports.com).
[b] The Nubian sandstone outcrop surface area at each station delineated by Thiessen polygon.
[c] Average weighted temperature based on Thiessen polygons and calculated by: [Area (%) x Temp[a] (°C)]/100

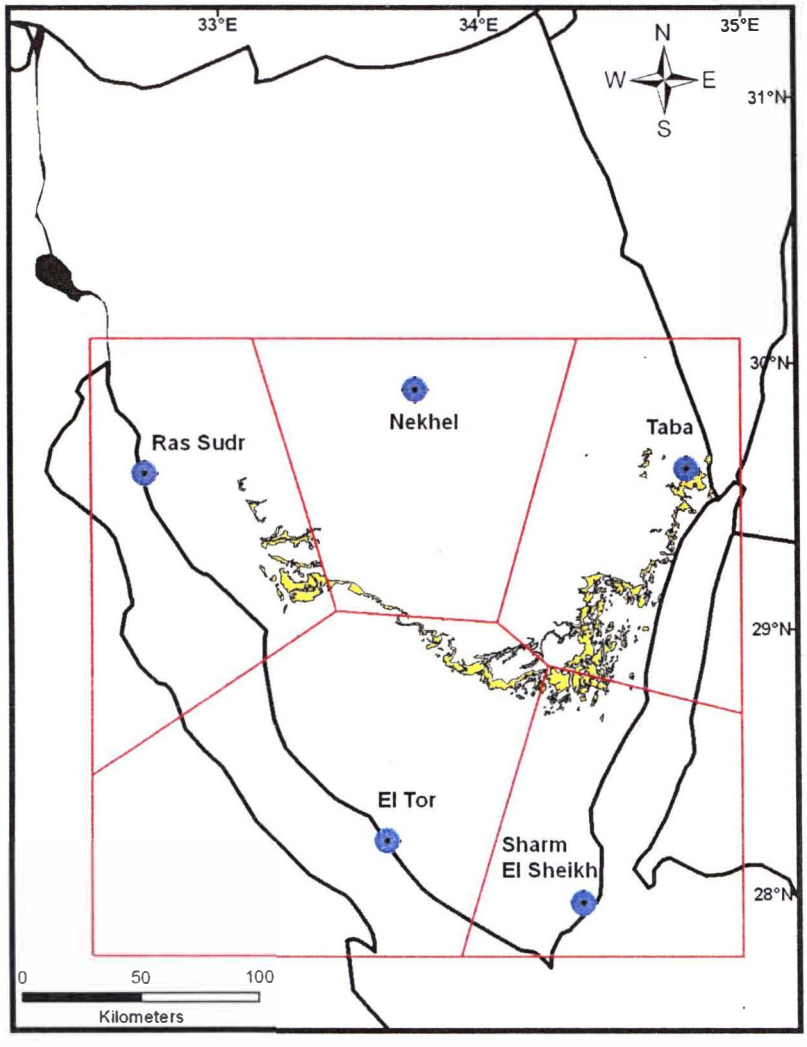

Figure 31: Graphical calculation of the modern mean weighted annual air temperature using Theissen method using five meteorological stations surrounding the Nubian Aquifer outcrops.

Examination of (Fig. 32) shows that the estimated noble gas recharge temperatures versus the ^{14}C ages for Group I samples (Late Pleistocene waters >10,000 yrs BP); Group II samples (Holocene waters <10,000 yrs BP); and three Holocene (4500-9000 yrs BP) groundwater samples collected from the Tertiary-Upper Cretaceous water-bearing formations that underlie southwestern Nile Delta, Egypt

(Aeschback-Hertig et al., 2006; 2007) provides a strong evidence of the prevalence of a cooler climatic regime during the late Pleistocene than the Holocene and present day climatic regimes. The concentrations of atmospheric noble gases indicate that the average groundwater temperature during the Late Pleistocene (Group I) was 4.0 °C lower than that of Holocene waters and 3.2 °C lower than that of present day over the recharge area.

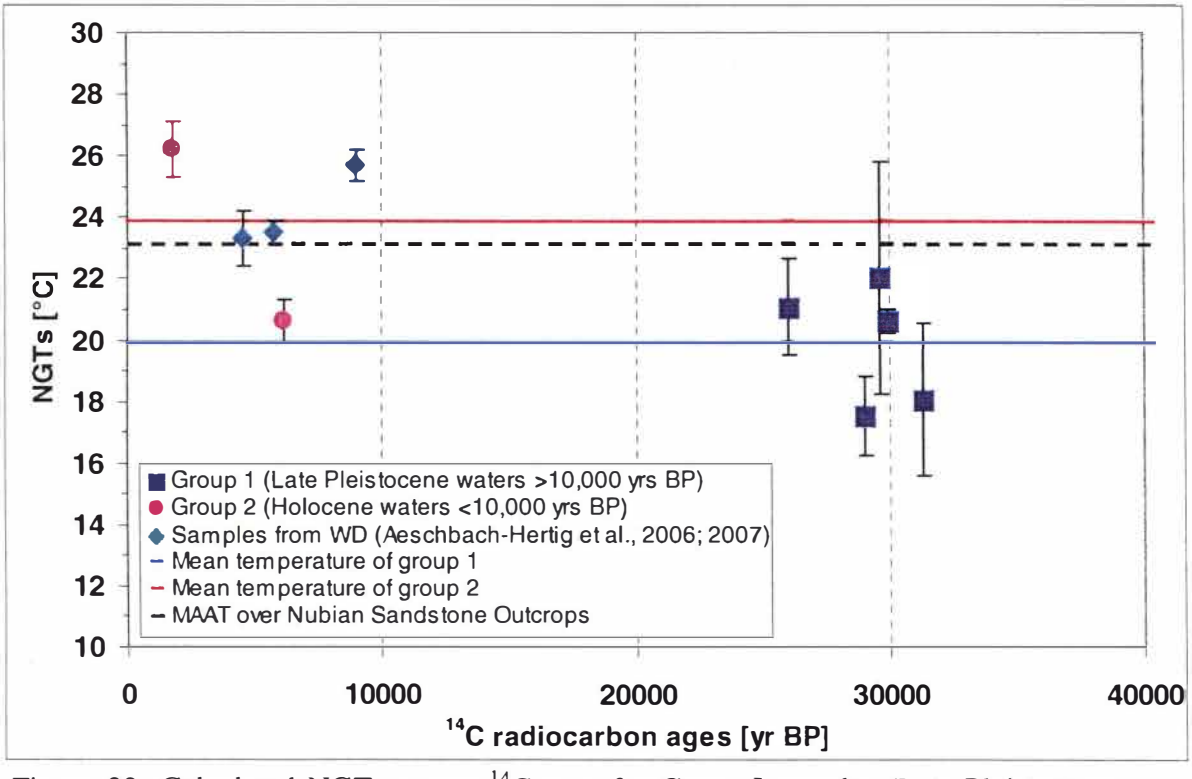

Figure 32: Calculated NGTs versus ^{14}C ages for Group I samples (Late Pleistocene waters > 10 k yrs BP); Group II (Holocene waters <10 k yrs BP) and three Holocene (4500-9000 yrs BP) groundwater samples collected from southwestern Nile Delta (Aeschbach-Hertig et al., 2006; 2007).

These findings are consistent with the previous work done on North African fossil groundwater aquifers. The recharge temperatures for the Northwestern Sahara Aquifer throughout a major recharge period that occurred 45,000 to 23,000 years ago

were estimated to be 2-3 °C lower than the modern MAAT (Guendouz et al., 1997). The Iullemeden Aquifer System was recharged between 28,000 and 23,200 years ago and the recharge temperatures were at least 5-6 °C lower than modern MAAT (Edmunds et al., 1999). The groundwater ages cited above correspond to glacial periods identified from North Atlantic marine record (Bond et al., 1993) and the extracted recharge temperatures are generally lower than modern MAAT in the investigated areas by 2-7 °C. Such lower temperatures are to be expected if the recharge was from precipitation during cool glacial periods.

CHAPTER VII

SUMMARY AND CONCLUSIONS

Comparisons of the stable isotopic composition of fossil water to modern precipitation showed that modern precipitation across the entire North African region is enriched compared to the fossil waters in these areas. Such depletions in the fossil water isotopic compositions are expected if the groundwater residing in these fossil aquifers resulted from precipitation during cooler glacial periods and are inconsistent with precipitation during interglacial warm periods. Such depleted values, compared to modern precipitation, suggest that the air mass history of precipitation recharging the fossil aquifers was different from what is normally the case today.

These suggestions are further supported by low recharge temperatures extracted from the concentration of dissolved noble gases in the Sahara fossil groundwater and the ^{14}C ages of the groundwater. Recharge temperatures for the Northwestern Sahara Aquifer throughout a major recharge period that occurred 45,000 to 23,000 years ago were estimated to be 2-3 °C lower than the current MAAT (Guendouz et al., 1997). The Iullemeden Aquifer System was recharged between 28,000 and 23,200 years ago and the recharge temperatures were at least 5-6 °C lower than modern MAAT (Edmunds et al., 1999). Age dating and noble gas analyses for groundwater from the Nubian Aquifer in Sinai indicated the aquifer was recharged 31,000 to 26,000 years ago and the recharge temperatures were ~3 °C lower than the current MAAT (Abouelmagd et al., 2011). The groundwater ages cited above

correspond to glacial periods identified from North Atlantic marine record (Bond et al., 1993) and the extracted recharge temperatures are generally lower than the current MAAT in the investigated areas by 2-7 °C. Such lower temperatures are to be expected if the recharge was from precipitation during cool glacial periods.

A progressive west-to-east isotopic depletion of the fossil aquifers of North Africa can be argued to be due to an enhanced "continental effect". In this explanation, the observed isotopic patterns are best explained by the classical Rayleigh type rain out process associated with water vapor from wet oceanic air masses travelling across wide stretches of the continent (Abouelmagd et al., 2012). As described earlier glacial models call on southward migration and intensification of paleowesterly regimes bringing moisture over North Africa (Sonntag et al., 1978; Bradley, 1999). The observed west-to-east pattern of isotopic depletion in the composition of the fossil groundwater in North Africa is similar to that observed in modern precipitation over southern Europe; this suggests that similar wind regimes might have extended as far south as the northern parts of Saharan Africa during previous wet climatic periods (Sonntag et al., 1978).

To better understand the nature of the wind regimes that produce the west-to-east isotopic depletions, I searched for modern analogs. Precipitation events were selected that cover the entire range of isotopic variations that were observed in modern precipitation recorded from the IAEA stations over Egypt and monitored the propagation of clouds that produced these events using temporal satellite imagery. My analysis indicates that the overwhelming majority of modern rain events over Egypt

were precipitated from northerly to northwesterly wind regimes and that these regimes produce precipitation with intermediate to enriched isotopic compositions (–39.7‰ to +34.6‰). However, I documented rare precipitation events (5 of 165 events) that produced depleted isotopic compositions (δ^2H: –56.9‰ to –43.7‰) approaching those of the fossil Nubian Aquifer groundwater (δ^2H: –86‰ to –53‰). Four of the five isotopically depleted precipitation events were found to be related to clouds that were generated over the Atlantic Ocean, and then traveled inland in an eastward direction, across the North African Sahara Desert, starting from Morocco, and crossing Algeria, Tunisia, and Libya, and finally reaching Egypt. I speculate that similar westerly wind regimes could have been the main source of precipitation during wet climatic periods that led to the recharge of the North African fossil groundwater aquifers during the glacial humid periods in the Pleistocene and early Holocene. I acknowledge the differences in vegetative cover, temperature, solar insolation, and source composition between present and glacial periods, yet maintain that such differences are unlikely to obscure the west to east isotopic trend described earlier. The suggested Atlantic source region was perhaps enriched by 1-1.5 ‰ in oxygen and correspondingly in hydrogen at maximum glacial conditions due to lowering of the sea level during glacial times (Fairbanks, 1989). This will not have any impact on the continental effect proposed here although it may affect the deuterium excess values at the source (Pfahl and Wernli, 2008). It is also likely that there was extensive vegetation cover over land along the air mass transport regions

during glacial times. This again will only have a modifying effect on the Rayleigh process (Rozanski et al, 1982; Krishnamurthy and Bhattacharya, 1991).

In search for potential modern analogs, I describe the North Atlantic Oscillation (NAO), that controls the temperature, moisture flux, and the wind patterns across North Africa and discuss their potential relevance to glacial periods. The NAO is the fluctuation in relative air pressure differences between a persistent low-pressure region centered around Iceland and a persistent high-pressure region centered around the Azores Islands in the subtropical Atlantic Ocean. This fluctuation controls wind strengths and wind directions, across the North Atlantic (Barnston and Livezey, 1987; Hurrell, 1995; Hurrell et al., 2003). When the pressure difference is relatively high (i.e., positive NAO index), westerly winds are strong and bring mild temperatures and moist weather to central Europe; when the pressure difference is relatively low (i.e., negative NAO index), central and northern Europe remain cold and westerly winds shift southward to bring mild and wet winter weather to the Mediterranean and North Africa. Moreover, I speculate that recharge of the Nubian Aquifer fossil waters may have been favored by a predominance of negative NAO index conditions for extended periods during recharge events that may have lasted for thousands of years. The decadal-scale synchronicity of the NAO index and climate variability in the Eastern Mediterranean and Ethiopian Highlands has been discussed recently in terms of the mechanism of teleconnection and its implications for climate prediction (Feliks et al., 2010). The hydrogeological impact of such climate variability persisting over longer time scales has been considered by several authors (e.g., Schroder and Rosbjerg,

2004; Holman et al., 2009). Further investigations are recommended to investigate the nature and the potential role of NAO throughout glacial periods.

On the basis of my findings and those of others reported in this work, I advocate the following: (1) during glacial periods paleo-westerly wind regimes intensified and migrated southward bringing moisture to North Africa, perhaps during periods of prolonged negative NAO; inter-tropical convergence zone (ITCZ) moved southward preventing moisture-bearing winds from the Gulf of Guinea from reaching southern Sahara (Sonntag et al., 1978; Sultan et al., 1997; Bradley, 1999; Brookes, 2003; Smith et al., 2004); (2) during interglacial periods, the ITCZ migrated northward increasing monsoonal precipitation in central and southern Africa (e.g., Rossignol-Strick, 1983; Prell and Kutzbach, 1987; Yan and Petit-Maire, 1994; Osmond and Dabous, 2004), however, the northward extent of the ITCZ during pluvial phases remain uncertain (Kieniewicz and Smith, 2009); and (3) while there is hardly any doubt that the intensification of the precessionally-forced tropical and subtropical monsoon circulation is largely responsible for paleo-wet periods over large segments of Africa, it is unlikely that these regimes could have advanced during these periods as far north as the recharge areas of the North African fossil aquifers. More likely, it is the intensified paleowesterly wind regimes during glacial periods that brought about the wet periods to these areas and recharged its aquifers.

BIBLIOGRAPHY

Abouelmagd, A., Sultan, M., Kehew, A., Milewski, A., and Sturchio, N., 2011. Source of groundwater recharge over the Nubian Sandstone Aquifer, Sinai Peninsula, Egypt: Geochemical and geochronological constraints. Abstract PP21A-1767 presented at 2011 Fall Meeting, AGU, San Francisco, CA, 5–9 Dec.

Abouelmagd, A., Sultan, M., Milewski, A., Kehew, A., Sturchio, N., Soliman, F., Krishnamurthy, R.V., Cutrim, E., 2012. Toward a better understanding of palaeoclimatic regimes that recharged the fossil aquifers in North Africa: Inferences from stable isotope and remote sensing data. Palaeogeography, Palaeoclimatology, Palaeoecology 329–330, 137–149.

Aeschbach-Hertig, W., El-Gamal, H., Dahab, K., Friedrich, R., Kipfer, R., Hajdase, I., 2007. Identifying and dating the origin of groundwater resources in reclamation areas of Egypt. In: Advances in Isotope Hydrology and its Role in Sustainable Water Resources Management (HIS-2007), Proceedings of a Symposium, Vienna, IAEA, Vienna, STI/PUB/1310, Vol. 2: 395-403.

Aeschback-Hertig, W., El-Gamal, H., Dahab, K., Kipfer, R., Bonani, G., 2006. Environmental tracer study of groundwater recharge near the Nile Delta, Egypt. DPG-Fruhjahrstagung Heidelberg, E-Verhandl. DPG, UPI.6.

Ahrens, C.D., 2008. Essentials of meteorology: An invitation to the atmosphere. 5th Ed. Brooks/Cole, Belmont, CA, USA, 485p.

Almogi-Labin, A., Bar-Matthews, M., Ayalon, A., 2004. Climate variability in the Levant and northeast Africa during the Late Quaternary based on marine and land records. In: Goren-Inbar, Naama, Speth, John D. (Eds.), Human Paleoecology in the Levantine Corridor. Oxbow Press, Oxford, 117–134.

Ambroggi, R.P., 1966. Water under the Sahara. Scientific American 214, 21–29.

Bakhbakhi, M., 2002. Hydrogeological framework of the Nubian Sandstone Aquifer System. In: Managing Shared Aquifer Resources in Africa, ISARM-Africa, IHP-VI, Series on Groundwater 8, 177–201.

Bakhbakhi, M., 2006. Nubian Sandstone Aquifer System. IHP-VI, series on groundwater 10, 75–81.

Ball, J., 1927. Problems of the Libyan Desert. Geographical Journal 70, 21–38, 105-128, 209-224.

Barakat, M.G., Milad, G.S., 1966. Subsurface geology of Dakhla Oasis. Journal of Geology 10, 145–154.

Bar-Matthews, M., Ayalon, A., Gilmour, M., Matthews, A., Hawkesworth, C.J., 2003. Sea–land oxygen isotopic relationships from planktonic foraminifera and speleothems in the Eastern Mediterranean region and their implication for paleorainfall during interglacial intervals. Geochimica et Cosmochimica Acta 67 (17), 3181–3199.

Barnston, A.G., Livezey, R.E., 1987. Classification, seasonality and persistence of low frequency atmospheric circulation patterns. Monthly Weather Review 115, 1083–1126.

Barthel, K.W., Hermann-Degen, W., 1981. Late Cretaceous and Early Tertiary stratigraphy in the Great Sand Sea and its SE margins (Farafra and Dakhla oases), SW Desert, Egypt. Mitt. Bayer. Staats, Paleont. Hist. Geol. 21, 141–182.

Bartov, Y., Stein, M., Enzel, Y., Agnon, A., Reches, Z., 2002. Lake levels and sequence stratigraphy of Lake Lisan, the late Pleistocene precursor of the Dead Sea. Quaternary Research 57, 9–21.

Bar-Yosef, O., Meadow, R., 1995. The origins of agriculture in the Middle East. In: Price, T.D., Gebauer, A.B. (Eds.), The Last Hunters–First Farmers: Perspectives on the Prehistoric Transition to Agriculture. School of American Research Press.

Bond, G., Broecker, W., Johnson, S., McManus, J., Labeyrie, L., Jouzel, J., Bonani, G.B., 1993. Correlation between climate records from North Atlantic sediments and Greenland ice. Nature 365, 507-508.

Bouchaou, L., Michelot, J.L., Qurtobi, M., Zine, N., Gaye, C.B., Aggarwal, P.K., Mara, H., Zerouali, A., Taleb, H., Vengosh, A., 2009. Origin and residence time of groundwater in the Tadla basin (Morocco) using multiple isotopic and geochemical tools. Journal of Hydrology 379, 323–338.

Bowen, G.J., Revenaugh, J., 2003. Interpolating the isotopic composition of modern meteoric precipitation. Water Resources Research 39, 1299. DOI 10.129/2003WR002086.

Bradley, R.S., 1999. Paleoclimatology: Reconstructing Climates of the Quaternary. Academic Press, 610 pp.

Broecker, W.S., Oversby, V.M., 1971. Chemical equilibria in the Earth. McGraw-Hill, New York, 318 p.

Brookes, I.A., 2003. Geomorphic indicators of Holocene winds in Egypt's Western Desert: Geomorphology 56, 155–166.

Burdon, D.J., 1982. Hydrogeological conditions in the Middle East. Q. J. eng. Geol. London 15, 71–82.

Bzioui, M., 2004. Report on the development of the water resources in Morocco. UN Water Africa.

CEDARE (Center for the Environment and Development for the Arab Region and Europe), 2001. Regional strategy for the utilization of the Nubian Sandstone Aquifer System (groundwater model), Cairo.

CEDARE, 2002. Regional strategy for the utilization of the Nubian Sandstone Aquifer System. Center for the Environment and Development for the Arab Region and Europe, Cairo, Egypt 22–82.

Clark, I., Fritz, P., 1997. Environmental isotopes in Hydrogeology. CRC Press, Boca Raton, Florida, USA, 328 p.

Claussen, M., Gayler, V., 1997. The greening of Sahara during the mid-Holocene: results of an interactive atmosphere–biome model. Glob. Ecol. Biogeogr. Lett. 6, 369–377.

Cook, P.G., Herczeg, A.L., 2000. Environmental tracers in subsurface hydrology. Kluwer Academic Publishers, Boston.

Coplen, T.P., 1996. New guidelines for reporting stable hydrogen, carbon, and oxygen isotope-ratio data. Geochim. Cosmochim. Acta 60, 3359–3360.

Craig, H., 1961. Isotopic variations in meteoric waters. Science 133, 1702–1703.

Crombie, M.K., Arvidson, R.E., Sturchio, N.C., El Alfy, Z., Abu Zeid, K., 1997. Age and isotopic constraints on Pleistocene pluvial episodes in the Western Desert, Egypt. Palaeogeography, Palaeoclimatology, Palaeoecology 130, 337– 355.

Dabous, A.A., Osmond, J.K., 2001. Uranium isotopic study of artesian and pluvial contributions to the Nubian Aquifer, Western Desert, Egypt. Journal of Hydrology 243, 242–253.

Dansgaard, W. 1964. Stable isotopes in precipitation. Tellus, 16, 436–467.

Edmunds, W.M., 2005. Groundwater as an archive of climatic and environmental change. In, P.K. Aggarwal, J. Gat, and K. Froehlich (eds.) Isotopes in the Water Cycle: Past, Present and Future of a Developing Science. Springer. pp. 341-352.

Edmunds, W.M., Fellman, E., Goni, I.B., 1999. Lakes, groundwater and palaeohydrology in the Sahel of NE Nigeria, evidence from hydrogeochemistry. J. Geol. Soc. London 156, 345-355.

Edmunds, W.M., Wright, E.P., 1979. Groundwater recharge and palaeoclimate in the Sirte and Kufra basins, Libya. Journal of Hydrology 40, 215–241.

El-Baz, F., 1998. Sand accumulation and groundwater in the eastern Sahara. Episodes, 21(3): 147–151.

El-Baz, F., 2000. Satellite observations of the interplay between wind and water processes in the Great Sahara. Photogrammetric Engineering and Remote Sensing, Vol. 66, No. 6: 777–782.

El-Ramly, M.F., 1972. A new geological map for the basement rocks in the Eastern and Southwestern Deserts of Egypt. Annals of the Geol. Surv. Egypt 2, 1–18.

EMA, 1996. Climatic Atlas of Egypt. Egyptian Meteorological Authority, Ministry of Transport and Communications, Cairo, Egypt.

Epstein, S., Mayeda, T., 1953. Variations of ^{18}O content of waters from natural sources. Geochimica et Cosmochimica Acta 4, 213–224.

Ezzat, M.A., 1974. Groundwater Series in the Arab Republic of Egypt: Exploitation of Groundwater in El-Wadi El Gedid Project Area. General Desert Development Authority, Ministry of Irrigation, Cairo, 149 p.

Fairbanks, R. 1989. A 17,000-year glacio-eustatic sea level record: influence of glacial melting rates on the Younger Dryas event and deep-ocean circulation. Nature 342, 637–642.

Faure, G., 1977. Principles of isotope geochemistry. John Wiley & Sons, New York, 464 p.

Feliks, Y., Ghil, M., Robertson, A.W., 2010. Oscillatory Climate Modes in the Eastern Mediterranean and Their Synchronization with the North Atlantic Oscillation. J. Climate 23, 4060–4079.

Forstel, H., Hutzen, H., 1983. Oxygen isotope ratios in German groundwater. Nature 304, 614–616.

Friedman, I., 1953. Deuterium content of natural waters and other substances. Geochimica et Cosmochimica Acta 4, 89–103.

Frumkin, A., Ford, D.C., Schwarcz, H.P., 2000. Paleoclimate and vegetation of the last glacial in Jerusalem from a speleothem record. Global Biogeochemical Cycles 14 (3), 863–870.

Gallaire, R. J.D. Taupin, G.M. Zuppi and Filly, A. 1998, Stable isotopes to study mechanism forming precipitations in West Africa. In: Study of Past and Current Environmental Changes in the Hydrosphere and the Atmosphere, IAEA, Vienna, pp. 141–149 STI/PUB/1024.

Gasse, F., 2000. Hydrological changes in the African tropics since the Last Glacial Maximum. Quaternary Science Reviews 19, 189–211.

Gat, J.R., Carmi, I., 1970. Evolution of the isotopic composition of atmospheric waters in the Mediterranean Sea area. Journal of Geophysical Research 75, 3039–3048.

Geb, M., 2000. Factors favouring precipitation in North Africa: seen from the viewpoint of present-day climatology. Global and Planetary Change 26, 85–96.

Geyh, M.A., 1994. The paleohydrology of the eastern Mediterranean. In: Bar-Yosef O., Kra, R.S., (Eds.), Late Quaternary Chronology and Paleoclimates of the Eastern Mediterranean. Tucson: Radiocarbon. pp. 131–145.

Gonfiantini, R., Conrad, G., Fontes, J.Ch., Sauzay, G., Payne, B.R., 1974. Etude isotopique de la nappe du Continental Intercalaire et de ses relations avec les autres nappes du Sahara septentrional. Isotope Techniques in Groundwater Hydrology, Vol. I. IAEA, Vienna, pp. 227–241.

Guendouz, A., Moulla, A.S., Edmunds,W.M., Shand, P., Poole, J., Zouari, K., Mamou, A., 1997. Palaeoclimatic information contained in groundwater of the Grand erg Oriental, North Africa. Proceedings Vienna Symposium 1997, IAEA SM 349/43: 555–571.

Hamilton, A., Perrott, R.A., 1979. Aspects of the glaciation of Mount Elgon, East Africa. Palaeoecol. Afr., 11, 153-161.

Hellström, B., 1940. The subterranean water in the Libyan Desert. Geografiska Annater, 22, 206–239.

Hermina, M., 1990. The surroundings of Kharga, Dakhla and Farafra oases. In Said, R(ed). The Geology of Egypt. Balkema, Rotterdam, 259–292.

Hermina, M.H., Ghobrial, M., Issawi, B. 1961. The geology of the Dakhla area. Geol. Surv. Min. Res. Dept., Cairo, 33 pp.

Hermina, M.H., Issawi, B., 1971. Rock-stratigraphic classification of the Upper Cretaceous–lower Tertiary exposures in southern Egypt. In: Gray, C. (Ed.), Symposium on the Geology of Libya, Faculty of Science, University of Libya, Tripoli, 147–154.

Hesse, K.H., Hissese, A., Kheir, O., Schnacker, E., Schneider, M., Thorweihe, U., 1987. Hydrogeological investigations in the Nubian Aquifer system, Eastern

Sahara. In: Kilitzsch, E., Schranck, E. (Eds.), Research in Egypt and Sudan: Berlin. Dietrich Reimer, Berlin, pp. 397–464.

Himida, I.H., 1969. Remarks on the absolute age determination of the artesian water of the Oases of the Western Desert with special reference to Kharga Oasis. Bull. Desert Inst. 17 (2), 53–63.

Himida, I.H., 1970. The Nubian artesian basin, its regional hydrogeological aspects and palaeohydrological reconstruction. Journal of Hydrology 9, 89–116.

Hoelzmann, P., Gasse, F., Dupont, L., Salzmann, U., Staubwasser, M., Leuschner, D., Sirocko, F., 2004. Palaeoenvironmental changes in the arid and subarid belt (Sahara-Sahel-Arabian Peninsula) from 150 kyr to present. In: R. W. Battarbee et al. (eds) 2004. *Past Climate Variability through Europe and Africa*. Springer, Dordrecht, The Netherlands, pp. 219–256.

Holman, I.P., Rivas-Casado, M., Howden, N.J.K., Bloomfield, J.P., Williams, A.T., 2009. Linking North Atlantic ocean–atmosphere teleconnection patterns and hydrogeological responses in temperate groundwater systems. Hydrological Processes 23, 3123–3126.

Hurrell, J.W., 1995. Decadal trends in the North Atlantic Oscillation: regional temperatures and precipitation. Science 269, 676–679.

Hurrell, J.W., Kushnir, Y., Visbeck, M., Ottersen, G., 2003. An overview of the North Atlantic Oscillation, in: Hurrell, J.W., Kushnir, Y., Ottersen, G., Visbeck, M. (Eds.), The North Atlantic Oscillation: Climate Significance and

Environmental Impact, Geophysical Monograph 134, American Geophysical Union, Washington D.C., pp. 1–35.

Ingraham, N.L., Taylor, B.E., 1986. Hydrogen isotope study of large-scale meteoric water transport in northern California and Nevada. Journal of Hydrology 85, 183–197.

Issar, A., Bein, A., Michaeli, A., 1972. On the ancient water of the Upper Nubian Sandstone aquifer in central Sinai and southern Israel. Journal of Hydrology 17, 353-374.

Issar, A., Bruins, J., 1983. Special climatological conditions in the deserts of Sinai and Negev during the Late Pleistocene. Palaeogeography, Palaeoclimatology and Palaeoecology 43, 63–72.

Issar, A.S., 2003. Climate Changes During the Holocene and Their Impact on Hydrological Systems, Cambridge University Press, Cambridge, UK.

Issar, A.S., 2010. Climate change as a draw bridge between Africa and the Middle East. Global and Planetary Change 72, 451–454.

Issar, A.S., Zohar, M., 2004. 2007. Climate Change — Environment and Civilization in the Middle East. Springer, Berlin. 252 pp.

Issawi, B., 1971. Geology of the Darb El Arba'in, Western Desert, Egypt. Annals of the Geological Survey of Egypt 1, 53–92.

Jenkins, D., 1990. North and Central Sinai. In: Said, R. (Ed.), Geology of Egypt: Balkema, Rotterdam, 361–380.

JICA, 1999. South Sinai Groundwater Resources Study in the Arab Republic of Egypt Report, In: Inc., P.C.I.A.S.C. (Ed.) Tokyo, Japan.

Johnson, T. C., Kelts, K. and Odada, E. O. 2000, The Holocene history of Lake Victoria. Ambio, 29(1), 2-11.

Joseph, A., Frangi, J. P., and Aranyossy, J. F. 1992, Isotope characteristics of meteoric water and groundwater in the Sahelo-Sudanese zone. Journalof Geophysical Research 97, 7543–7551.

Kazemi, G., Lehr, J., Perrochet, P., 2006. Groundwater Age. John Wiley & Sons, Hoboken, N.J., 325 p.

Kehew, A.E., Milewski, A., Soliman, F., 2010. Reconstructing an extreme flood from boulder transport and rainfall-runoff modeling: Wadi Isla, South Sinai, Egypt. Global and Planetary Change 70, 64– 75.

Kieniewicz, J.M., Smith, J.R., 2009. Paleoenvironmental reconstruction and water balance of a mid-Pleistocene pluvial lake, Dakhleh Oasis, Egypt. GSA Bulletin 121, 1154–1171, DOI: 10.1130/B26301.1.

Kipfer, R., Aeschbach-Hertig, W., Peeters, F., Stute, M. 2002. Noble gases in lakes and ground waters. In Porcelli, D., Ballentine, C., and Wieler, R., editors, *Noble gases in geochemistry and cosmochemistry*, volume 47 of *Rev. Mineral. Geochem.*, pages 615–700. Mineralogical Society of America, Geochemical Society.

Klitzsch, E., 1972. Salinität und Herkunft des Grundwassers im mittleren Nordafrika.- Geol. Jb., C2, 251–260, Hannover.

Klitzsch, E., 1984. Northwestern Sudan and bordering areas: Geological developments since Cambrian time. Berl. Geowiss. Abh. 50(A), 23-45.

Klitzsch, E., 1994. Geological exploration history of the Eastern Sahara. Geol. Rundsc., 83: 475– 483.

Klump, S., Tomonaga, Y., Kienzler, P., Kinzelbach, W. Baumann, T., Imboden, D. M., Kipfer, R. 2007. Field experiments yield new insights into gas exchange and excess air formation in natural porous media. Geochim. Cosmochim. Acta, 71(6):1385–1397.

Knetsch, G., Shata, A., Degens, E., Münnich, K.O., Vogel, J.C., Shazly, M.M., 1962. Untersuchungen an Grundwasser der Ost-Sahara. Geol. Rundschau 52, 587–610.

Knetsch, G., Yallouze, M., 1955. Remarks on the origin of the Egyptian Oasis depressions. Bull. Soc. Géograph. Égypte 28, 21–33.

Krishnamurthy, R.V., Bhattacharya, S.K., 1991. Stable oxygen and hydrogen isotope ratios in shallow groundwaters from India and a study of the role of evapotranspiration in the Indian monsoon. The Geochemical Society, special publication 3 ,187–193.

Majoube, M., 1971. Fractionnement en oxygene-18 et en deuterium entre l'eau et sa vapeur. Jour. Chim. Phys. 68, 1423–1436.

Mazor, E., 1972. Paleotemperatures and other hydrological parameters deduced from noble gases dissolved in groundwaters; Jordan Rift Valley, Israel. Geochimica et Cosmochimica Acta 36, 1321–1336.

McKee, E.D., 1962. Origin of the Nubian and similar sandstones. Geol. Rundschau 52, 551–587.

Meigs, P., 1953. World distribution of arid and semi-arid homoclimates. Reviews of Research on Arid Zone Hydrology. Paris: UNESCO.

Merlivat, L., Jouzel, J., 1979. Global climatic interpretation of the deuterium – oxygen-18 relationship for precipitation. Journal of Geophysical Research 84, 5029–5033.

Mills, A.C., Shata, A., 1989. Ground-water assessment of Sinai, Egypt. Groundwater, 27(6), 793–801.

Mokhtar, M.M., 1988. Some geological and hydrogeological studies on the southwestern area of Egypt. M.Sc. Fac. Sci. Menufia Univ., Egypt.

Münich, K.O., Vogel, J.C., 1962. Untersuchungen an Pluvialen Wassern der Ost-Sahara. Geologische Rundschau *52*, 611–624.

NASA (National Aeronautics and Space Administration), 2005. MODIS 32-day Composite MOD09A1, Goodes.AF.2005225, Collection 3, The Global Land Cover Facility, University of Maryland, College Park, Maryland, Day 225.

NCDC (National Oceanic and Atmospheric Administration, National Climatic Data Center), 2010. Surface data, global summary of the day and hourly global. URL: http://www7.ncdc.noaa.gov/CDO/cdo.

Nelson, S.T., 2000. A simple, practical methodology for routine VSMOW/SLAP normalization of water samples analyzed by continuous flow methods. Rapid Communications In Mass Spectrometry 14, 1044-1046.

Nicholson, S.E., Flohn, H., 1980. African environmental and climatic changes and the general atmospheric circulation in late Pleistocene and Holocene. Climatic Change 2, 313–348.

Osmond, J.K., Dabous, A.A., 2004. Timing and intensity of groundwater movement during Egyptian Sahara pluvial periods by U-series analysis of secondary U in ores and carbonates. Quaternary Research 61, 85–94.

Patterson, L.J., 2003. Chlorine-36 and stable chlorine isotopes in the Nubian Aquifer, Western Desert, Egypt. M. S. thesis, Univ. of Ill., Chicago, 81 p.

Patterson, L.J., Sturchio, N.C., Kennedy, B.M., van Soest, M.C., Sultan, M., Lu, Z. T., Lehmann, B.E., Purtschert, R., El Alfy, Z., El Kaliouby, B., Dawood, Y., Abdallah, A., 2005. Cosmogenic, radiogenic, and stable isotopic constraints on groundwater residence time in the Nubian Aquifer, Western Desert of Egypt. Geochem. Geophys. Geosystems, 6.

Pfahl, S., Wernli, H., 2008. Air parcel trajectory analysis of stable isotopes in water vapor in the eastern Mediterranean. J. Geophys. Res. 113, D20104,doi:10.1029/2008JD009839.

Prell, W.L., Kutzbach, J.E., 1987. Monsoon variability over the past 150,000 years. J. Geophys. Res. 92, 8411–8425.

Rossignol-Strick, M., 1983. African monsoons, an immediate climate response to orbital insolation. Nature 304, 46–49.

Rozanski, K., Sonntag, C., Münnich, K.O., 1982. Factors controlling stable isotope composition of European precipitation. Tellus 34, 142–150.

Said, R., 1962. The Geology of Egypt. Amsterdam, Elsevier, 377p.

Said, R., 1971. Explanatory notes to accompany the geological map of Egypt. Geol. Surv. Egypt, paper No. 56, 123p.

Salati, E., Dall'Olio, A., Matsui, E., Gat, J.R., 1979. Recycling of water in the Amazon basin, an isotope study. Water Resources Research 15, 1250–1258.

Salem, O.M., Pallas, P., 2002. The Nubian Sandstone Aquifer System. In: Appelgren, B. (editor). 2004. Managing Shared Aquifer Resources in Africa. ISARM-AFRICA. Proceedings of the International Workshop, Triploi, Libya, 2-4 June 2002. IHP-VI, Series on Groundwater No. 8. UNESCO, Paris.

Sandford, K.S., 1935a. Sources of water in north-western Sudan. Geographical Journal 85, 412–431.

Sandford, K.S., 1935b. Geological observations on the North-West frontiers of the Anglo-Egyptian Sudan and the adjoining part of the southern Libyan Desert. Quarterly Journal Geological Society 91, 323–381.

Sanlaville, P. 2000. Considérations sur l'environnement dans le sud du Levant durant les stades isotopiques 5 et 4, Paléorient, Volume XXVIII/1.

Sarazin, G., Michard, G., Prevot F. 1999. A rapid and accurate spectroscopic method for alkalinity measurements in sea water samples. Water Research 1, 290–294.

Schroder, TM., Rosbjerg, D. 2004. Groundwater recharge and capillary rise in a clayey catchment: modulation by topography and the Arctic Oscillation. Hydrology and Earth System Sciences 8, 1090–1102.

Sefelnasr, A.M., 2007. Development of groundwater flow model for water resources management in the development areas of the Western Desert, Egypt. Ph.D. Thesis, Nat. Sci. Martin Luther Univ. Germany, 171 p.

Shata, A., 1953. New light on the structural development of the Western Desert of Egypt. Bull. Inst. Desert Egypt.

Shata, A., 1982. Hydrogeology of the Great Nubian Sandstone basin, Egypt. Q.J.Eng. Geol. London, Vol.15, 127–133.

Shata, A., 1991. Water resources and the future of arid lands: (RTM-91). RIGW/IWACO. Cairo-Rotterdam, 35–49.

Shata, A., Knetsch, G., Degens, E.T., Münnich, K.O., El-Shazli, M.M., 1962. The geology, origin and age of the ground water supplies in some desert areas of U.A.R. Bull. Inst. Desert Egypt 2, 61–124.

Smith, J.R., Giegengack, R., Schwarcz, H.P., 2004. Constraints on Pleistocene pluvial climates through stable-isotope analysis of fossil-spring tufas and associated gastropods, Kharga Oasis, Egypt. Palaeogeography, Palaeoclimatology, Palaeoecology 206, 157–175.

Solomon, D.K., Cook, P.G., Sanford, W.E., 1998. Dissolved gases in subsurface hydrology. In: Kendall, C., McDonnell, J.J. (Eds.), Isotope Tracers in Catchment Hydrology, Elsevier, Amsterdam, 291–318.

Sonntag, C., 1986. A time dependent groundwater model for the Eastern Sahara. Berliner Geowiss. Abh., (A), 72: 124–134.

Sonntag, C., Neureuther, P., Kalinke, C., Munnich, K.O., Klitzch, E., Weistroffer, K., 1976. Zur palaeoklimatik der Sahara: Kontinental effekt im D und O-18 Gehalt pluvialer Saharawaesser. Naturewiss 63, 749–765.

Srdoč, D., Obelić, B., Horvatinčić, N., Sliepčević, A., Stichler, W., Moser, H., Geyh, M.A., 1982. Isotope analyses of groundwaters of the North African Plain. Catena 9, 253–263.

Stern, R.J., Kroner, A., 1993. Late Precambrian crustal evolution in NE Sudan: isotopic and geochronologic constraints. Journal of Geology 101, 555–574.

Street-Perrott, F.A., Marchand, D.S., Roberts, N., Harrison, S.P., 1989. Global lake-level variations from 18,000 to 0 years ago: A Palaeoclimatic Analysis. Washington, DC, United States Department of Energy, 213pp.

Sturchio, N.C., Du, X., Purtschert, R., Lehmann, B.E., Sultan, M., Patterson, L.J., Lu, Z.T., Muller, P., Bigler, T., Bailey, K., O'Connor, T.P., Young, L., Lorenzo, R., Becker, R., El Alfy, Z., El Kaliouby, B., Dawood, Y., Abdallah, A.M.A., 2004. One million year old groundwater in the Sahara revealed by krypton-81 and chlorine-36. Geophysical Research Letters, 31, L05503, doi:10.1029/2003GL019234.

Stute, M., Clark, J.F., Schlosser P., Broecker, W.S. 1995. A 30,000 yr continental paleotemperature record derived from noble gases dissolved in groundwater from the San Juan Basin, New Mexico. Quaternary Research 43, 209–220.

Stute, M., Schlosser, P., 1993. Principles and applications of the noble gas paleo-thermometer. In Climatic Change in Continental Isotopic Records, eds. P.K.

Swart, K. C. Lohmann and S. Savin, pp. 89-100. American Geophysical Union, Geophysical, Monograph 78.

Stute, M., Talma, S., 1998. Glacial temperatures and moisture transport regimes reconstructed from noble gases and $\delta^{18}O$, Stampriet aquifer, Namibia. Isotope Techniques in the Study of Past and Current Environmental Changes in the Hydrosphere and Atmosphere. IAEA, Vienna, 307-318.

Sultan, M., Ahmed, M., Sturchio, N., Yan, E., Milewski, A., Becker, R., Wahr, J., Becker, D., Chouinard, K., 2012. Assessment of the vulnerabilities of the Nubian Sandstone Fossil Aquifer, North Africa, In: Climate Vulnerability, In Press.

Sultan, M., Arvidson, R.E., Duncan, I.J., Stern, R.J., El Kaliouby, B., 1988. Extension of the Najd shear system from Saudi Arabia to the central Eastern Desert of Egypt based on integrated field and Landsat observations. Tectonics 7, 1291–1306.

Sultan, M., Metwally, S., Milewski, A., Becker, D., Ahmed, M., Sauck, W., Soliman, F., Sturchio, N., Yan, E., Rashed, M., Wagdy, A., Becker, R., Welton, B., 2011. Modern recharge to fossil aquifers: Geochemical, geophysical, and modeling constraints. J. Hydrol.403, 14–24, DOI: 10.1016/j.jhydrol.2011.03.036.

Sultan, M., Sturchio, N., Hassan, F.A., Hamdan, M.A.R., Mahmood, A.M., El Alfy, Z., Stein, T., 1997. Precipitation source inferred from stable isotopic

composition of Pleistocene groundwater and carbonate deposits in the Western Desert of Egypt. Quaternary Research 48, 29–37.

Sultan, M., Yan, E., Sturchio, N., Wagdy, A., Abdel Gelil, K., Manocha, N., Becker, R., Milewski, A., 2007. Natural discharge: A key to sustainable utilization of fossil groundwater. J. Hydrol. 335, 25–36, DOI:10.1016/j.jhydrol.2006.10.034.

Taupin, A., Coudrain-Ribstein, R., Gallaire, G.M. Zuppi and Filly, A., 2000, Rainfall characteristics (δ18σ, δ2H, up triangle, openT and up triangle, openHr) in western Africa, regional scale and influence of irrigated areas: Journal of Geophysical Research 105 D9, p. 11911–11924.

Thorweihe, U., 1982. Hydrogeologie des Dakhla Beckens (Ägypten). Berliner geowiss. Abh. 38, 1–58.

Thorweihe, U., 1990. Nubian aquifer system. In: Said, R. (Ed.), Geology of Egypt: Balkema, Rotterdam, 601–611.

Thorweihe, U., Heinl, M., 2000. Map hydrogeology of the Nubian Aquifer System, Scale 1:2,500,000. Annex to Thorweihe and Heinl (1996), 23 pp.

Thorweihe, U., Heinl, M., 2002. Groundwater resources of the Nubian Aquifer System, NE-Africa. Modified synthesis submitted to: Observatoire du Sahara et du Sahel. OSS, Paris, 23 pp.

USGS, United States Geological Survey, 2003. USGS Global Visualization Viewer GLOVIS site <http://glovis.usgs.gov/>.

Vaks, A., Bar- Matthews, M., Ayalon, A., Matthews, A., Frumkin, A., Dayan, U., Halicz, L., Almogi- Labin, A., Schilman, B., 2006. Paleoclimate and location of the border between Mediterranean climate region and the Saharo- Arabian Desert as revealed by speleothems from the northern Negev Desert, Israel. Earth Planet. Sci. Lett. 249, 384–399.

Vaks, A., Bar-Matthews, M., Ayalon, A., Schilman, B., Gilmour, M., Hawkesworth, C.J., Frumkin, A., Kaufman, A., Matthews, A., 2003. Paleoclimate reconstruction based on the timing of speleothem growth and oxygen and carbon isotope composition in a cave located in the rain shadow in Israel. Quaternary Research 59, 182–193.

Vogel, J.S., Southon, J.R., Nelson, D.E., Brown T.A., 1984. Performance of catalytically condensed carbon for use in accelerator mass spectrometry. In Wölfli, W., Polach, H.A. and Anderson, H.H., eds., Proceedings of the 3rd International Symposium on Accelerator Mass Spectrometry. Nuclear Instruments and Methods in Physics Research 233 (B5): 289-293.

Wallin, B., Gaye, C., Gourcy, L., Aggarwal, P., 2005. Isotope Methods for Management of Shared Aquifers in Northern Africa. Ground Water 5, 744–749.

Weiss, R.F., 1968. Piggyback samplers for dissolved gas studies on sealed water samples. Deep-Sea Res. 15, 695–699.

WISER/IAEA (Water Isotope System for data analysis, visualization, and Electronic Retrieval, International Atomic Energy Agency), 2010. WISER Version 0.7, copyright 2003–2008, URL: http://nds121.iaea.org/wiser.

WPP (World Population Projects), 2009. Population Division of the Department of Economic and Social Affairs of the United Nations Secretariat 2009. World Population Prospects: The 2008 Revision. Highlights. New York: United Nations.

Wycisk, P., 1993. Outline of the geology and mineral resources of the southern Dakhla Basin, SW Egypt. In: Meissner, B. & Wycisk, P. (eds). Geopotential and Ecology: Analysis of a desert region. CATENA Supplement 26, 67–97.

Yan, Z., Petit-Maire, N., 1994. The last 140 Ka in the Afro-Asian arid/semi-arid transitional zone. Glob. Planet Change 40:79–91. Palaeogeography, Palaeoclimatology, Palaeoecology 110, 217–233.

Zuppi GM, Sacchi E 2004, Hydrogeology as a climate recorder: Sahara–Sahel (North Africa) and the Po Plain (Northern Italy). Glob Planet Change 40:79–91.

Appendix A

Fossil Groundwater Wells Inventory

Fossil Groundwater Wells Collected for Processing Rayleigh Distillation Model (Gonfiantini, 1974; Edmunds and Wright, 1979; Srdoč et al., 1982; Thorweihe, 1982; Sultan et al., 1997; Bouchaou, 2009).

Box No.	Well Code	Country	Aquifer/Basin	$\delta^{18}O$ (‰)	$\delta^{2}H$ (‰)	^{14}C yr (BP)
1	M-1	Morocco	Tadla	–6.67	–40.7	32,964
	M-2			–6.57	–39.4	21,643
	M-3			–6.47	–39.6	33,371
	M-4			–6.93	–41.3	16,885
	M-5			–6.57	–40.7	35,175
	M-6			–6.91	–43.4	29,839
	M-7			–6.29	–40.1	19,873
	M-8			–5.2	–34.8	12,793
	M-9			–6.55	–38.6	27,347
	M-10			–5.82	–38.1	26,618
2	A-1	Algeria	NW Sahara	–6.5	–54	11,701
	A-2			–8.7	–54	12,447
3	A-3	Algeria	NW Sahara –	–8.3	–59	37,409
	A-4			–8.2	–62	36,024
	A-5			–8.6	–62	33,798
	A-6			–8.5	–61	30,599
	A-7			–8.4	–63	24,524
	A-8			–6.7	–56	39,074
	A-9			–8.9	–58	23,910
	A-10			–8.4	–58	12,867
	A-11			–6.8	–60	18,936
	A-12			–9.1	–60	14,698
4	A-13	Algeria	NW Sahara	–8.1	–56	32,046
	A-14			–8.8	–62	35,409
	A-15			–8.6	–61	26,496
	A-16			–8.5	–60	30,938
	A-17			–8	–60	14,553
	A-18			–7.5	–60	12,263
5	T-1	Tunisia	NW Sahara	–8.6	–62	51,550
	T-2			–7.9	–62	39,074
	T-3			–8.4	–60	22,547
	T-4			–9.1	–64	45,801
	T-5			–8.8	–62	29,368
	T-6			–8.3	–61	23,337
	T-7			–8.5	–58	36,688
	T-8			–8	–57	33,324
	T-9			–7.8	–53	22,802

Fossil Groundwater Wells Collected for Processing Rayleigh Distillation Model (Gonfiantini, 1974; Edmunds and Wright, 1979; Srdoč et al., 1982; Thorweihe, 1982; Sultan et al., 1997; Bouchaou, 2009).

Box No.	Well Code	Country	Aquifer/Basin	$\delta^{18}O$ (‰)	$\delta^{2}H$ (‰)	^{14}C yr (BP)
6	L-1	Libya	NW Sahara	–9.16	–68.2	32,500
	L-2			–9.16	–68.0	30,700
	L-3			–6.69	–45.3	>40,000
	L-4			–9.47	–68.7	35,300
	L-5			–9.55	–67.4	>40,000
	L-6			–7.08	–46.3	17,250
	L-7			–9.59	–69.0	22,700
	L-8			–9.88	–72.7	24,900
7	L-9	Libya	Sirte	–6.8	–76	35,760
	L-10			–8.6	–74	33,300
	L-11			–9.0	–74	33,220
	L-12			–8.3	–73	27,210
	L-13			–8.5	–70	25,188
	L-14			–8.7	–74	28,630
	L-15			–9.9	–76	35,530
	L-16			–9.5	–78	39,850
	L-17			–9.6	–79	>40,360
	L-18			–10.5	–80	>40,360
	L-19		NSSA	–11.6	–	>42,870
	L-20			–10.5	–	36,330
8	E-1	Egypt	NSSA	–11.3	–77	37,520
	E-2			–10.9	–72	>48,500
	E-3			–11.0	–77	>46,600
	E-4			–10.7	–75	32,110
	E-5			–10.9	–82	>27,400
	E-6			–10.6	–81	32,300
	E-7			–10.8	–81.7	34,800
	E-8			–10.4	–78.09	15,100

Appendix B

Meteorological and Isotopic Compositions Data

Isotopic compositions and Meteorological Data of the Modern Rainfall over Cairo, Egypt (WISER/IAEA, 2010; NCDC, 2010).

Month/Year	δ^2H‰	$\delta^{18}O$‰	PPT (mm)	Air Temp (°C)	Detailed Analysis of Rainfall Event				
					NRD	PPT (mm)	Contribution (%)	Day	Time
Mar-1987	–17	–3.05	24.63	15.3	7	7.87	31.95	3/3/1987	6:00 AM
						3.05	12.38	3/10/1987	6:00 AM
						7.87	31.95	3/11/1987	12:00 PM
						0.25	1.015	3/14/1987	6:00 AM
						1.02	4.14	3/17/1987	6:00 AM
						4.06	16.48	3/19/1987	6:00 AM
						0.51	2.07	3/25/1987	6:00 AM
Dec-1987	–56.9	–8.18	34.7	16.1	2	2.03	28.55	12/20/1987	6:00 AM
						5.08	71.45	12/23/1987	6:00 AM
Mar-1988	10.25	0.51	3.3	18.5	2	3.05	92.42	3/7/1988	6:00 AM
						0.25	7.58	3/8/1988	6:00 AM
Feb-1989	0.2	0.75	2.04	14.2	2	1.02	50	2/10/1989	6:00 AM
						1.02	50	2/22/1989	6:00 AM
Jan-1990	–2.55	–1.55	1.78	14.0	3	0.25	14.04	1/17/1990	12:00 AM
						1.02	57.3	1/26/1990	6:00 AM
						0.51	28.65	1/28/1990	6:00 AM
Jan-1991	9.5	–0.61	5.08	14.5	2	2.03	39.96	1/25/1991	6:00 AM
						3.05	60.04	1/31/1991	6:00 AM
Feb-1991	0.1	1.73	2.29	15.4	3	1.02	44.54	2/8/1991	6:00 AM
						1.02	44.54	2/25/1991	6:00 AM
						0.25	10.92	2/27/1991	6:00 AM

Isotopic compositions and Meteorological Data of the Modern Rainfall over Cairo, Egypt (WISER/IAEA, 2010; NCDC, 2010).

Month/Year	δ^2H‰	$\delta^{18}O$‰	PPT (mm)	Air Temp (°C)	Detailed Analysis of Rainfall Event				
					NRD	PPT (mm)	Contribution (%)	Day	Time
Apr-1991	17.35	2.4	1.02	22.9	1	1.02	100	4/27/1991	6:00 AM
Dec-1991	–39.7	–6.6	7.62	13.4	6	1.02	13.39	12/16/1991	6:00 AM
						0.25	3.28	12/21/1991	6:00 AM
						1.02	13.39	12/24/1991	12:00 PM
						4.06	53.28	12/25/1991	6:00 AM
						1.02	13.39	12/26/1991	6:00 AM
						0.25	3.28	12/31/1991	6:00 AM
Dec-2000	–18.9	–4.55	12.7	16.7	5	2.03	15.99	12/8/2000	6:00 PM
						5.08	40.03	12/9/2000	6:00 AM
						4.06	31.99	12/10/2000	6:00 AM
						0.76	5.99	12/13/2000	3:00 PM
						0.76	5.99	12/14/2000	12:00 AM
Jan-2001	22.35	2.68	1.52	16.0	2	0.76	50	1/18/2001	3:00 PM
						0.76	50	1/20/2001	6:00 AM
Feb-2001	–8.7	–3.3	2.79	18.8	2	2.03	72.76	2/17/2001	6:00 AM
						0.76	27.24	2/20/2001	6:00 PM
Mar-2001	–21	–2.63	3.05	21.3	1	3.05	100	3/13/2001	6:00 AM
Feb-2002	34.6	1.29	5.08	16.6	1	5.08	100	2/10/2002	6:00 PM
Jan-2003	–6.8	–0.92	0.51	16.2	1	0.51	100	1/22/2003	6:00 AM
Feb-2003	–17.9	–1.1	1.02	14.7	1	1.02	100	2/12/2003	6:00 AM
Mar-2003	–3.6	–2.87	110.2	16.0	3	106.17	96.32	3/11/2003	3:00 PM
						2.03	1.84	3/24/2003	6:00 PM
						2.03	1.84	3/25/2003	6:00 AM

Isotopic compositions and Meteorological Data of the Modern Rainfall over El-Arish, Egypt (WISER/IAEA, 2010; NCDC, 2010).

Month/Year	δ^2H‰	$\delta^{18}O$‰	PPT (mm)	Air Temp (°C)	Detailed Analysis of Rainfall Event				
					NRD	PPT (mm)	Contribution (%)	Day	Time
Jan-2001	1.1	–0.61	11.19	13.6	7	1.02	9.12	1/4/2001	12:00 PM
						0.51	4.56	1/12/2001	12:00 PM
						0.51	4.56	1/19/2001	12:00 PM
						0.51	4.56	1/23/2001	6:00 AM
						5.08	45.4	1/24/2001	6:00 AM
						3.05	27.26	1/25/2001	6:00 AM
						0.51	4.56	1/26/2001	6:00 AM
Feb-2001	–9.5	–3.67	25.13	14.2	6	0.25	0.99	2/4/2001	12:00 PM
						2.03	8.08	2/7/2001	6:00 PM
						7.11	28.29	2/8/2001	6:00 AM
						0.76	3.02	2/17/2001	6:00 AM
						7.87	31.32	2/18/2001	6:00 AM
						7.11	28.29	2/21/2001	6:00 AM
Mar-2001	–18.2	–3.32	16	18.2	2	3.05	19.06	3/9/2001	6:00 AM
						12.95	80.94	3/10/2001	6:00 AM
Apr-2001	–10.3	–2.88	5.84	20.4	2	5.08	86.99	4/8/2001	6:00 AM
						0.76	13.01	4/30/2001	12:00 AM
Oct-2001	7.1	–1.36	2.03	23.4	1	2.03	100	10/28/2001	6:00 PM
Nov-2001	12.6	–0.71	8.38	18.5	5	0.51	6.09	11/16/2001	6:00 PM
						1.02	12.17	11/17/2001	6:00 PM
						4.06	48.45	11/18/2001	6:00 AM
						0.76	9.07	11/21/2001	6:00 PM
						2.03	24.22	11/23/2001	12:00 AM

Isotopic compositions and Meteorological Data of the Modern Rainfall over El-Arish, Egypt (WISER/IAEA, 2010; NCDC, 2010).

Month/Year	δ^2H‰	$\delta^{18}O$‰	PPT (mm)	Air Temp (°C)	Detailed Analysis of Rainfall Event				
					NRD	PPT (mm)	Contribution (%)	Day	Time
Dec-2001	–5.6	–3.83	10.16	14.3	3	2.03	19.98	12/5/2001	6:00 PM
						1.02	10.04	12/15/2001	6:00 PM
						7.11	69.98	12/20/2001	6:00 AM
Jan-2002	–32.7	–7.05	54.09	11.4	10	7.87	14.55	1/3/2002	6:00 AM
						2.03	3.75	1/9/2002	6:00 AM
						7.11	13.14	1/10/2002	6:00 AM
						9.91	18.32	1/11/2002	6:00 AM
						7.87	14.55	1/12/2002	6:00 AM
						2.03	3.75	1/21/2002	6:00 AM
						3.05	5.64	1/22/2002	6:00 AM
						7.11	13.14	1/23/2002	6:00 AM
						2.03	3.75	1/27/2002	12:00 PM
						5.08	9.39	1/28/2002	6:00 PM
Feb-2002	28.7	1.78	104.7	13.8	5	0.76	0.73	2/10/2002	6:00 PM
						6.1	5.83	2/11/2002	12:00 AM
						0.76	0.73	2/12/2002	6:00 PM
						5.08	4.85	2/13/2002	6:00 AM
						91.95	87.86	2/18/2002	3:00 AM
Mar-2002	–24.2	–5.43	9.4	16.3	3	0.51	5.43	3/27/2002	6:00 PM
						1.02	10.85	3/28/2002	6:00 AM
						7.87	83.72	3/29/2002	6:00 PM
Apr-2002	–44.9	–8.3	2.03	17.8	1	2.03	100	4/2/2002	6:00 PM

Isotopic compositions and Meteorological Data of the Modern Rainfall over El-Arish, Egypt (WISER/IAEA, 2010; NCDC, 2010).

Month/Year	δ^2H‰	$\delta^{18}O$‰	PPT (mm)	Air Temp (°C)	Detailed Analysis of Rainfall Event				
					NRD	PPT (mm)	Contribution (%)	Day	Time
Oct-2002	–16.4	–4.08	2.28	23.9	2	0.25	10.96	10/14/2002	6:00 PM
						2.03	89.04	10/17/2002	6:00 AM
Dec-2002	–8.5	–3.91	30.49	15.2	7	5.08	16.66	12/11/2002	6:00 PM
						5.08	16.66	12/12/2002	1:00 AM
						0.51	1.67	12/17/2002	6:00 PM
						6.1	20.01	12/18/2002	6:00 AM
						0.76	2.49	12/20/2002	6:00 PM
						3.05	10	12/21/2002	6:00 AM
						9.91	32.5	12/22/2002	6:00 AM
Jan-2003	–1.2	–2.73	15.5	14.4	4	4.06	26.19	1/15/2003	6:00 AM
						9.91	63.94	1/16/2003	6:00 AM
						1.02	6.58	1/17/2003	6:00 AM
						0.51	3.29	1/20/2003	6:00 AM
Feb-2003	–6.9	–2.15	5.09	13.3	4	1.02	20.04	2/11/2003	6:00 AM
						2.03	39.88	2/12/2003	6:00 AM
						1.02	20.04	2/13/2003	6:00 AM
						1.02	20.04	2/22/2003	6:00 AM
Mar-2003	–12	–3.28	40.64	14.2	6	2.03	4.99	3/7/2003	6:00 AM
						0.51	1.25	3/12/2003	6:00 AM
						11.94	29.38	3/13/2003	6:00 AM
						6.1	15.01	3/24/2003	6:00 PM
						16	39.37	3/25/2003	6:00 AM
						4.06	9.99	3/26/2003	6:00 AM

Isotopic compositions and Meteorological Data of the Modern Rainfall over Rafah station, Egypt (WISER/IAEA, 2010; NCDC, 2010).

Month/Year	δ^2H‰	$\delta^{18}O$‰	PPT (mm)	Air Temp (°C)	Detailed Analysis of Rainfall Event				
					NRD	PPT (mm)	Contribution (%)	Day	Time
Jan-2001	–11.8	–3.57	63.5	13.6					
Feb-2001	–17.1	–4.28	44.2	14.5					
Mar-2001	–14.4	–4.29	5.2	18.6					
Apr-2001	–12.9	–3.9	9.6	19.2					
May-2001	–12.3	–3.62	0.7	19.7					
Nov-2001	4.8	–1.67	10.6	17.6					
Dec-2001	–12.2	–4.25	49.4	14.9					
Jan-2002	–13.5	–4.85	68	11.8					
Feb-2002	30.7	1.53	10.3	16.3	**No Available Records**				
Mar-2002	–40.75	–7.34	29.4	16.6					
Apr-2002	–37.8	–6.65	4.2	18.3					
May-2002	–3.6	–1.42	1.5	20.6					
Oct-2002	–3.8	–2.92	3.1	23.1					
Nov-2002	4.3	–1.64	8.9	18.6					
Dec-2002	–7.4	–4.13	75.7	14					
Jan-2003	–14.2	–3.99	NR	NR					
Feb-2003	–1.6	–2.05	NR	NR					
Mar-2003	–14	–3.64	NR	NR					

Isotopic compositions and Meteorological Data of the Modern Rainfall over Sidi Barrani station, Egypt (WISER/IAEA, 2010; NCDC, 2010).

Month/Year	δ^2H‰	$\delta^{18}O$‰	PPT (mm)	Air Temp (°C)	Detailed Analysis of Rainfall Event				
					NRD	PPT (mm)	Contribution (%)	Day	Time
Oct-1978	–9.5	–2.52	37	20.8					
Nov-1978	–25.1	–5.07	30	16					
Dec-1978	–21.5	–3.74	10	14.8					
Jan-1979	6	–0.82	3	14.2					
Feb-1979	–23.3	–4.72	18	16.7					
Mar-1979	17	1	18	17.1					
Apr-1979	12.6	1.27	2	19.6					
Oct-1979	–24.3	–4.67	23	22.6					
Nov-1979	–24.3	–4.74	16	17.6					
Dec-1979	–30.2	–5.78	63	14.5					
Jan-1980	–5.4	–1.9	10.3	12.6	**No Available Records**				
Feb-1980	–17.4	–3.56	42.9	13.1					
Mar-1980	–2.9	–2.66	7.2	14.7					
Apr-1980	–27.2	–4.53	1	17.4					
Dec-1980	–21.4	–4.49	7.9	14.8					
Jan-1981	–11.8	–4.26	29.7	11.5					
Feb-1981	–30.6	–6.05	27.6	13.3					
Mar-1981	–1.6	–1.4	2.4	16.2					
Nov-1981	–25.1	–5.18	9	17.6					
Jan-1982	–23.3	–5.62	21.9	13.7					
Feb-1982	–26.3	–6.05	72.7	12.7					
Mar-1982	–43.7	–7.98	6.9	14.6					

Isotopic compositions and Meteorological Data of the Modern Rainfall over Sidi Barrani station, Egypt (WISER/IAEA, 2010; NCDC, 2010).

Month/Year	δ^2H‰	$\delta^{18}O$‰	PPT (mm)	Air Temp (°C)	Detailed Analysis of Rainfall Event				
					NRD	PPT (mm)	Contribution (%)	Day	Time
Apr-1982	–24.3	–3.88	1.5	17.9	**No Available Records**				
Jan-1983	–10.2	–4	72.9	12.5					
Oct-1983	–21.1	–4.75	20.6	20.2					
Nov-1983	–11.9	–2.99	25.4	18.7					
Jan-1984	–0.7	–1.35	6.3	12.9					
Feb-1984	3.2	–1.32	5.3	13.7					
Mar-1984	–0.1	–1.28	11.6	15.7					
Apr-1984	–23.8	–4.63	6.2	16.7					
Oct-1984	–8.1	–0.86	40.3	22.1					
Nov-1984	–29	–4.4	51.9	18.1					
Jan-1985	–12.8	–3.2	35.2	14.4					
Feb-1985	–23.6	–4.95	11	14.1					
Oct-1985	–27	–5.41	19.6	20.2					
Nov-1985	–26.4	NR	15.1	18.5					
Jan-1986	–5.3	–1.31	12.7	14.2					
Feb-1986	–12.2	–3.78	20.6	14.7					
Mar-1986	–24.8	–5	16.2	15.4					
May-1986	–29.6	–4.33	9	18.8					
Nov-1986	–14.8	–3.48	26.6	17.6					
Dec-1986	–25.8	–4.1	26.4	14.3					
Jan-1987	–24.9	–3.99	11.8	15.2					
Feb-1987	–11.5	–2.4	1	15.7					

Isotopic compositions and Meteorological Data of the Modern Rainfall over Sidi Barrani station, Egypt (WISER/IAEA, 2010; NCDC, 2010).

Month/Year	δ^2H‰	$\delta^{18}O$‰	PPT (mm)	Air Temp (°C)	Detailed Analysis of Rainfall Event				
					NRD	PPT (mm)	Contribution (%)	Day	Time
Mar-1987	–28.6	–3.93	24.1	14.3	**No Available Records**				
Dec-1987	–38	–5.58	58.5	15.7					
Jan-1988	–20.1	–4.74	30.9	13.2					
Feb-1988	4.7	0.31	52.5	13.5					
Oct-1988	–19.7	–4.73	85	21.4					
Nov-1988	–19.9	–5.04	19.7	16					
Dec-1988	–24.2	–5.37	45.7	13.3					
Jan-1989	2.7	–1.01	58.7	12.4					
Mar-1989	–27.5	–5.88	8	15.5					
Oct-1989	–7.9	–2.51	18.8	21.2					
Dec-1989	–19.7	–4.08	10.1	15.1					
Jan-1990	16.2	2.68	41.2	13.8					
Feb-1990	–19.7	–3.87	48.9	13.8					
Nov-1990	4.8	–1.71	11.2	19.3					
Dec-1990	–34.9	–6.07	27.8	15.6					
Jan-1991	–12.6	–4.04	65.4	13.3					
Feb-1991	–24.8	–4.83	19.6	13.8					
Dec-1991	–46.4	–7.85	73.7	12.5					
Jan-1992	–12.4	–3.46	77.9	13					
Feb-1992	50.05	8.68	25.4	11.7					
Mar-1992	–20.8	–3.14	7	13.8					
Nov-1992	–27.9	–5.97	4.8	18.9					

Isotopic compositions and Meteorological Data of the Modern Rainfall over Sidi Barrani station, Egypt (WISER/IAEA, 2010; NCDC, 2010).

Month/Year	δ^2H‰	$\delta^{18}O$‰	PPT (mm)	Air Temp (°C)	Detailed Analysis of Rainfall Event				
					NRD	PPT (mm)	Contribution (%)	Day	Time
Dec-1992	–10.9	–2.96	50.7	13.6	**No Available Records**				
Jan-1993	–6.1	–3.3	43.5	12.9					
Feb-1993	–18.9	–4.89	20.5	12.2					
Oct-1993	–14.4	–3.35	31.3	22.7					
Nov-1993	–22.3	–5.04	5.2	19					
Dec-1993	–4.3	–2.01	41.5	15.7					
Jan-1994	–11.3	–2.64	37.8	14.2					
Feb-1994	–13.9	–3.07	6.5	14.1					
Oct-1994	–15.8	–3.62	57.4	23.5					
Nov-1994	–14.4	–3.54	69.3	18.4					
Dec-1994	–0.4	–2.28	30.3	14.1					
Feb-1995	–19.9	–4.51	62.4	13.8					
Oct-1995	–0.5	–1.52	10.7	23					
Nov-1995	4.3	–1.67	8.5	16.9					
Jan-1996	–32	–6.36	46.6	13.4					
Feb-1996	–18.1	–3.51	7.3	14.2					
Sep-1996	9.9	0.78	3.4	26.6					
Oct-1996	–15.6	–3.72	24.8	21.6					
Nov-1996	–26.8	–5.3	1	19.6					
Jan-1997	–20.7	–5.03	21.1	14.6					
Feb-1997	–19.9	–4.55	15.9	13.7					
Mar-1997	–14.5	–3.33	21.4	15					

Isotopic compositions and Meteorological Data of the Modern Rainfall over Sidi Barrani station, Egypt (WISER/IAEA, 2010; NCDC, 2010).

Month/Year	δ^2H‰	$\delta^{18}O$‰	PPT (mm)	Air Temp (°C)	Detailed Analysis of Rainfall Event				
					NRD	PPT (mm)	Contribution (%)	Day	Time
Nov-1997	–16.2	–3.86	25	18.8					
Apr-1997	–1.2	–1.75	10.4	16.3					
Jan-1998	–14.8	–3.4	8.1	14.5					
Feb-1998	–7.2	–3.11	16.5	15.3					
Mar-1998	–27	–5.85	45.8	14.6					
Feb-1999	–19.5	–4.71	21	13.5					
Nov-1999	8.2	–0.75	9	20					
Nov-2000	–26.2	–4.99	14.8	19.4					
Dec-2000	10	–0.89	59.3	15.9					
Jan-2001	–20.6	–4	11.2	14.5					
Feb-2001	–20.7	–4.42	9.4	14.6					
Mar-2001	3.5	–0.3	0.5	16.7	**No Available Records**				
Apr-2001	6.1	–0.41	3.1	17.8					
Jan-2002	–19.25	–5.22	67.1	17.1					
Feb-2002	–15.35	–4.27	7.2	16.5					
Mar-2002	–14.73	–4.13	8.7	17.2					
Apr-2002	–6.36	–2.89	12.9	18.7					
Oct-2002	1.1	–1.16	1.4	22.5					
Nov-2002	–11.2	–2.53	4.7	19.2					
Dec-2002	–12.7	–4.01	48.1	15.9					
Jan-2003	–23.5	–5.19	NR	NR					
Feb-2003	21.6	2.63	NR	NR					
Mar-2003	–11.3	–2.75	NR	NR					

Appendix C

Chemical Analyses of Groundwater Wells in Sinai Peninsula

Chemical Analyses of Groundwater Wells that Tap the Nubian Aquifer in Sinai Peninsula.

ID	Name	Cations (ppm)				Anions (ppm)		
		Ca^{2+}	Mg^{2+}	Na^{+}	K^{+}	HCO^{-}_3	SO_4	Cl^{-}
SN4-1	Arif El Naqa 2	548	182	440	26	358	1100	1160
SN4-2	El Themd 2	230	97.4	183	14.4	261	520	523
SN4-3	El Hasana 3	632	129	297	26.5	239	780	1160
SN4-4	Sudr El Hetan 3	222	68.4	206	23.5	236	565	417
SN4-5	El Rueikna 3	62	18.6	39.3	5.1	131	129	94.8
SN4-6	Feiran 3	120	28.5	103	6.6	224	154	212
SN4-7	El Kuntella 3	284	68.7	193	23.4	254	511	490
SN4-8	Nekhel 5	195	70.8	195	20.7	247	529	363